GEOGRAPHICA
BERNENSIA

P 40

The Hydrological Modelling System PREVAH

Part II – Physical Model Description

Daniel Viviroli,
Joachim Gurtz,
and Massimiliano Zappa

University of Berne, Switzerland • Institute of Geography

This document contains the physical description of the hydrological modelling system PREVAH. It is Part II of the extensive model documentation by Viviroli, Gurtz and Zappa (2007) and is complemented by Part I, which gives an overview of PREVAH, and Part III, the user manual for the modelling system. Part IV is a sample project containing selected components of the modelling system. For more information and updates, visit http://www.hydrologie.unibe.ch/PREVAH.

Publication Part	**Part I**	**Part II**	**Part III**	**Part IV**
Contents	Overview and selected applications	Physical model description	User manual	Sample project and selected executables
Availability	Printed only	On-line only (pdf)	On-line only (pdf)	On-line only (zip)

Last change of this document: December 11, 2007

Authors Daniel Viviroli[1], Joachim Gurtz[2] and Massimiliano Zappa[3]

[1] Institute of Geography, University of Berne (GIUB)
[2] Institute for Atmospheric and Climate Science, ETH Zurich (IACETH)
[3] Swiss Federal Institute for Forest, Snow and Landscape Research, Birmensdorf (WSL)

with contributions from
Karsten Jasper, Simon Jaun, Herbert Lang, Jörg Schulla and Mark Verbunt

Editorial assistant Sabina Steiner (GIUB)

Publisher Geographica Bernensia
Hallerstrasse 12, CH-3012 Berne

Citation Viviroli, D., Gurtz, J. and Zappa, M. (2007): The Hydrological Modelling System PREVAH. Geographica Bernensia P40. Berne: Institute of Geography, University of Berne.

ISBN 978-3-905835-01-0

Table of contents

1. Introduction

A sound simulation of hydrological processes at catchment scale requires the development and application of physically congruous hydrological models, including careful parameterisation, calibration and evaluation (Gurtz et al., 2003; Refsgaard, 1997; Uhlenbrook and Leibundgut, 2002). In the past decade, spatially distributed modelling became an established tool for studying both the components and the possible changes of the hydrological cycle. Beven (2000) gives a thorough review on the evolution of rainfall-runoff models. Hydrological models were first idealised in distributed configuration in the early 20's (Ross, 1921). The development of the unit hydrograph method (Sherman, 1932) as well as early works on the investigation and calculation of key processes like effective rainfall, saturation excess and infiltration capacity (Horton, 1933) were among the principles leading to the development of more advanced modelling packages as summarised in the blueprint for physically-based hydrological simulations proposed by Freeze and Harlan (1969). An important result of the development was the first easily usable hydrological "Stanford Watershed Model IV" (Crawford and Linsley, 1966). Further model developments – alongside the progress in computer sciences – can be considered as the turning point towards the transition to spatial and temporal distributed modelling approaches (Bergström, 1976 and 1992; Beven and Kirkby, 1979; Ross et al., 1979; Abbott et al., 1986a and 1986b; Singh, 1995). The configuration and structure of developed hydrological models depends on the modelling task and the strong relationship between these tasks and the used temporal and spatial scale (see Figure 1-1 and 1-2; Klemes, 1990).

Mountainous catchments, in particular, are characterised by highly variable morphology, soil and vegetation types and by pronounced temporal and spatial variations of the climatic elements (Klemes, 1990; Gurtz et al., 1999). Mountain discharge regimes depend, according to location and elevation of the watersheds, on glacial melt, snowmelt, rainfall and their spatial and temporal superposition. The quality of the hydrological simulations depends on how well the available models are able to describe and accurately represent the heterogeneity of such hydrological systems at the different spatial and temporal scales (Figure 1-2, see also Blöschl and Sivapalan, 1995; Zappa, 2002).

The availability of geographic information systems (GIS) and digital elevation models (DEM), the improved reliability, precision and resolution of meteorological and hydrological networks and the availability of remotely sensed data allowed the development and application of spatially distributed hydrological models within mountainous landscapes (Gurtz et al., 1999) and their calibration and evaluation with respect to observed time series and spatial patterns of hydro-meteorological variables. The development of the distributed hydrological catchment models PREVAH (Precipitation-Runoff-Evapotranspiration-Hydrotope model; Gurtz et al., 1997a, 1999 and 2003; Zappa et al., 2003) and WaSiM-ETH (Wasserhaushalts-Simulations-Modell, Schulla and Jasper 2000; Klok et al., 2001; Verbunt et al., 2003) has been initiated to allow the application of such new knowledge for mountain hydrology in Switzerland and other basins of the world.

WaSiM-ETH is a model relying on a very solid physically based formulation of the hydrological processes describing the water fluxes within a mountainous watershed. WaSiM-ETH spatial discretisation is based on grids with regular mesh sizes. The entire fluxes are computed for each time step for each grid within the modelled domain. This makes of WaSiM-ETH a computationally highly demanding model.

To allow for more flexibility, and in order to make reliable research with a reduced need of computational resources, a simpler distributed model was needed. PREVAH is such a model. To reduce the computational time, three solutions are implemented:

– The spatial discretisation relies on the Hydrological Response Units (HRU) approach.

– The formulation of the relevant processes is simplified and some algorithms are related to more conceptual approaches.

– The required meteorological information is processed only once and assimilated from tables during each simulation.

In the new century, the computational core of PREVAH has been steadily integrated with new components and tools that allow for a user friendly application of the model. Currently, PREVAH has grown into a fully functional modelling system able to manage all the work needed for its application. Tools are available for

the preprocessing management and interpolation of the required meteorological information. Tools are also available for the transformation, parameterisation and preprocessing of the physiogeographical spatial information. An in-built-calibration routine reduces the need of knowledge of the model structure and sensitivities during the process of calibration. Monte Carlo model runs can be started in order to obtain estimates of parameter uncertainties. Finally, tools have been developed to visualise the output of the model (grids, tables and output of the calibration module). These features have improved the usability of PREVAH and support new users in their first experiences with our model.

This document should provide the basis for comprehension of the content and computational structure of the hydrological catchment model system PREVAH, its parameterisation, calibration and verification, as well as its use for simulation and prediction.

Firstly, a general overview of the elementary structure of the PREVAH model is given in Chapter 2. The preparation of a model application, including preprocessing and parameterisation of spatial data, is described in Chapter 3, along with the respective tools available. Subsequently, the theoretical basis of the model and its modules are explained, describing the specific hydrological processes considered (Chapter 4). The possibilities for processing hydrological data are presented in Chapter 5. A successful application of the model for a specific catchment area requires a thorough calibration and validation, whereon Chapter 6 addresses. All in all, this document is intended to enable the reader to understand and use the complex model system PREVAH for solving a given problem in a most efficient way.

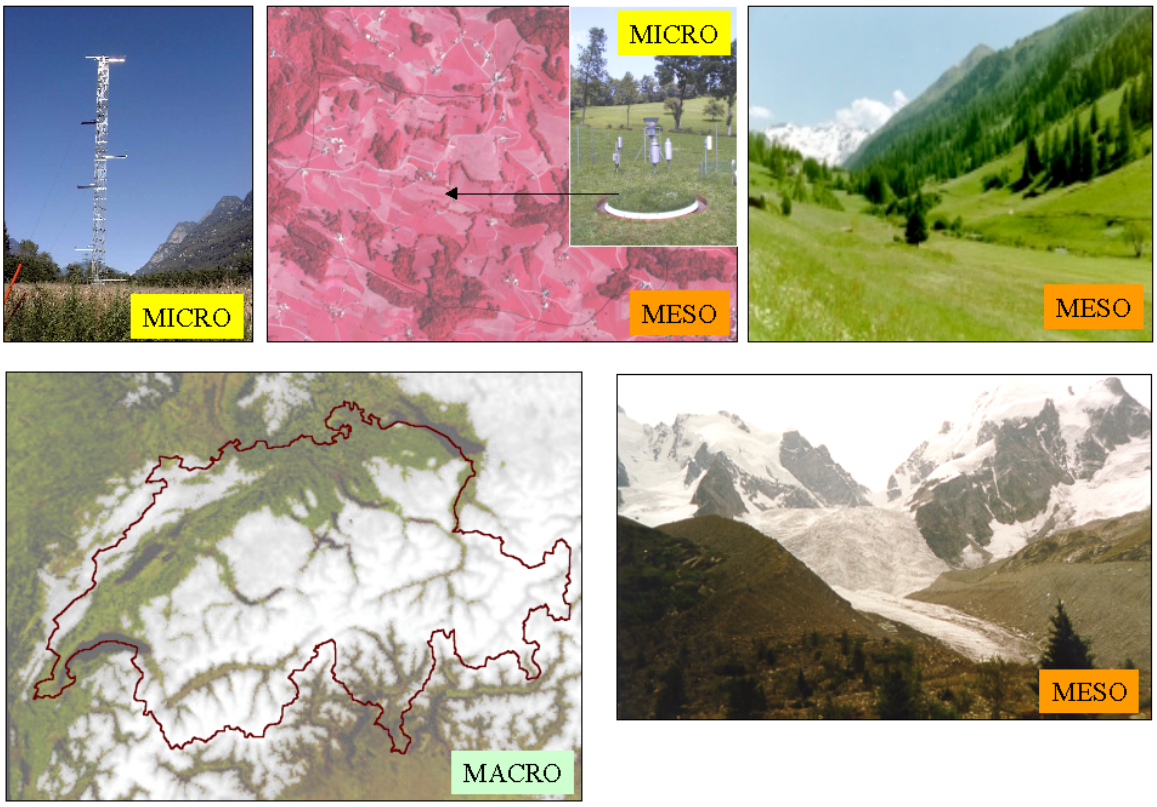

Figure 1-1: Complexity of the hydrological system Alps at different spatial scales. From top left clockwise: a meteorological tower in an alpine valley, an infrared airborne picture of the 3.3 km^2 hydrological research catchment Rietholzbach, the lysimeter site within the Rietholzbach catchment, a picture of the high alpine valley Dischma, a picture of the partly glaciated catchment of the Rosegbach and a processed satellite shot of the snow cover distribution in Switzerland (Zappa, 2002).

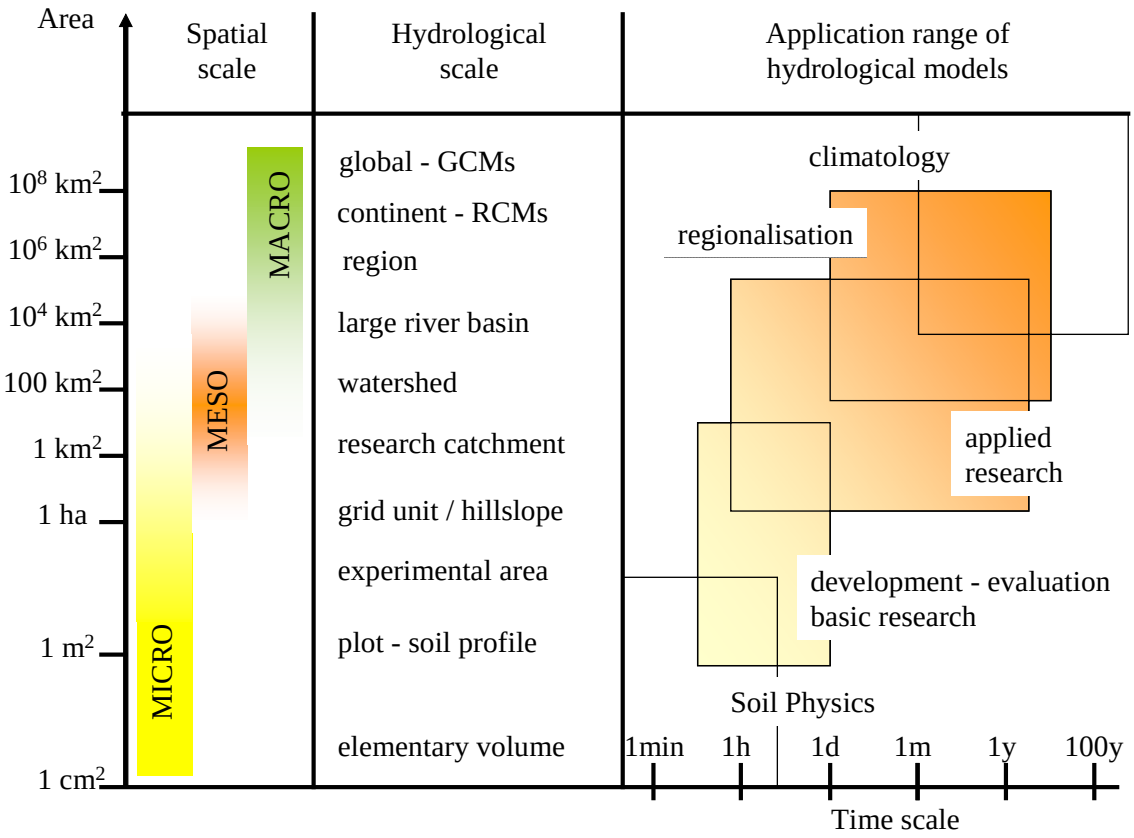

Figure 1-2: Application range of hydrological models at different spatial and temporal scales (Zappa, 2002, based on a concept of Becker and Nemec, 1987).

2. Basic structure of PREVAH

The heterogeneous character of mountainous areas requires a relatively detailed areal distributed description of the hydrological system and its spatial distributed application. The hydrological catchment model PREVAH (Precipitation-Runoff-Evapotranspiration-Hydrotope model) uses parameters which are based, as far as possible, on physical principles (Gurtz et al., 1997a). The spatial distributed model application is based on the concept of use Hydrological Response Units HRU (Flügel, 1995; Zappa, 2002). The preprocessing of digital information for distributed hydrological models requires the use of GIS-packages. The procedure includes the topographical analysis of the investigated catchments based on a DEM, the aggregation of the land-use classes to hydrologically relevant land-use classes and the parameterisation of the soil properties from digital maps of soil types. Grid based models assimilate the spatial information directly from the grids during model initialisation and apply it for the simulation of the hydrological cycle. HRU-models (Ross et al., 1979; Flügel, 1997; Kouwen et al., 1993) require a further step in the preprocessing since the spatial information has first to be aggregated into HRUs. The most important rules for generating HRUs consist of assigning all the grid elements located in the same meteorological sub-unit to a HRU (e.g. the same range of elevation), as well as showing similar aspect, using the same land-use classification and similar soil properties and, eventually, having the same position with respect to the mass balance equilibrium line of a glacier (Zappa, 1999; Zappa, 2002). The HRU-specific spatial information is stored in a table and assimilated by PREVAH during the model initialisation. The HRU size is smaller where the ensemble of the characteristics of the soils, land surface and topography shows higher spatial variability. Each HRU, and consequently, each grid cell, must be provided with a set of parameters based on information derived from the DEM, from soil maps (plant-available soil field capacity, soil depth, hydraulic conductivity) and from digital maps of land-use and land surface characteristics. The model core consists of several subsystems (Figures 2-1 and 2-2).

- A snow model
- A glacier model
- An interception model
- A model of soil water storage and depletion by evapotranspiration
- A runoff generation model
- A discharge concentration and a flood-routing model

The snow model describing the accumulation and melting of the snow cover relies on the combination of a temperature index (Braun, 1985) and an energy balance approach (Anderson, 1973), distinguishing radiation-dependent melt in periods without precipitation and advectively induced ablation periods. Retention and freezing of liquid water within the snow cover is also taken into account.

The glacier model is based on a distributed temperature-index ice-melt model including potential direct solar radiation, which can also be used for snow-melt modelling (Hock, 1999; Klok et al., 2001; Zappa et al., 2003; Verbunt et al., 2003).

Snowmelt can also be computed by adopting the algorithms physically based snowmelt model ESCIMO (Zappa et al., 2003).

The interception model considers variations in interception storage as a function of vegetation type, including vegetation density (leaf area index, LAI) and the extent of the vegetation cover. Evaporation of intercepted water occurs from plant-covered surfaces at potential rate as long as the reservoir contains sufficient humidity. The surface depression storage capacity of rocky soils and urban areas is also defined for the calculation of direct evaporation.

Particular attention was paid to evaluating evapotranspiration. Potential evapotranspiration is calculated following equations by Penman, Penman-Monteith (Penman, 1948; Penman, 1956) and others. The adjustment to different surface characteristics (i.e. land-use types) is done by varying the albedo. The calculation of actual evapotranspiration is based on the direct relation to the available moisture at the land surface and in soil depending on the soil characteristics. In the case of applying the Penman-Monteith equation (Monteith, 1965), the actual evapotranspiration can be estimated by using temporally changing minimum stomatal re-

sistances for the various vegetation classes (Gurtz et al., 1999). In case of a large soil moisture deficit, the stomatal resistance is decreased depending on soil moisture ranging below a given threshold. The computations of evapotranspiration require the availability of different meteorological input variables. The amount of net radiation is site-adjusted and determined as a function of exposure, slope and albedo of the relevant surface. Further, the temperature is adapted according to the local topographical characteristics.

In the case that only a limited number of meteorological variables are available, PREVAH also offers the opportunity of computing potential evapotranspiration. The formulations of Turc/Ivanov, Wendling and Hamon are implemented (Zappa, 2002; Zappa and Gurtz, 2003).

The important link between the loss of water by evapotranspiration and by runoff is provided through the plant-available water content in the aeration zone of the soil. The respective storage capacity is determined by the soil depth available for the roots and the plant-available field capacity of the soil. Specific rules have been developed for rocky surfaces, bare surfaces, urban surfaces and wet areas. In these cases, the actual evapotranspiration is assumed to be the potential Penman evaporation depending on the moisture available in soils and/or in surface depression storages.

Input to the soil water reservoir and runoff storages are calculated in a spatially distributed manner as a function of soil moisture content and soil characteristics of different HRUs. The sub-models for runoff formation originate in an ETH-version of the HBV-model (Bergström, 1976; Jensen, 1986) but have been strongly modified and adapted to the HRU-based spatially distributed modelling of runoff formation. In the runoff reservoirs of the model, three runoff components are distinguished: quick surface runoff, interflow (delayed runoff) and groundwater flow (baseflow). In detail, there are two groundwater storages representing a fast and a more delayed baseflow component, respectively (Gurtz et al., 2003). Each runoff component is governed by the corresponding specific storage time which holds valid for the whole sub-catchment. The percolation into the baseflow storages is calculated depending on soil conductivity and moisture content of the upper storages. Flood-routing is based on the combination of linear storages and translation components.

To represent the high dynamics typical for runoff formation processes in mountainous regions, a one-hour time interval is recommended. PREVAH always run at an internal time step of one hour. Depending on the choice of the evapotranspiration scheme, up to six meteorological input variables are required:

- Precipitation [mm per time step]
- Air temperature [°C], corrected for slope and aspect
- Global radiation [W m^{-2}], corrected for slope and aspect
- Relative sunshine duration [-]
- Wind speed [m s^{-1}]
- Relative air humidity [-] or water vapour pressure [hPa]

If only daily values of the meteorological elements are available, 24 identical values are assumed for every hour in the case of air temperature, wind speed, water vapour pressure and relative humidity; precipitation is divided into 24 identical values which sum up to the observed daily total. Daily values of global radiation are subdivided between sunrise and sunset according to the calculated potential clear-sky direct radiation (Schulla, 1997; Hock, 1999).

This assumption of uniform precipitation intensity and air temperature may principally affect the accuracy of the simulation of snow accumulation, snowmelt and runoff-generation. Zappa and Gurtz (2003) discuss this problem in the case of plot-scale simulations of soil moisture and evapotranspiration and conclude that the underestimation of the rain intensities leads to systematic errors in the computation of the soil water content but has a reduced effect on the estimation of daily evapotranspiration rates.

Interpolation is necessary if the data available do not completely cover the domain of interest. In this case, it is used for conversion of the data from sets of sample points, e.g. measured values from rainfall stations, to a discretised, continuous surface. The rationale behind spatial interpolation and extrapolation is the very common observation that, on average, values at points close together in space are more likely to be similar than points further apart (Sonderegger, 2004).

Interpolation methods are distinguished between exact and inexact interpolators. An interpolation method that predicts a value of an attribute at a sample point which is identical to that measured is called an exact interpolator. All other interpolation methods are inexact interpolators. The ideal situations are the exact interpolators, because it is only at the data points that we have direct knowledge of the attribute in question Inverse distance weighting (IDW) detrended IDW, ordinary kriging (OK) and detrended OK are exact interpolators, but elevation dependent regression is an inexact interpolator (Sonderegger, 2004). All these interpolation techniques are implemented in the preprocessing tools of the PREVAH modelling system and are available for generating the meteorological tables that are required to feed the model core.

The application of PREVAH requires thorough calibration and verification. The most sensitive tuneable parameters are the adjustment factors for scaling snowfall and rainfall (Zappa, 2002), the parameters of the snowmelt module (Zappa et al., 2003), the non-linearity factor controlling the soil moisture recharge (Zappa and Gurtz, 2003) and the parameters of the runoff generation module (Gurtz et al., 2003). In the case of glaciated basins, two additional parameters controlling the melt of glaciated areas are introduced and require calibration (Klok et al., 2001).

PREVAH can be calibrated manually. Model output is compared with observed values and evaluated by means of objective statistical criteria (Nash and Sutcliffe, 1970; Legates and McCabe, 1999). A graphical comparison between observations and simulations can be made in the calibration phase as an additional subjective assessment of model performance. Several hydrometeorological variables may be considered for manual model calibration and verification.

The in-built supervised automatic calibration procedure relies on the maximisation of an index of agreement based on nine different scores derived by comparing observed and simulated discharges (Sonderegger, 2004; Verbunt et al., 2006). A total of about 200 model runs is needed to calibrate PREVAH. The result of all model runs provides information on parameter sensitivity and related uncertainties (Zappa and Kan, 2007). The same index of agreement can be used to sort a series of Monte Carlo model runs, where the parameters requiring calibration are varied randomly. For this kind of analysis, thousands of model runs are required. The computing time for such analyses for a standard medium-size basin is of the order of 3 to 4 weeks.

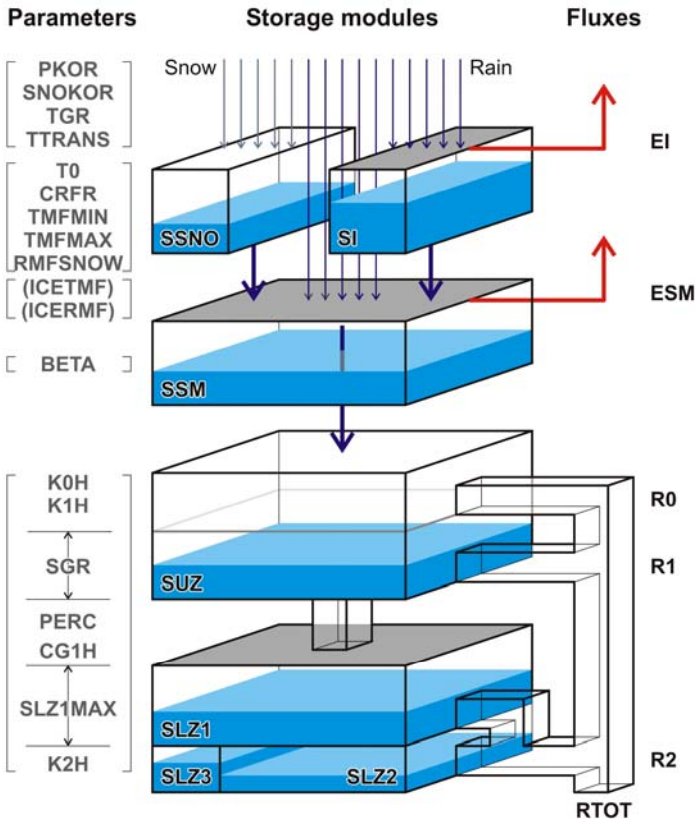

Figure 2-1: Schematic of the hydrological model core of PREVAH.

PARAMETERS

Precipitation

PKOR	Precipitation adjustment for rain [%]
SNOKOR	Precipitation adjustment for snow [%]
TGR	Threshold temperature rain-snow [°C]
TTRANS	Transition temperature range rain-snow [°C]

Snowmelt

T0	Threshold temperature snowmelt [°C]
CRFR	Coefficient for re-freezing [-]
TMFMIN	Minimum temperature melt factor for snow [mm d^{-1} K^{-1}]
TMFMAX	Maximum temperature melt factor for snow [mm d^{-1} K^{-1}]
RMFSNOW	Constant radiation melt factor snow [mm h^{-1} K^{-1} W^{-1} m^2]

Icemelt (glaciated catchments only)

ICETMF	Constant temperature melt factor for ice [mm d^{-1} K^{-1}]
ICERMF	Constant radiation melt factor for ice [mm h^{-1} K^{-1} W^{-1} m^2]

Soil moisture recharge

BETA	Non-linearity parameter for infiltration module [-]

Runoff formation

K0H	Storage time for surface runoff [h]
K1H	Storage time for interflow [h]
SGR	Threshold for quick runoff formation [mm]
PERC	Percolation rate [mm h^{-1}]
CG1H	Storage time for quick baseflow [h]
SLZ1MAX	Maximal content of the quick baseflow storage [mm]
K2H	Storage time for slow baseflow [h]

STORAGE MODULES

SSNO	Snow storage [mm]
SI	Interception storage [mm]
SSM	Soil moisture storage [mm]
SUZ	Upper zone (unsaturated) runoff storage [mm]
SLZ1–3	Lower zone (saturated) runoff storages [mm]

FLUXES

EI	Evaporation from interception storage [mm h^{-1}]
ESM	Evapotranspiration from soil moisture storage [mm h^{-1}]
R0	Quick runoff (surface runoff) [mm h^{-1}]
R1	Delayed runoff (interflow) [mm h^{-1}]
R2	Slow runoff (baseflow) [mm h^{-1}]
RTOT	Total runoff [mm h^{-1}]

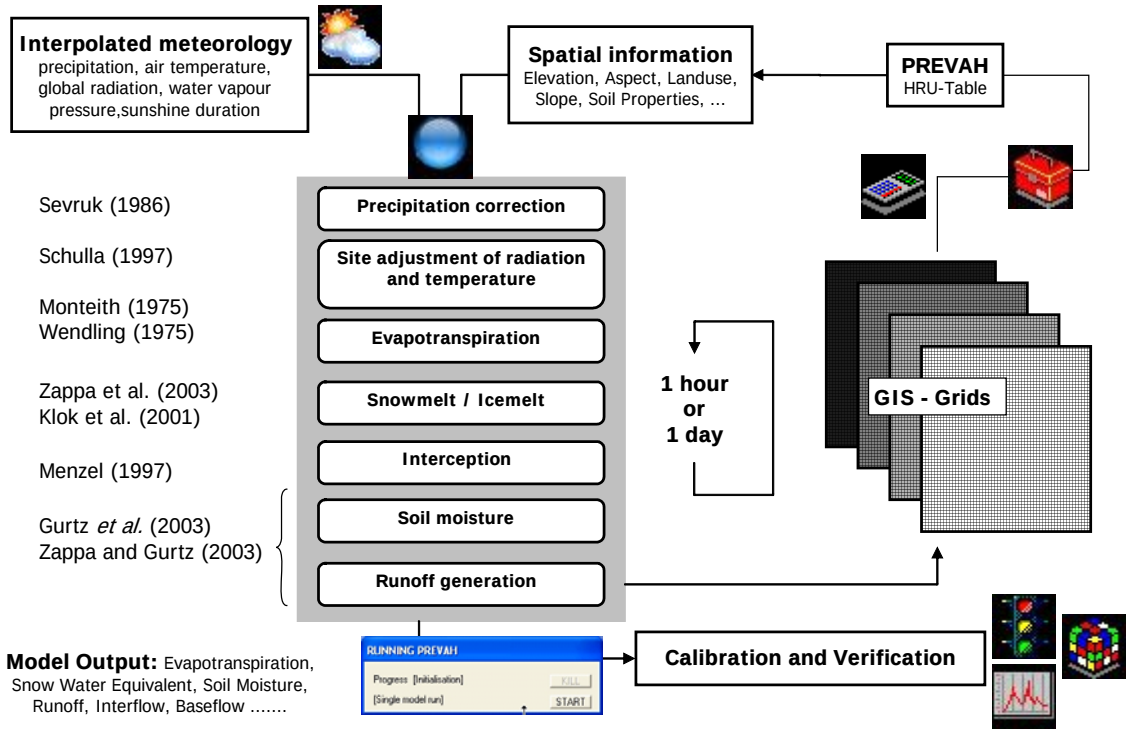

Figure 2-2: Flow chart of the PREVAH modules, including the assimilation of physiographic and meteorological information and the gridded or table-oriented model outputs. Icons refer to the tools of the modelling system linked to the specific tasks in the preprocessing and postprocessing of PREVAH.

3. Preprocessing of spatial information

Two methods are most commonly adopted for the spatial discretisation of a watershed (Singh, 1997): the grid-oriented approach and the response units approach (Ross et al., 1979; Moore et al., 1993). Grid-oriented hydrological models (Abbott et al., 1986a and 1986b; Klok et al., 2001) assimilate the spatial information for cell-by-cell simulations from grids with a prescribed spacing. Response units based models (Flügel, 1995 and 1997; Gurtz et al., 1999; Becker and Braun, 1999) rely on a physiographically-oriented discretisation of the investigated domain into irregular-shaped hydrologically similar areas as determined by the ensemble of the soils, land surface and topographic characteristics. The needed spatial information can be assimilated from a database consisting of: a digital elevation model (DEM), a land use map and soil maps.

The basic concept of the spatial distribution used in hydrological models is the subdivision of the model domain into a regularly spaced grid. This is a very effective subdivision for computational purposes. Further, the development and application of such a model is relatively easy because of the broadly available databases in gridded formats like digital elevation models and images from remote sensing devices. Compared to other methods, e.g. a subdivision into triangles, a disadvantage of a regular grid is the inflexibility in following small but important landscape features like river beds, valleys or ridges.

The preprocessing of the spatial digital information includes a complete topographic analysis (determination of slope, aspect, elevation zones, digital river network and other topographic characteristics), the possibility of summarising the land use classes to hydrological relevant classes and of assigning the parameterisation of the soil properties from the map of soil types.

3.1 Model requirements

Physiogeographical data are usually temporally constant, spatially distributed data describing the properties of the basin. Most of the spatial data can be derived from three basic data sets:

– The digital elevation model (DEM)

– The land use data

– The soil type data (e.g. FAO Soil classes)

DEMs and land use data are relatively exact and high resolution data whereas the soil types with their related soil properties are only more ore less rough estimates. For a full functionality, the PREVAH modelling system needs at least these three aforementioned data. Most of the other data sets can be derived from these grids during the preprocessing with WINHRU (see separate documentation). If, for each of the 3 basic data sets, a specific spatial resolution would be used, the data sets could be combined only after a resample of all data. This should be completed using a geographical information system GIS or similar software during the preprocessing. For all the tools of our modelling system, it is imperative that all grids are in the same format (same number of columns and rows, same co-ordinates, same cell spacing, same *NoData* value). The spatial resolution of the model grids must be chosen depending on the modelled basin. Typically, mountainous basins require a finer resolution than low land basins. In the case of catchments with an area ranging between 10 and 500 km^2, the critical resolution for a sound simulation of the discharge from mountainous environments is 500x500 m^2 (Figure 3.1-1). The resolution depends also on the computer's capacity of installed memory and processor performance.

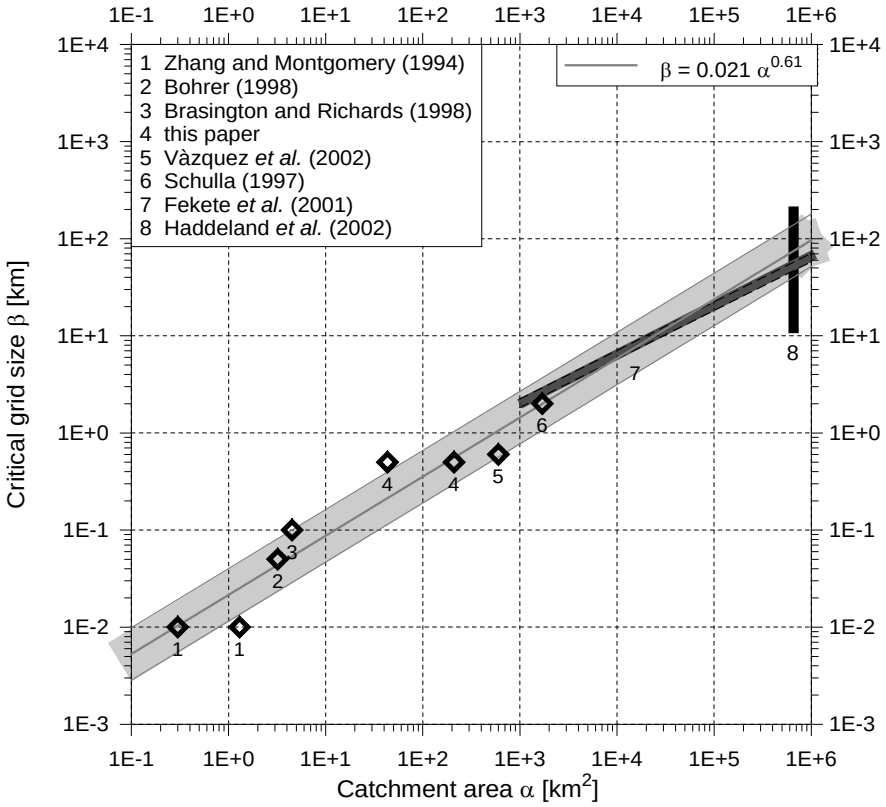

Figure 3.1-1: Visualisation of the critical grid size β *as a function of the catchment area* α*. A grid size below the value indicated by the computed regression (thick grey line) indicates an increase of computational time without increase of model ability (from Zappa, 2002). A grid size above the value diagnosed by the proposed log-log regression may cause a significant reduction in ability in the simulation of hydrological processes within the investigated catchment. The dark grey area indicates the recommended grid size proposed by Fekete et al. (2001). The black area represents the range of grid sizes adopted by Haddeland et al. (2002) for the simulation of the discharge from two macroscale basins.*

3.1.1 Digital elevation model

One of the most important data sets for using hydrological models is a digital elevation model (DEM), especially when applying the model to mountainous regions. The DEM can be used to calculate a number of derived data sets, such as local slope and aspect. It is also useful to determine some important hydrological information by using this derived information. These include, for example, flow directions, flow accumulations (for a specific catchment area), the river network and the sub-basin structure. It is also possible to calculate topographic shading and sky view factors for parameterising radiation sensitive models. The DOS program TANALYS (Schulla, 1997) performs a complex analysis of the DEM. The data sets are generated in a series of steps, as shown in Figure 3.1-2.

Only the shaded data sets are essential for the hydrological model PREVAH. Aspect and slope are required for the radiation correction, temperature modification, and the characterisation of hydrological response units.

Slope, aspect and curvatures are determined using the algorithms given by e.g. Binley and Beven (1993) or Tarboton et al. (1993). A 3 × 3 moving window is used to construct a 2nd-order parabolic surface fitting the 9 points. For each of the 9 points, Equation (3.1-1) holds:

$$z = Ax^2y^2 + Bx^2y + Cxy^2 + Dx^2 + Ey^2 + Fxy + Gx + Hy + I \qquad (3.1\text{-}1)$$

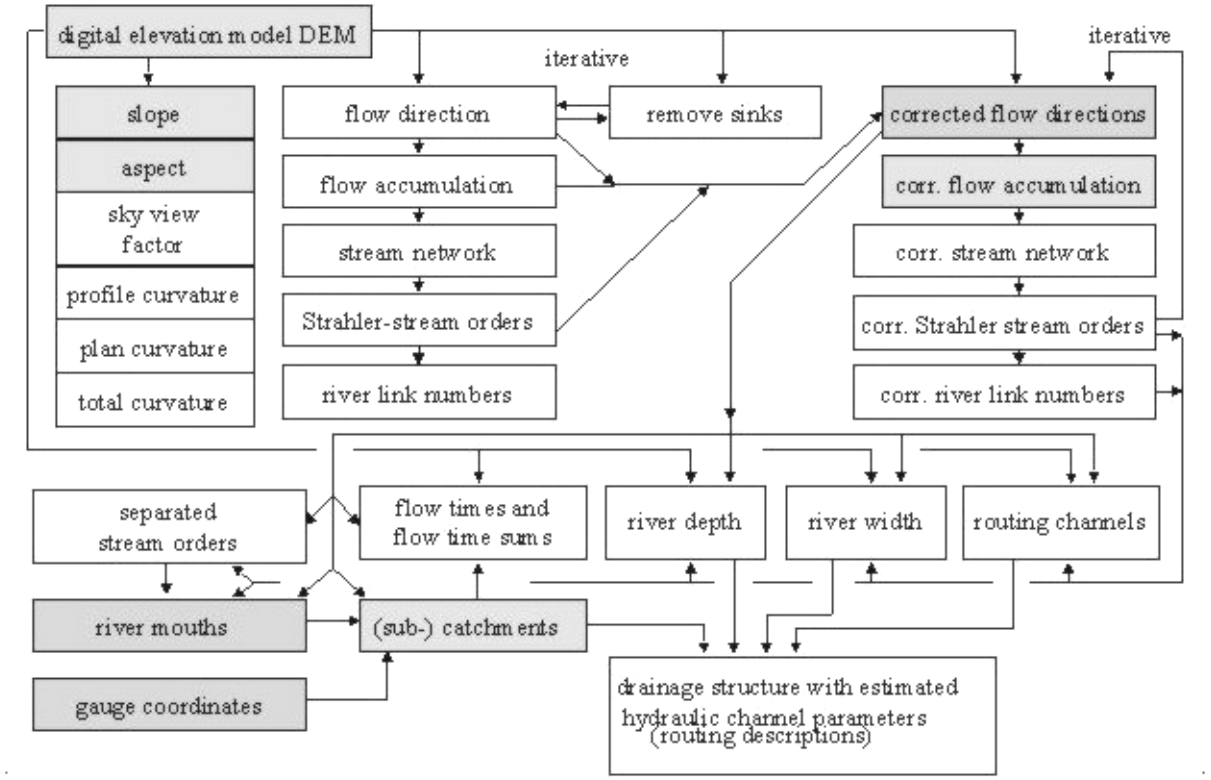

Figure 3.1-2: Topographic analysis of a digital elevation model by TANALYS. Arrows are indicators that a data set can only be generated if the arrow source already exists.

If local co-ordinates are used with (1, 1) in the upper left cell, and if the distance between the points is normalised and set to L=1 (which is allowed for quadratic grid cells), it is easy to derive a solution of the linear equation system (co-ordinates x, y ϶ {1, 2, 3}). The coefficients A to I are then given by:

$$I = z_{2,2}$$
$$H = (z_{2,1} - z_{2,3})/(2L)$$
$$G = (z_{3,2} - z_{1,2})/(2L)$$
$$F = (-z_{1,1} + z_{3,1} + z_{1,3} - z_{3,3})/(4L^2)$$
$$E = [(z_{2,1} + z_{2,3})/2 - z_{2,2}]/L^2$$
$$D = [(z_{1,2} + z_{3,2})/2 - z_{2,2}]/L^2$$
$$C = [(-z_{1,1} - z_{1,3} + z_{3,1} + z_{3,3})/4 + (z_{1,2} - z_{3,2})/2]/L^3$$
$$B = [(z_{1,1} + z_{3,1} - z_{1,3} - z_{3,3})/4 - (z_{2,1} - z_{2,3})/2]/L^3$$
$$A = [(z_{1,1} + z_{1,3} + z_{3,1} + z_{3,3})/4 - (z_{1,2} + z_{2,1} + z_{2,3} + z_{3,2})/2 + z_{2,2}]/L^4$$

	x=1	x=2	x=3
y=1	$z_{1,1}$	$z_{1,2}$	$z_{1,3}$
y=2	$z_{2,1}$	$z_{2,2}$	$z_{2,3}$
y=3	$z_{3,1}$	$z_{3,2}$	$z_{3,3}$

(3.1-2)

Some local parameters can by derived directly from these parameters by:

slope angle $$\hat{\beta} = \arctan\left(\sqrt{G^2 + H^2}\right) \quad (3.1\text{-}3)$$

aspect angle $$\hat{\Omega} = 180 - \arctan(H/G) + 90(G/|G|) \quad (3.1\text{-}4)$$

profile-curvature $$\varphi = -2(DG^2 + EH^2 + FGH)/(G^2 + H^2) \quad (3.1\text{-}5)$$

plan-curvature $$\omega = 2(DH^2 + EG^2 - FGH)/(G^2 + H^2) \quad (3.1\text{-}6)$$

total curvature $$\chi = \omega - \varphi = 2E + 2D \quad (3.1\text{-}7)$$

Flow directions are determined from the steepest slope observed in the maximum 8 neighbouring cells. Flow is allowed into only *one* of these cells. Artefacts like sinks or flat areas, which may be the result of generating the elevation model, but can also be real, natural sinks, e.g. in karst regions, are filled iteratively. Sinks are removed by finding the lowest point of all points outside but connected to the border of the sink which has a higher elevation than the sink itself. This elevation is then used to replace the value for all cells within the sink. If, after filling all boundary cells of the sink, which has grown by at least one cell, there is still no gradient to the outside of the sink, the filling is redone, now looking for the next higher elevation of the surrounding cells. This is completed iteratively until at least one cell of the (usually now much larger) sink has a flow gradient to the sink's outer side or until the growing sink reaches a *NoData* value or the boundary of the grid, which are both handled as pour points. Then, the sink has become a "flat region". Now, the flow directions within the flat regions are directed to the one or more pour points in an iterative way starting at the pour points and looking for undefined flow directions in their neighbourhood.

After calculating the flow directions and filling the sinks, the flow accumulation can be calculated. Flow accumulation is the catchment area for each grid cell in units of grid cells draining directly or indirectly through each cell. The accumulation is completed by following the flow directions of each cell until the grid boundary or a *NoData* value have been reached and summing up the number of touched cells. The result includes the cell itself, so the cells at the catchment boundary already have a flow accumulation value of 1 to avoid errors e.g. in calculating the topographic index. For calculating the topographic index, the flow accumulation value should be scaled by the cell size, in order to obtain grid scale independent results.

By setting a threshold for the flow accumulation, the river network can be extracted as a first approximation. The extraction of river networks is a rather complicated task; see e.g. Tarboton et al. (1993). The river network is used together with the flow direction grid to determine the flow orders after Strahler (1952) and to identify each river link with a river link number.

If the extracted stream network still shows artefacts like parallel rivers in neighbouring grid cells, these artefacts can be removed by applying a flow direction correction algorithm. This is also an iterative task. In a first step, rivers of Strahler order 1 are checked (head waters). If they are flowing alongside a river of higher order or alongside a river of the same order but with a larger catchment and if there is at maximum of 1 no-river grid cell between the rivers (which must have an elevation less or equal to the lower of the river cells), then the smaller river's flow direction is redirected by 45° to the larger river. After processing the entire grid, the same procedure is completed for rivers of Strahler order 2 and then for rivers of Strahler order 3. Then, the correction is completed again for rivers of Strahler order 1 and 2, respectively, in order to correct new artefacts which may have been introduced by the correction of higher order flow directions. After each single correction step, a recalculation of the flow accumulations, river network and Strahler orders has to be performed.

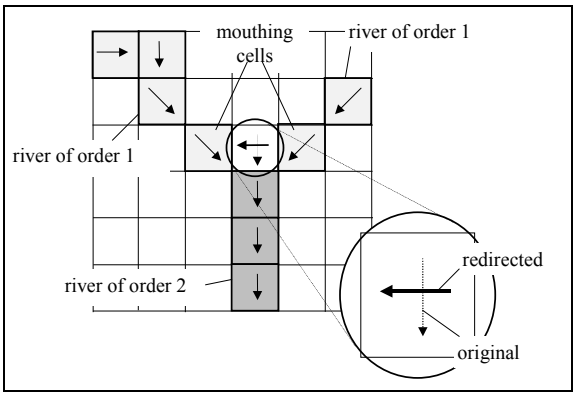

Figure 3.1-3: Flow direction correction at mouths.

A further correction may be necessary if grid cells drain between the mouthing points of two rivers directly into the higher order river. In this case, a redirection of flow directions has to be performed. Figure 3.1-3 shows the principle of this correction. Without this correction, the sub-basin for a river of order 2 would extend upstream between the catchments of the mouthing rivers of order 1. This is an artefact which does not reflect reality. Therefore, the flow direction of the last in-between-grid-cell is redirected to the last cell of the nearest or, if both mouthing rivers have the same distance to the redirected cell, to the larger river.

By separating rivers of order 2 and higher or order 3 and higher and so on, the stream network can be limited to rivers of a given minimum order (or corresponding catchment area). The separated rivers are newly numbered and then the mouths are determined, where these rivers are flowing to higher order rivers. Mouthing points are the last grid cells of a river when observing it in flow direction (Figure 3.1-3).

Sub-catchments are delineated using the mouthing points or any other pour points given in separate grids, e.g. locations of gauging stations as numbered grid cell codes in a pour point grid. The flow times for crossing the grid cells are now also summed for each cell until the next pour point is reached. Grid cells which are part of a routing channel are coded with the number of the largest of its tributaries.

The soil-topographic index (*TI*) is determined using the local catchment area a, the local transmissivity T_0 and the local slope angle β.

$$TI = \ln \frac{a}{T_0 \tan \beta} \tag{3.1-8}$$

Since it is very difficult to obtain spatially distributed information on the thickness of an aquifer, we approximate the transmissivity through the hydraulic conductivity. In opposition to the usual definition of the soil topographic index, a is the local catchment, not the local specific catchment (this is a program restriction). In order to compare our topographic index results to the topographic indices of other software developers, the value ln (cellsize) must be subtracted from all grid cells. The hydraulic-topographic index is not influenced by the transmissivity; in this case, a grid with constant cell values of 0.001 is used for T_0.

3.1.2 Land use – land cover map

The land use is a key physiographical property for spatially distributed application of hydrological models. Remote sensing platforms are fundamental for the large scale detection of the spatial distribution of different land use types. Land use (or land cover) can be determined by digitalisation, analysis and interpretation of remotely sensed images. A short definition of land use and land cover is:

Land cover:

Land cover is defined as the observed physical cover including the vegetation (natural or planted) and human constructions which cover the earth's surface. Water, ice, bare rock or sand surfaces count as land cover. Changes in land cover drive changes in the climatic system and are affected by climate change either directly or indirectly through human response. Land cover determines water, energy, and trace gas balances.

Land use:

Land use is based on the function of the land, i.e. the purpose for which the land is being used. Thus, a land use can be defined as a series of activities undertaken to produce one or more goods or services. A given land use may take place on one or more pieces of land and several land uses may occur on the same piece of land.

Land use is needed by PREVAH for the a priori parameterisation of vegetation specific parameters, which are linked to several processes of the hydrological cycle.

– *Surface roughness:* Roughness is a vegetation and topographical, structural variable and is important in models since it is used to calculate wind effects on evapotranspiration, which effects the rate of moisture transfer from the vegetation to the atmosphere. Hence, atmospheric and hydrological models require accurate estimates of surface roughness. For the same reason, hydrological models require the accurate estimation of the vegetation-atmosphere linkage. The *surface roughness* shows minimal temporal variation. Only meadows and crops show a seasonal course. The average height of the different types of vegetation is assumed as the index for the surface roughness. The surface roughness of forests, rocky areas, urban areas and water bodies must also be estimated.

– *Minimal stomata resistances:* Water evaporates at cell surfaces inside the leaves. A prerequisite for this evaporation is that the air inside the stomata cavities is released to the ambient air outside the leaves. The stomata regulate this pathway to the atmosphere. During the night, stomata are closed and transpiration is practically zero. However, as solar radiation falls on the leaves after sunrise, chemical processes take place in the stomata guard cells and the stomata open. The efficiency by which the driving force (the vapour pressure difference) moves water vapour molecules out of the leaves depends on the degree of stomata opening. This efficiency is expressed as a stomatal resistance (a resistance is the reciprocal of the conductance; see Figure 3.1-4). As the solar radiation increases, the resistance decreases. The stomatal resistance of the whole canopy, i.e. the stomata resistance expressed per unit of soil surface, also depends on the number of stomata, which is in turn related to the leaf area. Since the resistances are coupled in parallel, the stomata resistance of the canopy decreases with leaf area index (LAI). The stomata resistance is a parameter which has to be estimated for each class of vegetation. Its value is strongly related to the physiological and biological characteristic of a specific type of vegetation. This specific parameter of vegetated surfaces is related to the reaction of stomata on changes in the available moisture content in the soil. The closure of stomata causes a reduction in transpiration, and therefore a limitation in potential evapotranspiration. Stomata resistances increase during dry periods and are equal to the defined minima if enough water is available for transpiration. Increased stomata resistances cause a limitation in actual evapotranspiration, as compared to the potential value.

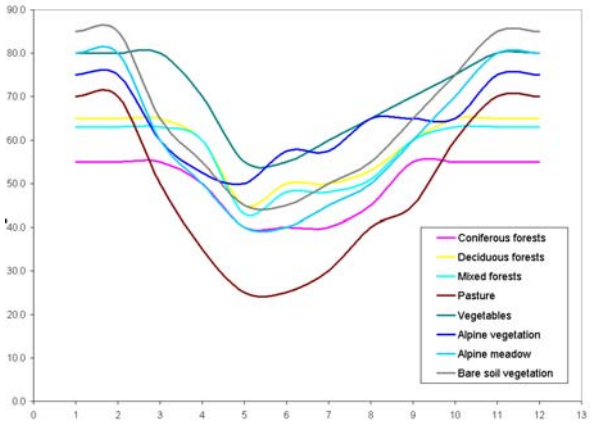

Figure 3.1-4: Monthly changing parameterisation of the minimal stomatal resistances for different standard land use categories of PREVAH.

– *Root depth:* The root depth is defined as the vertical distance from the soil surface up to which 95% of all plant roots are found. Data of rooting depth are important to properly quantify interactions between the climate, soil and plants, as root growth is very sensitive to climate change and soil properties (especially moisture). The soil moisture content available for evapotranspiration is controlled by the actual saturation of the soil and structure of the soil's root zone. The parameter "root depth" is adopted by

PREVAH for the estimation of the depth of the soil horizon that is involved in the exchange processes between soil, vegetation and atmosphere. The plant available soil moisture capacity, soil depth and root depth are used to determine the maximal depth of the water column, which the soil can store as soil moisture and that the vegetation can assimilate through the roots. The root depth has to be estimated and assigned for each class of vegetation.

– *Leaf Area Index (LAI) and vegetation density:* The seasonal cycle of vegetated surfaces can be well described through two seasonally varying parameters: LAI and the density of the vegetation. In this way, it is possible to capture the different phenological behaviour of the different classes of vegetation. LAI (see Figure 3.1-5) is the total area of leaves in relationship to the ground below them. LAI describes a fundamental property of the plant canopy in its interaction with the atmosphere, especially concerning radiation, energy, momentum, and gas exchange. Leaf area plays a key role in the absorption of radiation, in the deposition of photosynthates during the diurnal and seasonal cycles, and in the pathways and rates of biogeochemical cycling within the canopy-soil system. Various soil-vegetation-atmosphere models and hydrological models use LAI. Globally, it varies from less than 1 to above 10 but there is also significant variation within biomes at regional, landscape and local levels. Coniferous forests have high LAI and vegetation density throughout the year. Deciduous forests have a much lower LAI in winter when compared to the summer-half-year. The main hydrological processes related to seasonal development of these vegetation specific parameters are interception and evapotranspiration. Higher LAI means higher water storage capacity on leaves, which determines a higher potential for interception evaporation in the seasons with higher LAI.

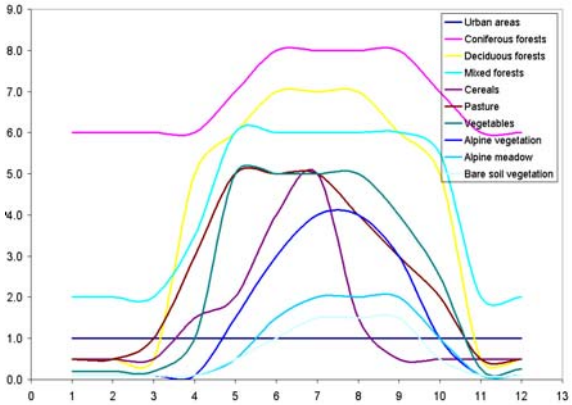

Figure 3.1-5: Monthly changing parameterisation of the leaf area index *for different standard land use categories of PREVAH.*

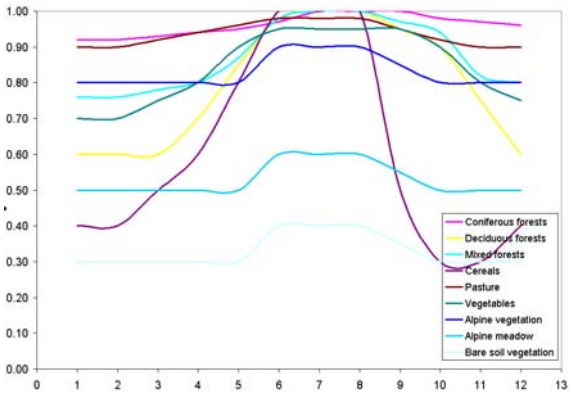

Figure 3.1-6: Monthly changing parameterisation of the vegetation density for different standard land use categories of PREVAH.

– *Albedo*: Albedo is the fraction of radiation that is reflected by the earth's surface. Surface albedo is fundamental to the surface energy balance, as it is the ratio of the downwelling to upwelling short-wave radiative fluxes at the earth's surface. Surface albedo and clouds are two of the most important parameters

modulating the earth's climate, especially over land. Although it does not change temporally as significantly as clouds, surface albedo undergoes considerable variation over space, and shows strong seasonal cycles and inter-annual variability. Surface albedo data have been obtained from in situ observations and space-borne measurements by means of remote-sensing techniques. The former are site-specific as they usually represent very small areas but have high temporal resolution, whereas the opposite is true for the latter. Therefore, the two types of measurements are complementary. Albedo is a key parameter for modellers and analysts concerned with climate, weather, ecosystem and hydrological issues. During short time periods, albedo can show an important dependence on weathering and air temperature. Snowfall causes a large increase in albedo (the albedo of fresh snow is 0.8-0.9). Snow albedo leads to reduced energy reaching the surface. This reduces evapotranspiration. The hydrological model must be able to update the albedo at the surface after snowfall events.

– *Soil heat flux*: Soil heat flux is the rate at which heat is conducted through the soil. A simple parameterisation of the soil heat flux consists of assigning a fraction of the net radiation at the soil surface. While this approximation is fairly crude, and does not recognise the phase difference between the diurnal net radiation and soil heat flux curves, it yields an adequate estimate given that the soil heat flux is typically small in comparison to the other energy budget components.

– *Available water content:* If no reliable parameterisations on soil depth and plant available volumetric water content are possible, the maximal plant-available soil water content has to be parameterised a priori for each type of vegetation.

– *Maximal interception storage*: The interception storage (Figure 3.1-7) represents the storage of moisture on the leaves of trees, grasses etc. Moisture is added to this storage from rainfall or snowmelt. The first call on this storage is for evaporation which, experiments have shown, can take place at more than the potential rate. It is possible to represent this in the model. Any moisture in excess of the storage limit reaches the soil storage. The maximal value of the interception storage may be proportional to the LAI.

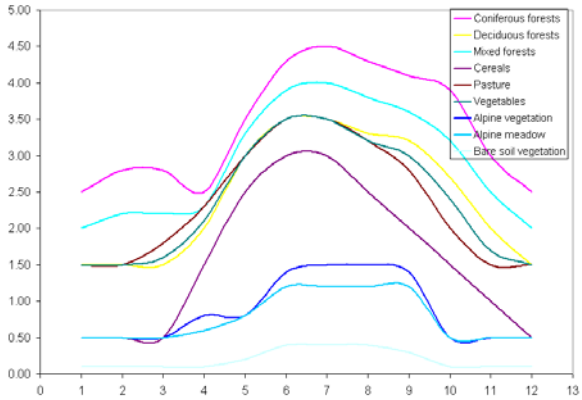

Figure 3.1-7: Monthly changing parameterisation of the maximal interception storage *for different standard land use categories of PREVAH.*

The PREVAH modelling system uses the information on land use and land cover for the parameterisation of vegetation specific parameters (see the next Sections). Only hydrological relevant land cover classes are currently implemented in PREVAH (see Table 3.1-1). The different types of land use can be aggregated for hydrological considerations into three main families:

– Vegetation: forests, meadows, bushes, agricultural land etc.

– Unproductive land forms: urban areas, rocks, bare soils

– Water bodies: rivers, lakes, snow, glaciers

Table 3.1-1: PREVAH implements parameterisation for following land use types:

Internal ID	Land cover type	Internal ID	Land cover type
1	Water	18	Fruits
2	Urban areas	19	Vegetables
3	Coniferous forests	20	Wheat
4	Deciduous forests	21	Alpine vegetation
5	Mixed forests	22	Wetlands
6	Cereals	23	Rough pasture
7	Pasture	24	Sub-Alpine meadow
8	Bush	25	Alpine meadow
13	Firn	26	Bare soil vegetation
14	Bare ice	28	Corn
15	Rock	29	Grapes

Secondary land cover types have to be aggregated into one of the PREVAH standard land use types. If another identifier is assigned to these categories, then the tools WINHRU and/or GRIDMATH allow the reclassification into the Internal ID required by PREVAH.

3.1.3 Soil map

Institutes and organisations involved in applied research at a global scale have a definite need for soil information because these data are a crucial input in models that simulate crop growth and calculate anticipated yields and water balance, or to assess the environmental impact of different land-use practices. A parameterisation of the soil's characteristics helps analysts, scientist, planners and decision-makers concerned with: development and land use research and planning; assessing and combating soil degradation and desertification; planning, monitoring and evaluating sustainable development; and modelling the interactions between soil, vegetation and atmosphere.

The a priori parameterisation of the soil's specific parameters is based on information derived from digital soil maps. Such maps should allow the classification of hydrologically relevant soil parameters like plant-available soil field capacity, soil depth and soil conductivity. These parameters are assigned during the preprocessing of the spatial data.

Soil depth

Soil depth is the vertical distance between the surface and the parent material of a soil. Soil depth indicates the state of pedogenesis; its changes can indicate degradation and other transformation processes. Soil depth usually remains the same over very long periods of time. Sudden changes will most likely be the result of a change of the soil itself (erosion, soil removal or allocation). The following tables (Table 3.1-2 and 3.1-3) indicate recommended parameterisations for soil depth in meters in the case of categorical data from the Soil Capability Map of Switzerland (BfR, 1980) and FAO "Digital soil map of the world" (FAO-UNESCO, 1988).

Table 3.1-2: Classification of soil depth from the Soil Capability Map of Switzerland.

Category	Soil depth	Parameterisation [m]
6	Very deep	4.00
5	Deep	2.00
4	Norm	1.00
3	Moderately shallow	0.50
2	Shallow	0.25
1	Very shallow	0.10
-	Rock, Glaciers, Urban areas	0.00

Table 3.1-3: Classification of soil depth from the FAO soil map (FAO-UNESCO, 1988).

Category	Soil depth	Parameterisation [m]	Recommended [m]
5	Very Deep	1.5-3.0	2.00
4	Deep	1.00-1.5	1.25
3	Norm	0.5-1.0	0.75
2	Shallow	0.1-0.5	0.35
1	Very shallow	<0.10	0.10

Plant available field capacity

Soil moisture storage capacity (also referred to as field capacity) is the water content of a soil at a defined time after its complete wetting and after free drainage has become negligible. Soil moisture storage capacity is an important soil characteristic for two reasons: together with the permanent wilting point, it defines the ability of a soil to satisfy the vegetation's water needs during periods without precipitation. Thus, the plant-available field capacity is defined as the amount of soil water that can be extracted by the plant, and is the difference in soil moisture content between the field capacity and the wilting point. It is expressed as millimetres of plant-available water within the root zone. Secondly, it describes a soil's effectiveness as a buffer in the vertical transfer of water after precipitation, thus determining a soil's water retention and purification properties. Changes in the soil moisture storage capacity occur very slowly under natural conditions. Significant changes are most probably only found after land use changes or changes to the soil itself. The following tables (Tables 3.1-4 and 3.1-5) indicate the recommended parameterisation for plant available field capacity in percent by volume in the case of categorical data from the Soil Capability Map of Switzerland (BfR, 1980) and FAO "Digital soil map of the world" (FAO-UNESCO, 1988). Table 3.1-5: Classification of maximal plant available filed capacity (AFC) from the FAO soil map (FAO-UNESCO, 1988).

Table 3.1-4: Classification of plant available field capacity (AFC) from the Soil Capability Map of Switzerland.

Category	AFC	Parameterisation [Vol%]
6	Very high	24.00
5	High	16.00
4	Norm	11.00
3	Moderately low	8.0
2	Low	4.5
1	Very low	1.5
-	Rock, Glaciers, Urban areas	0.00

Table 3.1-5: Classification of maximal plant available filed capacity (AFC) from the FAO soil map (FAO-UNESCO, 1988).

Category	AFC	Parameterisation [Vol%]	Recommended [Vol%]
1	Wetlands	-	-
2	Very High	> 20.0	25.0
3	High	15.0-20.0	17.5
4	Norm	10.0-15.0	12.5
5	Moderately low	6.0-10.0	8.0
6	Low	2.0-6.0	4.5
7	Very Low	<2.0	2.0

Hydraulic conductivity

Saturated hydraulic conductivity of a soil is a measure of a soil's ability to transmit water in a water-saturated state (Table 3.1-6). It is a key variable describing soil water fluxes. The entry of water into soil, movement of

water to plant roots, flow of water to drains and wells and its evaporation are some of the examples in which hydraulic conductivity plays a decisive role.

Table 3.1-6: Classification of saturated hydraulic conductivity from the Soil Capability Map of Switzerland.

Category	Hydraulic conductivity	Parameterisation [m s^{-1}]
7	Extremely high	1.4e-09
6	Very High	1.4e-08
5	High	1.4e-07
4	Norm	1.4e-06
3	Moderately low	1.4e-05
2	Low	1.4e-04
1	Very Low	1.4e-03

Ecologists use the saturated hydraulic conductivity to estimate or model vegetation composition and vegetation structure. Water and agricultural resource managers, hydrological modellers and atmospheric modellers use it for estimating land-atmosphere water fluxes.

3.2 Binary format

In the PREVAH modelling system, a binary grid format is used. In order to exchange grids between different computer platforms and exchange grids with other software, e.g. with ArcInfo, an ASCII-format is required.

The following rows represent the grid data from top left to lower right (rows 1 to 6: grid header including number of columns and rows, co-ordinates of the lower left corner, cell size, *NoData* value).

```
ncols                7
nrows                12
xllcorner            680500
yllcorner            222200
cellsize             2000
NoData_value         -9999
-9999 -9999 -9999 -9999 -9999 -9999 -9999
-9999 -9999 -9999 -9999 -9999 -9999 -9999
-9999 -9999 586 559 595 601 585
584 -9999 -9999 -9999 -9999 -9999 -9999
-9999 449 -9999 -9999 454 511 551
-9999 561 529 509 498 487 499
521 523 523 534 -9999 -9999 -9999
-9999 -9999 -9999 -9999 -9999 -9999 -9999
-9999 -9999 -9999 -9999 -9999 345 234
567 453 456 478 789 576 482
123 -9999 1252 1211 876 564 825
-9999 -9999 234 1246 -9999 -9999 -9999
```

The PREVAH binary format is structured similarly to the ASCII-format. All values are stored in single precision (4 bytes in most computer systems, 6 to 7 digits precision). Records 1 to 6 correspond to the data of the ASCII-Format. Then 6 additional records describing the grid statistics follow:

Records 1 to 6: as in the ASCII-format.

Records 7 to 12:

- Count of valid cells (without *NoData*-values)
- Minimum value of all valid grid cells
- Maximum value of all valid grid cells
- Sum of all valid grid cells
- Mean value of all valid grid cells
- Standard deviation of all valid grid cells

After this header, all cells of the grid are following in the same order as in the ASCII-format, i.e. from the top left cell to the lower right cell in a row by row order. The tool GRIDMATH (see particular documentation) is available for format conversion. ASCII-formats can be exchanged between different systems using e.g. Ftp-programs, with an automatic conversion of carriage returns/line feeds. To exchange binary data, the data first have to be converted into ASCII-data, then the exchange can be completed, followed by a re-converting on the target platform.

3.3 Concept of the hydrological response units HRU

3.3.1 Basics

When hydrological modelling is applied to different spatial units, the nature and size of the units must account for the complexity of the landscape and the accuracy required by the modelling task (Gurtz et al., 1999). The spatially distributed hydrological model PREVAH (Gurtz et al., 1999 and 2003a; Zappa et al., 2003) can either be applied to each single grid cell or to an aggregation of spatially distributed grid cells, which are similar according to a set of structural and statistical differentiation characteristics. This implies a similar/homogeneous hydrological response, if the applied criteria for differentiation have a direct feedback with the most important processes controlling evapotranspiration and runoff-generation. Such an aggregation of hydrologically equal surface units is called a 'hydrological response unit' HRU (Ross et al., 1979; Engel, 1996; Moore et al., 1993; Flügel, 1997). The HRU approach allows for the discretisation of a catchment with an internally dynamical spatial resolution. The HRU size is smaller where the ensemble of the characteristics of the soils, land surface and topography shows higher spatial variability (Gurtz et al., 1997b; Zappa and Gurtz, 2002).

3.3.2 Use of the HRU concept in PREVAH

PREVAH and its GUI-based version WINPREVAH rely on the aggregation of grid elements into HRUs. For distributed simulations, a set of HRUs has to be defined.

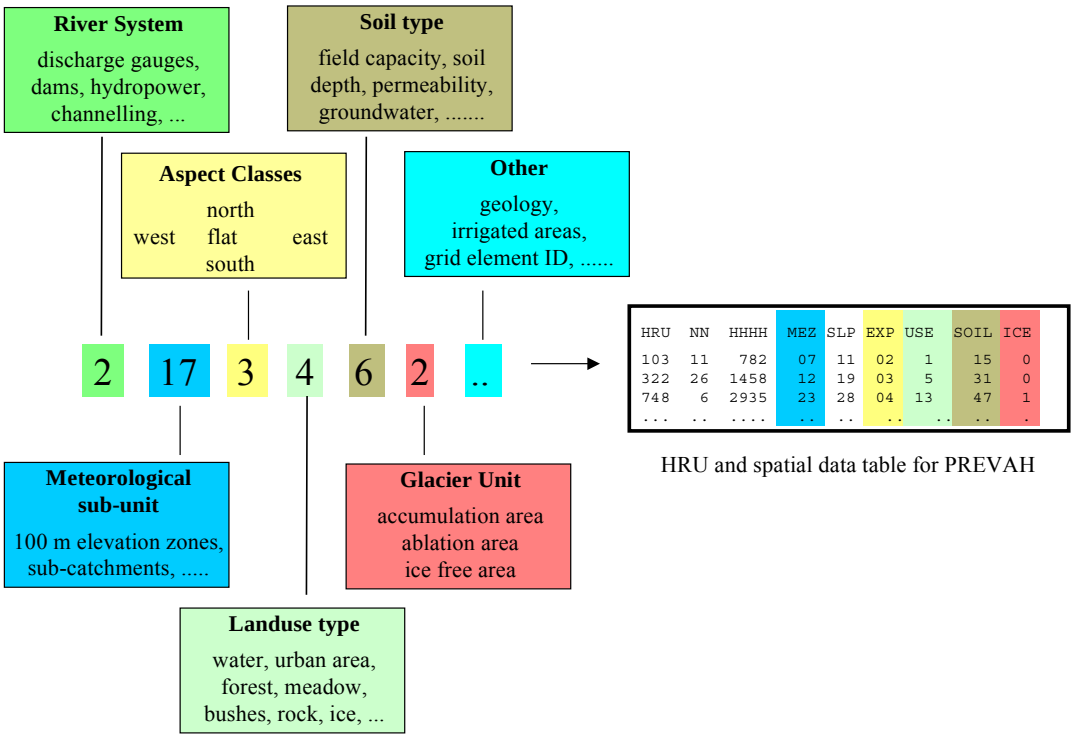

Figure 3.3-1: Preprocessing of spatial information for PREVAH including the possible criteria adopted for the aggregation of the HRUs. The typical rules for generating a code for the definition of HRUs assign, to a HRU, all the grid elements in the same meteorological sub-unit, with similar aspect, same land-use classification and, eventually, same position with respect to the equilibrium line of a glacier.

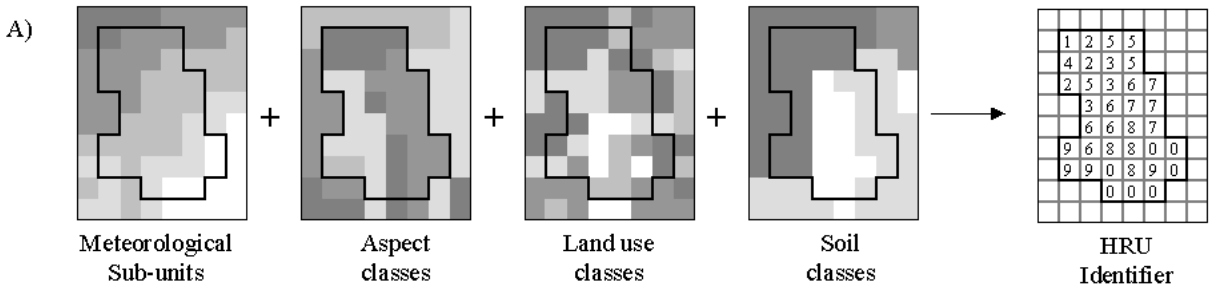

Figure 3.3-2: HRU based discretisation of idealised domain for distributed hydrological simulations in mountainous environments.

Different levels of information classes (Figures 3.3-1 and 3.3-2) are introduced and used to generate the HRUs (Nemec, 1993; Gurtz et al., 1999):

- Level of the *river system*: In particular the sub-catchment areas and channel network can be identified from the topography and position of gauging stations;
- The *topographic* level is characterised by elevation, aspect (typically five classes: north, east, south, west or flat) and slope. The amount of energy available for evapotranspiration is strongly controlled by these factors in combination with surface albedo;
- Level of the *meteorological input variables*: The definition of meteorological sub-units is typically related to the delimitation of 100 meters elevation zones on the basis of the available digital elevation model (DEM). The use of other criteria for such differentiation is possible;
- The level of *land-use characteristics*, which is an important control on evapotranspiration as well as processes involved in runoff-generation. In the case of glaciated catchments, a further classification is

required. The disposition of the grid elements with respect to the equilibrium line of the glacier (accumulation, ablation or ice-free area) has to be determined;

– The level of *soil properties and geology* includes field capacity, soil depth, permeability, groundwater recharge and storage characteristics. The extrapolation of those properties allows the description of the feedback between soils and water balance components.

3.3.3 Algorithm

Figure 3.3-2 shows the recommended rules for generating HRUs in mountainous environments. In the following example, all grid elements located in the same meteorological sub-unit, having similar aspect and soil properties and the same land-use classification are assigned to a HRU. Equations (3.3-1) and (3.3-2) illustrate the formulation of the algorithm adopted for the generation of the code HRU^{ID}:

$$HRU^{ID}{}_{(i,j)} = \sum_{n=1}^{m} CLASS^{ID}(n)_{(i,j)} \cdot 10^{D_n} \tag{3.3-1}$$

$$D_n = \begin{cases} \sum_{k=n+1}^{m} D^{ID}(k) & for\ n < m \\ 0 & for\ n = m \end{cases} \tag{3.3-2}$$

HRU^{ID} is computed for all grid elements (*i,j*) located in the investigated domain. *i* defines the grid columns (e.g. the *x* co-ordinate in metric units or the longitude in degrees) and *j* defines the grid rows (e.g. the *y* co-ordinate or latitude). *m* is the number of layers (physiographic properties) that are considered for generating HRU^{ID}. *n* is the identifier of a specific layer (Table 3.3-1). $CLASS^{ID}$ is a grid index where an integer number is assigned to every (*i,j*)-pair. That integer number represents a classification for a layer's attribute.

Table 3.3-1: Recommended physiographic layers for the discretisation of a mountainous catchment into HRUs. n *is the identifier of the layer.* $CLASS^{ID}$ *is a grid containing, for each* (i,j) *element, an integer number as an identifier for the attributes of a particular layer.* D^{ID} *is the required number of digits by a specific layer in the HRU-code. The right-part of the table shows the attributes* $CLASS^{ID}_{(x,y)}$ *for an arbitrary* (x,y) *grid point.*

n	Layer	$CLASS^{ID}_{(i,j)}$	D^{ID}	(x,y)	$CLASS^{ID}_{(x,y)}$
1	Elevation zone	0-99	2	Valley floor	15
2	Aspect	0-9	1	South-exposed	3
3	Land-use	0-99	2	Pasture	24
4	Soil type	0-99	2	Sand	13

A $CLASS^{ID}$ equal to "*3*", for example, for the layer "*aspect*" means that the (*i,j*)-pairs carrying this $CLASS^{ID}$ are south-exposed. The exponent D_n is required to build HRU^{ID}, appending a layer $CLASS^{ID}$ to the $CLASS^{ID}$ of the layers already defined. D^{ID} is the number of digits occupied by a layer $CLASS^{ID}$ in the HRU^{ID}.

Table 3.3-1 shows a selection of physiographic layers for the generation of HRUs in mountainous catchments. In the presented example, the HRU^{ID} can consider up to 100 meteorological sub-units (all the grid elements in the same 100 m range of elevation, in this experiment), land-use classes and soil types, and up to ten aspect classes.

An idealised (*x,y*) grid element located in the lower part of the investigated domain (south-exposed, used as a pasture and characterised by sandy soils) can be identified by a HRU^{ID} equal to "*1532413*", using equation (21), and the idealized $CLASS^{ID}$ reported on Table 3.3-1. Other (*i,j*)-pairs may share that HRU^{ID}. Thus, they are assumed to have a similar hydrological response to this example.

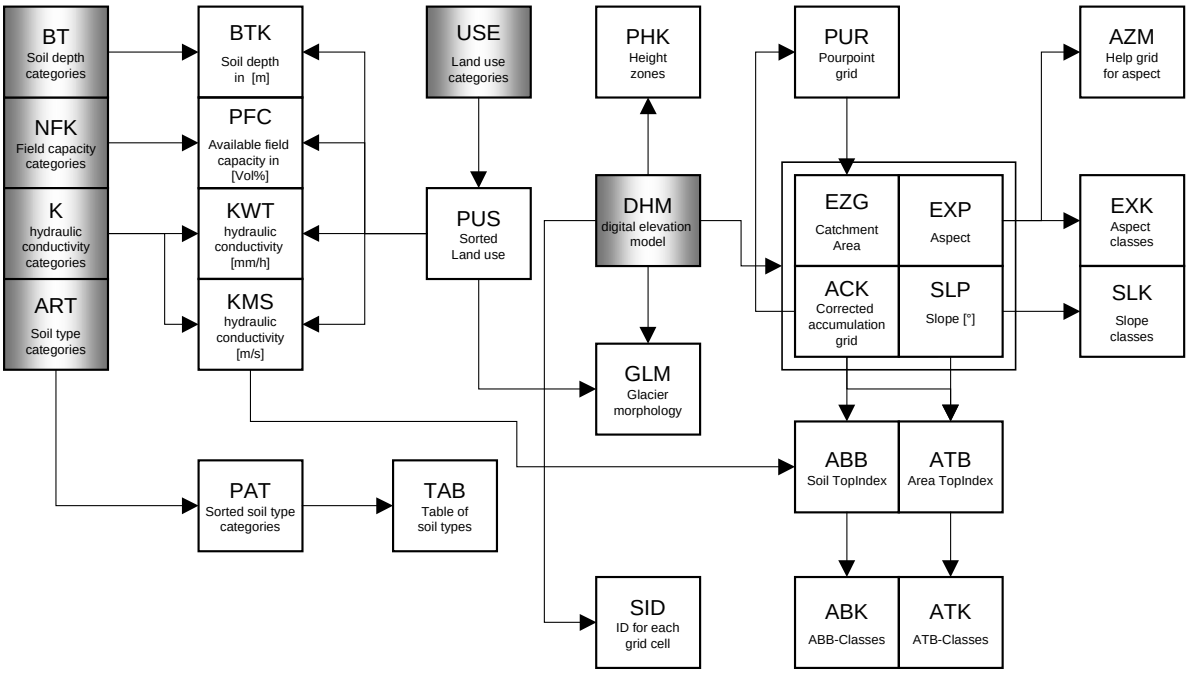

Figure 3.3-3: Project preprocessing with WINHRU. Summary of the required extensions and data flow. Grey boxes are the inputs, white boxes the output.

3.4 Meteorological model input

3.4.1 Required meteorological variables

PREVAH always runs at an internal time step of one hour. Depending on the choice of evapotranspiration scheme, up to six meteorological input variables are required:

- Precipitation [mm per time step]
- Air temperature [°C]. Air temperature is then corrected for slope and aspect
- Global radiation [W m^{-2}]. Global radiation is also corrected for slope and aspect
- Relative sunshine duration [-]
- Wind speed [m s^{-1}]
- Relative air humidity [-] or water vapour pressure [hPa]

Should only daily values of the meteorological elements be available, 24 identical hourly values are assumed for air temperature, wind speed, water vapour pressure and relative humidity. Precipitation is divided into 24 identical values, while global radiation values are subdivided between sunrise and sunset according to the calculated potential clear-sky direct radiation (Schulla, 1997; Hock, 1999).

This assumption of uniform precipitation intensity and air temperature may principally affect the accuracy of the simulation of snow accumulation, snowmelt and runoff-generation. Zappa and Gurtz (2003) discuss this problem in the case of plot-scale simulations of soil moisture and evapotranspiration and conclude that the underestimation of the rain intensities leads to systematic errors in the computation of the soil water content but has a reduced effect on the estimation of daily evapotranspiration rates.

3.4.2 Spatial interpolation of meteorological input data

Interpolation is necessary if the data available do not completely cover the domain of interest. In this case, it is used for conversion of the data from sets of sample points, e.g. measured values from rainfall stations, to a discretised, continuous surface. The rationale behind spatial interpolation and extrapolation is the very com-

mon observation that, on average, values at points close together in space are more likely to be similar than points further apart (Burrough and McDonnell, 2000).

"*Interpolation is the procedure of predicting the value of attributes at unsampled sites from measurements made at point locations within the same area or region. Predicting the value of an attribute at sites outside the area covered by existing observations is called extrapolation*" (Burrough and McDonnell, 2000:98). It is not possible to eliminate the problems associated with extrapolation but it should be considered carefully, perhaps by an investigation of extremes in the model input data plus a comparison with any other independent data.

Interpolation methods can be distinguished between exact and inexact interpolators. An interpolation method that predicts a value of an attribute at a sample point which is identical to that measured is called an exact interpolator. All other interpolation methods are inexact interpolators. The ideal situations are the exact interpolators, because it is only at the data points that we have direct knowledge of the attribute in question (Burrough and McDonnell, 2000). Inverse distance weighting (IDW) detrended IDW, ordinary kriging (OK) and detrended OK are exact interpolators but elevation dependent regression (EDR) is an inexact interpolator.

The pattern of spatial continuity of the variable to interpolate is one the most important facets for the problem of estimation. If the pattern is highly continuous, estimates based on only the closest available samples may be quite reliable, but erratic phenomenon may require the consideration of many more sample data beyond the closest points (Isaaks and Srivastava, 1989). The spatial variability and discontinuity of precipitation fields increases the shorter the reference period (Dyck and Peschke, 1995).

A. Elevation dependent regression (EDR)

The interpolation method Elevation Dependent Regression belongs to the family of polynomial regressions methods. It is a stochastic, global technique which fits the variable of interest to some linear combination of regressor variables. In this case, the variable of interest is fitted to the elevation of the used stations. Typically, the goal when using polynomial regression is to obtain the best fit with the simplest model. Using this method, the interpolation result is estimated using the altitude dependence of a variable. To use this method, it is necessary to generate the appropriate files containing the altitudinal gradients for each variable needed by PREVAH. The gradients can be given for a maximum three variable ranges separated by inversions (Figure 3.4-1). The estimation of the altitude of these inversions is completed semi-automatically by searching for cross sections of the regressions of neighbouring altitudinal ranges.

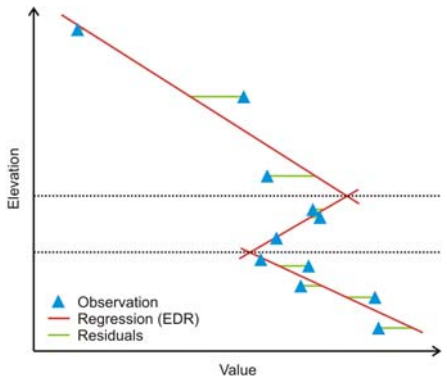

Figure 3.4.1: Elevation dependent regression.

Using this method, the interpolation result is estimated with the altitude dependence of a variable. As initial values, typical altitudinal ranges of inversions are specified for each of the two possible inversions. Separate regressions are then estimated for the range below and the range above the lower inversion. If the regressions intersect between the lower and upper (theoretical) inversion, it is assumed that there is only one inversion. Otherwise, i.e. if the regressions intersect outside the inter-inversion range, a twofold inversion is assumed, making only the lower regression valid below the lower inversion and the upper regression valid above the upper inversion. In-between, a third gradient is assumed to link both regressions linearly.

The interpolation to a specified point in the model is then completed by:

$$T(h_M) = a_{r,i} + b_{r,i} \cdot h_M \tag{3.4-1}$$

with h_M altitude [m a.s.l.]
T variable (e.g. air temperature)
i index for lower, medium and upper regression, respectively (i=1..3)
$a_{r,i}$, $b_{r,i}$ parameter of the respective regression

EDR is an "inexact" interpolation method, as defined above. The interpolated value in the location where an observation is available does not necessarily correspond to the observed value. The difference between interpolated value and observed value is called the "residual". To adopt this interpolation method, it is imperative to know the altitude of all the available meteorological stations. The computation of the altitudinal gradients is currently achieved using WINMET, a preprocessing tool of the PREVAH modelling system.

B. Inverse distance weighting interpolation (IDW)

Methods built on inverse distance interpolation combine the idea of proximity, introduced by the Thiessen polygons, with the gradual change of the trend surface. It is assumed that a value of an attribute z at an unvisited point is a distance-weighted average of data points within the neighbourhood of the unvisited point (Burrough and McDonnell, 2000). The fact that only the neighbourhood is considered in the calculations makes the inverse distance weighted method a local interpolator. The weight assigned to a particular value decreases as distance from the prediction location increases, thus sample data closest to the unmeasured point contribute more to the calculated average. The input data are read in as a table. For the IDW-method, all stations within a specified search radius are used for the interpolation. If all stations have identical values, interpolation is skipped and the constant value is used. If all stations have no-data values, the interpolation is also skipped, and the results from the last time step are used. If the distance is equal to 0 (a point to interpolate is at a gauging station), no interpolation is performed (avoiding division by 0), but the value is simply brought forward causing the IDW to be an exact interpolator. The interpolation result is the sum of all contributing weighted station data. The form of the inverse distance predictor is:

$$\hat{z}(u) = \sum_j \left(w_j \cdot z(u_j) \right) \tag{3.4-2}$$

with $w_j = \frac{1}{d(u,u_j)^p} \cdot \frac{1}{C}$ and $C = \sum_j \frac{1}{d(u,u_j)^p}$ follows: $\sum_j w_j = 1.0$

and with $\hat{z}(u)$ interpolated value at location u
w_j weight of the observed value at station j
$z(u_j)$ observed value at station j
$d(u,u_j)$ distance to station j
p weighting power of the inverse distance (between 1 and 3, 2 is recommended)

The IDW method is an averaging technique that produces highly smoothed surfaces. The original data points are honoured and, therefore, calculated values can never be higher than a local maximum or lower than a local minimum. To adopt this interpolation method, it is imperative to know the northing and easting (y and x co-ordinates) of all the available meteorological stations.

C.1 Geostatistical interpolation methods

Most earth science applications are not understood in sufficient detail to permit a deterministic approach to estimation. There is a large uncertainty pertaining to what happens at unsampled locations. For this reason, the geostatistical approach to estimation is based on a probabilistic model that recognises these inevitable uncertainties. Probabilistic, geostatistical models have been proven in cases where the available sample data is considered to be the result of a random process. They also give some ability to gauge the accuracy of estimates and assign confidence intervals. The strength of geostatistical methods over more classical approaches is their ability to recognise spatial variability at both the large and small scale, or in statistical parlance, it models both spatial trends and spatial correlation. IDW only recognises spatial correlation without spatial trend, whereas elevation detrending (EDR) only recognises horizontal dependency. Parts of the widely available geostatistical package GSLIB (Deutsch and Journel, 1997) were implemented into WINMET.

C.2 Regionalised variable theory

Geostatistical methods for interpolation start with the recognition that the spatial variation of any continuous attribute is often too irregular to be modelled by a simple, smooth mathematical function. Instead, the variation can be better described by a stochastic surface. The attribute is then known as a *regionalised variable*. Regionalised variable theory assumes that the spatial variation of any variable can be expressed as the sum of following three major components:

– A structural component ($m(\vec{x})$), having a constant mean or trend (deterministic function)

– The variation of the regionalised variable ($\varepsilon'(\vec{x})$) (a random, but spatially correlated component)

– A residual error term, "noise" (ε'') (spatially uncorrelated, Gaussian distributed)

These three components result in the random function $Z(\vec{x})$.

$$Z(\vec{x}) = m(\vec{x}) + \varepsilon'(\vec{x}) + \varepsilon'' \tag{3.4-3}$$

To calculate $Z(\vec{x})$ a suitable function for $m(\vec{x})$ has to be defined. If no trend or drift is present, $m(\vec{x})$ equals the mean value in the sampling area and the expected difference between any two places $\vec{x}$ and ($\vec{x}+\vec{h}$) separated by a distance vector $\vec{h}$.

$$E\left[Z(\vec{x}) - Z\left(\vec{x}+\vec{h}\right)\right] = 0 \tag{3.4-4}$$

$Z(\vec{x}+\vec{h})$ and $Z(\vec{x})$ are the values of the random function Z at locations ($\vec{x}+\vec{h}$) and $\vec{x}$. It is assumed that the variance of differences depends only on the distance ($\vec{h}$) between sites and not on the location.

$$E\left[\left\{Z(\vec{x}) - Z(\vec{x}+\vec{h})\right\}^2\right] = E\left[\left\{\varepsilon'(\vec{x}) - \varepsilon'(\vec{x}+\vec{h})\right\}^2\right] = 2\gamma\left(\vec{h}\right) \tag{3.4-5}$$

$\gamma\left(\vec{h}\right)$ is known as the semivariance. The *intrinsic hypothesis* of the regionalised variable theory is defined by the two conditions: stationarity of difference and variance of difference. Stationarity of difference presumes that the expected outcome of the random variable is only dependent on the distance between two points and not on the location. Thus, stationarity of difference is similar to the unbiasedness condition. Bias is unlike error, which can be defined as the difference between a true value and the prediction, model-based value in that it depends on a statistical model fitted to an ensemble of data values. Bias is most often predicted by the mean error, thus it is an expectation of over- or under- prediction based on some statistical model.

The main gain of probabilistic models is their ability to set the estimation error to zero. The solution derived from the model (attained by the intrinsic hypothesis) is then assumed to apply to reality. This means that, once structural effects have been taken in account, the remaining variation is homogeneous in its variation so that differences between sites are merely a function of the distance between them. For a given distance h, the variance of the random component of $Z(x)$ equals twice the semivariance.

$$\text{var}\left[\varepsilon'(\vec{x}) - \varepsilon'(\vec{x}+\vec{h})\right] = 2\gamma\left(\vec{h}\right) \tag{3.4-6}$$

If the conditions of the intrinsic hypothesis are fulfilled, the semivariance can be estimated from sample data.

$$\hat{\gamma}\left(\vec{h}\right) = \frac{1}{2n}\sum_{i=1}^{n}\left\{z\left(\vec{x}_i\right) - z\left(\vec{x}_i+\vec{h}\right)\right\}^2 \tag{3.4-7}$$

Where n is the number of pairs of observed sample points of attribute z separated by the distance $\vec{h}$.

C.3 Variogram models

Choosing a variogram model is an important step for the application of kriging. This does make kriging more time consuming than common deterministic approaches but, on the other hand, makes it more flexible as well. Basic variogram models can be conveniently divided into two types: those that reach a plateau (sill), often referred to as transition models, and those that do not. Transitive models have a variation of the spatial correlation structure with the lag h. Models not reaching a sill are often used when there is a trend or drift in the data. In the case study described in this manual, only transitive models were tested.

The advantage of a procedure that can assign weights smaller than 0 or greater than 1 (but still respecting the constraint that weights sum to 1) is that it can yield estimates exceeding maximum or under-running the minimum sample value. This behaviour is eligible because it is unlikely that the sample data set includes the most extreme values. The disadvantage of negative weights is the possibility of producing negative estimates, which is completely unrealistic in most cases, e.g. precipitation interpolation, but can be solved by setting such estimates to 0.

There are four different variogram models: the spherical model; exponential model; Gaussian model; and combination model (Figures 3.4-2 and 3.4-3).

The *Spherical model* is perhaps the most commonly used variogram model. Its standardised equation is:

$$\begin{aligned} \gamma_s(h) &= c_o + c_1\left\{1.5\frac{h}{a} - 0.5\left(\frac{h}{a}\right)^3\right\}, \quad for \quad 0 < h \le a \\ &= c_o + c_1 \qquad\qquad\qquad , \quad for \quad h > a \\ \gamma_s(0) &= 0 \end{aligned} \tag{3.4-8}$$

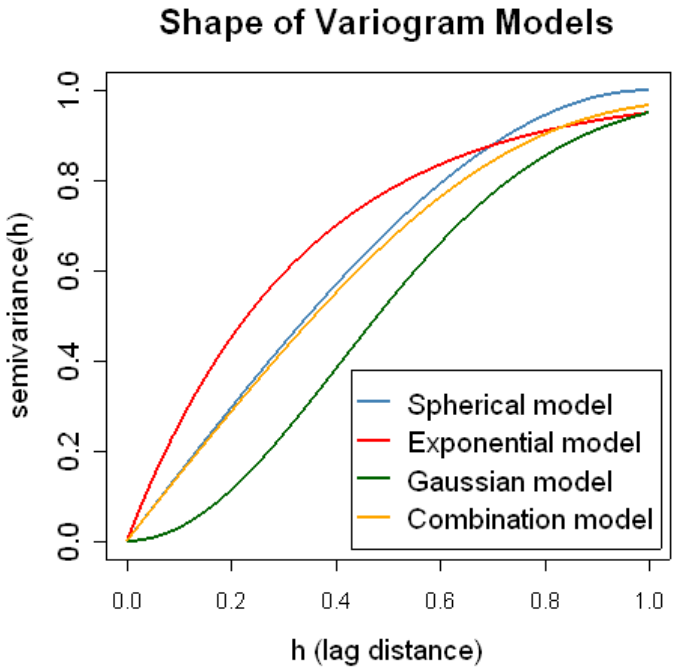

Figure 3.4-2: Shape comparison of the different variogram models. The nugget effect is set to zero for this image.

a is the range, c_o is the nugget effect (noise) and c_o+c_1 is the sill. It has a linear behaviour at small separation distances near the origin but flattens at larger distances and reaches the sill at a. If the nugget variance is important but not too large, and there is a clear range and sill, the spherical model usually fits observed variograms with reasonable accuracy.

The *Exponential model* is another commonly used transition model given by:

$$\gamma_e(h) = c_o + c_1\left\{1 - e^{\left(\frac{-3h}{a}\right)}\right\} \tag{3.4-9}$$

This model reaches its sill asymptotically, but is linear at very short distances to the origin as in the spherical model. However, it rises more steeply and then flattens more gradually. It is usually a good choice if there is a clear nugget and sill, but only a gradual approach to the range.

The *Gaussian model* is a transition model often used to model extremely continuous phenomena. The equation of this model is:

$$\gamma_g(h) = c_o + c_1\left\{1 - e^{\left(\frac{-3h^2}{a^2}\right)}\right\} \tag{3.4-10}$$

As in the exponential model, the Gaussian model reaches the sill asymptotically and the parameter *a* is defined as the practical range or distance at which the variogram value is 95% of the sill. However, its parabolic behaviour near the origin distinguishes it from the exponential model. Samples close to the location of interpolation produce smaller semivariances in the Gaussian model than in the other models. The Gaussian model is indicative of very continuous phenomena so this estimation procedure makes much more use of the closest samples. If a sample falls between a particular sample and the point being estimated, the particular sample will be "screened", resulting in negative stochastical weights. A model with a parabolic behaviour near the origin will cause the screen effect to be much more pronounced. Variogram models with parabolic behaviour near the origin are avoided in practice since the negative weights they may produce tend to make the estimation very erratic.

The *Combination model* is the fourth implemented model. It is a weighted combination of the spherical, exponential and Gaussian model.

$$\gamma(h) = \omega_1\gamma_s(h) + \omega_2\gamma_e(h) + \omega_3\gamma_g(h) \tag{3.4-11}$$

where ω_1, ω_2 and ω_3 are the weights assigned to each model. Near the origin, the combination model is almost equal to the spherical model, although it flattens earlier than this method.

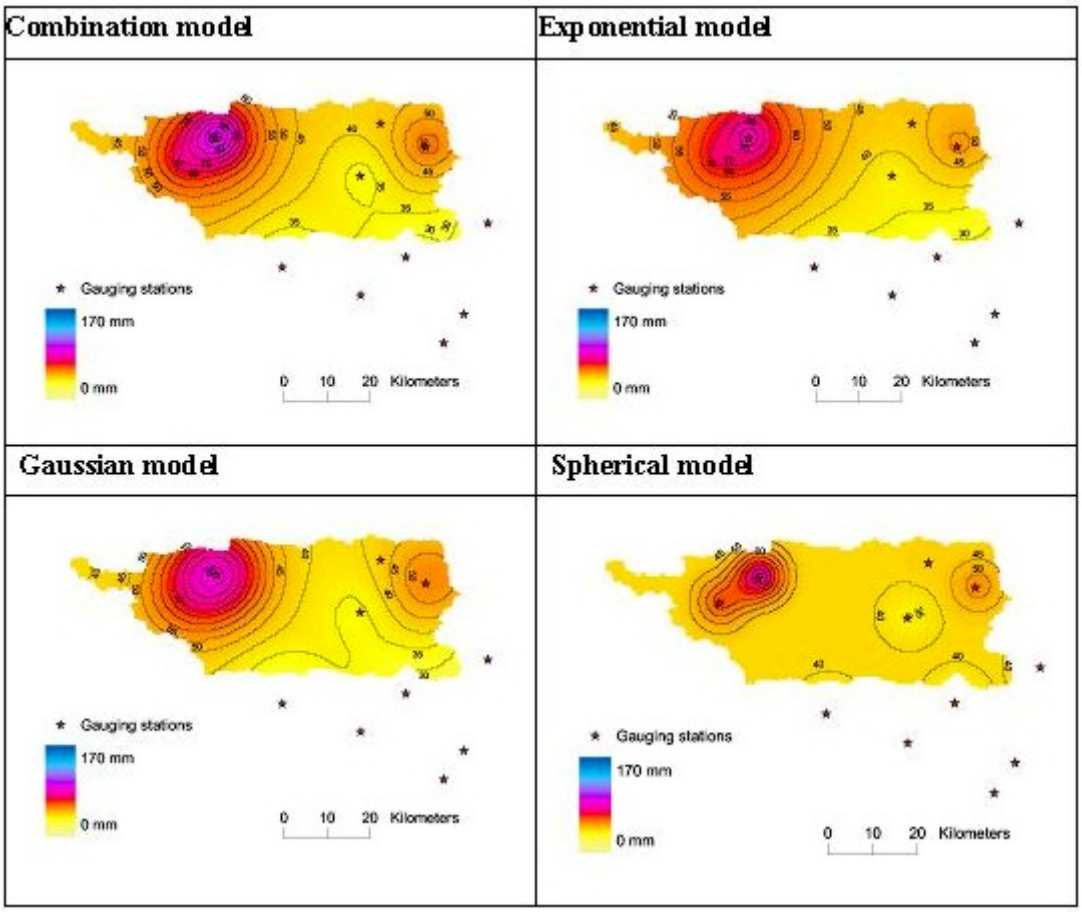

Figure 3.4-3: Resulting map of precipitation interpolation from the 14th May 1990 depicted for a visual comparison of the influence of each variogram model. Data from the Daning River (Sonderegger, 2004).

C.4 Ordinary Kriging (OK)

Ordinary kriging is often associated with the acronym BLUE for "Best Linear Unbiased Estimator". The estimates of ordinary kriging are weighted linear combinations of the available data, thus it is: "linear"; "unbiased", since it attempts to force the mean residual or error equal to 0; and "best" since it aims to minimise the variance of errors, which distinguishes ordinary kriging from most other interpolation methods. To accomplish an estimation error of zero, which leads to the unbiased nature of the interpolation, the weights λ_i for interpolation (according to the IDW interpolation, but using semivariances rather than distances) must sum to one.

$$\hat{z}(x_0) = \sum_{i=1}^{n} \lambda_i \cdot z(x_i) \qquad \text{with} \quad \sum_{i=1}^{n} \lambda_i = 1 \tag{3.4-12}$$

$\hat{z}(x_0)$ is the estimated value at location x_0 and $z(x_i)$ are the measured values of the points considered for the estimated value. The prediction error, minimum variance of $\left[\hat{z}(x_0) - z(x_0)\right]$ or "Kriging variance" is given by

$$\hat{\sigma}_e^2 = \sum_{i=1}^{n} \lambda_i \gamma(x_i, x_0) + \varphi \tag{3.4-13}$$

and is obtained by

$$\sum_{i=1}^{n} \lambda_i \gamma(x_i, x_j) + \phi = \gamma(x_j, x_0) \quad \text{for all } j \tag{3.4-14}$$

where ϕ is the lagrangian multiplicator. The number of points needed to estimate a location *(j)* varies with the local density and arrangement of control and the continuity of the regionalised variable.

For the prediction of $\hat{z}(x_0)$, the variogram model with its parameters first has to be chosen. Then, the weights for interpolation must be calculated following Equation 3.1-15:

$$A^{-1} \cdot b = \begin{bmatrix} \lambda \\ \varphi \end{bmatrix} \tag{3.4-15}$$

b is a vector containing the semivariances between the point to estimate and each data point included for estimation of the attribute value of that point. The matrix *A* contains the semivariances of all data point pairs and λ is the weight vector to be derived.

To find the values of matrix *A* and vector *b*, a distance *h* between the point pairs, for which the semivariances have to be calculated, must be computed and inserted into the variogram model equation. To perform detrended Ordinary Kriging, it is first checked whether precipitation was registered at any station during the time step to be interpolated. If the first condition is fulfilled, an EDR is conducted. The variance correlation rate (R^2) for the EDR has to exceed a minimum correlation rate (e.g. 0.3) for an elevation dependency to be accepted. By accepting the elevation dependency, the residuals of the regression are interpolated using OK. Otherwise, an OK interpolation without the EDR, thus without a trend, is conducted. By acceptance of the elevation dependency, the EDR map is superposed to the interpolated OK map resulting in the detrended OK map.

C.5 Simple Kriging

Simple Kriging (SK) is based on three assumptions:

1. Observations are a partial realisation of a random function $Z(\vec{x})$
2. The realisation is second order stationary (mean, spatial covariance and semivariance are independent of $\vec{x}$)
3. The mean *m* is known.

This are the same conditions as for OK except that the third condition is more restrictive; in OK, the mean only has to be stationary.

The kriging estimator $\hat{Z}(\vec{x}_0)$ is a weighted average of *k* values at control points $\hat{Z}(\vec{x})$ inside a neighbourhood around the location $\hat{Z}(\vec{x})$ where the estimate is to be made. The SK estimate, which can be derived from the OK estimate, is defined as:

$$\hat{Z}(\vec{x}_0) = m + \sum_{i=1}^{k} \lambda_i \left[Z(\vec{x}_i) - m \right] \tag{3.4-16}$$

The weights λ_i have to be estimated with the requirement that they must result in estimates $\hat{Z}(\vec{x}_0)$ having minimum variance of the errors $\hat{Z}(\vec{x}_0) - Z(\vec{x})$.

Simple kriging should not be used for the estimation of precipitation because of the violation of the third condition, the known mean. The precipitation mean of the gauging stations is an estimate of the mean of the measurements and not a known parameter of the distribution.

D. Detrended Inverse Distance Weighting (DTIDW) and Detrended Kriging (DTKRI)

The residuals (difference between interpolated and observed values for the considered meteorological stations) of the EDR-method can be spatially interpolated with the Inverse Distance Weighting (IDW^{RES}) and/or Kriging (KRI^{RES}) technique. Thus, a map of residuals is obtained. Through the addition of the map interpolated by regression and residuals map, the bias derived by the Elevation Dependent Regression method at the observation points can be accounted and corrected:

$$DTIDW_{(x,y)} = EDR_{(x,y)} + IDW_{(x,y)}^{RES} \quad (3.4\text{-}17)$$

or $$DTKRI_{(x,y)} = EDR_{(x,y)} + KRI_{(x,y)}^{RES}$$

This procedure is called detrended interpolation. The idea of the procedure is to separate the sources of variability into a vertical (elevation) component and a horizontal (spatial) component (Garen and Marks, 2001; Susong et al., 1999).

E. Laps Rate IDW (LIDW) and Laps Rate Kriging (LKRI)

From the Laps Rate Method, the temperature data at the stations are transformed applying a constant trend dT dh^{-1} (about -0.007 K m^{-1}). Data are reduced to sea level values. The new data are then spatially interpolated by IDW or Kriging and are then reprojected at the elevation of the grid points by using the same laps rate dT dh^{-1}.

$$LAPS_i = T_i + dT/dh \cdot (0 - H_i)$$

$$LIDW_{(x,y)} = IDW_{(x,y)}^{LAPS} + dT/dh \cdot DHM_{(x,y)} \quad (3.4\text{-}18)$$

or $$LKRI_{(x,y)} = KRI_{(x,y)}^{LAPS} + dT/dh \cdot DHM_{(x,y)}$$

To adopt these interpolation methods, it is imperative to know the northing and easting (y and x co-ordinates) and the elevation (H_i) of all available meteorological stations. A reliable digital elevation model (DHM) of the investigated domain is also essential.

3.5.1 Meteorological zones

The spatially interpolated meteorological information required for driving PREVAH is averaged for so called meteorological sub-units.

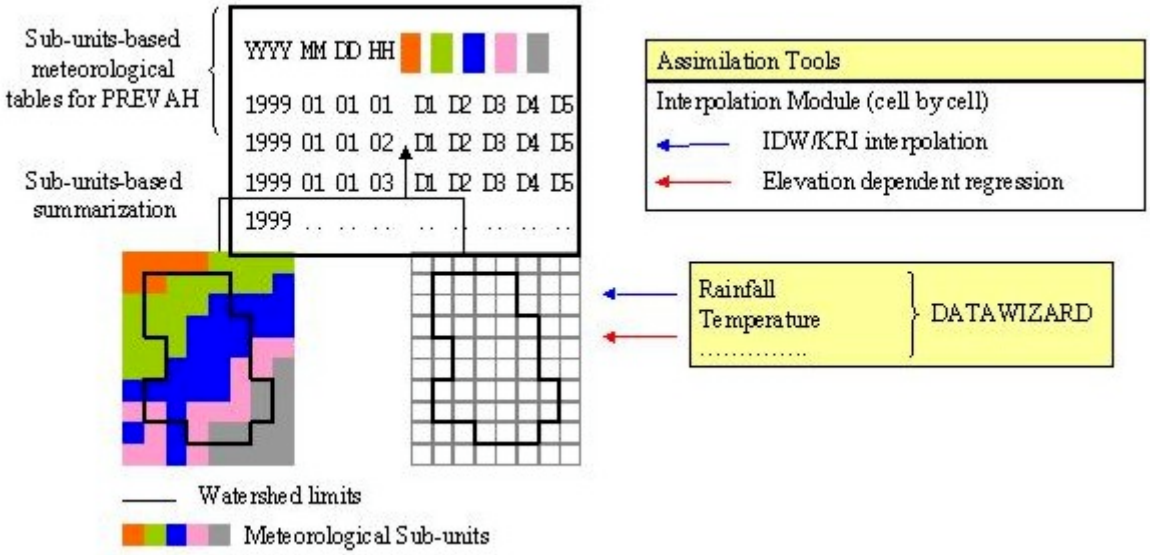

Figure 3.5-1: Assimilation of meteorological information for PREVAH using the interpolation module dtidw.exe.

Output tables for PREVAH:

Figure 3.5-1 shows the concept of averaging the interpolated meteorological fields for so called *meteorological sub-units*. Meteorological sub-units can be defined through WINHRU (see separate documentation).

A table is written for each year and variable.

We recommend the following rules for the definition of meteorological zones:

Watershed Area	First GRID	Second GRID
< 100 km^2	Elevation Zones	None
100 km^2 < 300 km^2	1st Order Streams	Elevation Zones
300 km^2 < 1000 km^2	2nd Order Streams	Elevation Zones
≥ 3000 km^2	4th Order Streams	Elevation Zones

The meteorological file for PREVAH is formatted as follows:

```
Meteorological file for PREVAH
YYYY MM DD HH     17     18     19     20     21     22     23     24     25     26     27     28     29     30     31     32      0
YYYY MM DD HH 0.0028 0.0253 0.0428 0.0679 0.0672 0.0773 0.0884 0.1151 0.1308 0.1381 0.1068 0.0642 0.0430 0.0242 0.0055 0.0005 1.0000
2000  1  1  1   0.00   0.00   0.00   0.00   0.00   0.00   0.00   0.00   0.00   0.00   0.00   0.00   0.00   0.00   0.00   0.00   0.00
2000  1  1  2   0.11   0.11   0.12   0.13   0.14   0.15   0.16   0.17   0.18   0.19   0.20   0.21   0.21   0.22   0.23   0.24   0.17
2000  1  1  3   0.02   0.03   0.05   0.07   0.08   0.10   0.12   0.14   0.16   0.17   0.19   0.21   0.23   0.25   0.26   0.28   0.14
2000  1  1  4   0.10   0.10   0.10   0.10   0.10   0.10   0.10   0.10   0.10   0.10   0.10   0.10   0.10   0.10   0.10   0.10   0.10
2000  1  1  5   0.00   0.00   0.00   0.00   0.00   0.00   0.00   0.00   0.00   0.00   0.00   0.00   0.00   0.00   0.00   0.00   0.00
2000  1  1  6   0.00   0.00   0.00   0.00   0.00   0.00   0.00   0.00   0.00   0.00   0.00   0.00   0.00   0.00   0.00   0.00   0.00
2000  1  1  7   0.00   0.00   0.00   0.00   0.00   0.00   0.00   0.00   0.00   0.00   0.00   0.00   0.00   0.00   0.00   0.00   0.00
2000  1  1  8   0.00   0.00   0.00   0.00   0.00   0.00   0.00   0.00   0.00   0.00   0.00   0.00   0.00   0.00   0.00   0.00   0.00
2000  1  1  9   0.00   0.00   0.00   0.00   0.00   0.00   0.00   0.00   0.00   0.00   0.00   0.00   0.00   0.00   0.00   0.00   0.00
2000  1  1 10   0.00   0.00   0.00   0.00   0.00   0.00   0.00   0.00   0.00   0.00   0.00   0.00   0.00   0.00   0.00   0.00   0.00
2000  1  1 11   0.00   0.00   0.00   0.00   0.00   0.00   0.00   0.00   0.00   0.00   0.00   0.00   0.00   0.00   0.00   0.00   0.00
2000  1  1 12   0.00   0.00   0.00   0.00   0.00   0.00   0.00   0.00   0.00   0.00   0.00   0.00   0.00   0.00   0.00   0.00   0.00
2000  1  1 13   0.00   0.00   0.00   0.00   0.00   0.00   0.00   0.00   0.00   0.00   0.00   0.00   0.00   0.00   0.00   0.00   0.00
2000  1  1 14   0.00   0.00   0.00   0.00   0.00   0.00   0.00   0.00   0.00   0.00   0.00   0.00   0.00   0.00   0.00   0.00   0.00
2000  1  1 15   0.00   0.00   0.00   0.00   0.00   0.00   0.00   0.00   0.00   0.00   0.00   0.00   0.00   0.00   0.00   0.00   0.00
2000  1  1 16   0.00   0.00   0.00   0.00   0.00   0.00   0.00   0.00   0.00   0.00   0.00   0.00   0.00   0.00   0.00   0.00   0.00
2000  1  1 17   0.00   0.00   0.00   0.00   0.00   0.00   0.00   0.00   0.00   0.00   0.00   0.00   0.00   0.00   0.00   0.00   0.00
2000  1  1 18   0.00   0.00   0.00   0.00   0.00   0.00   0.00   0.00   0.00   0.00   0.00   0.00   0.00   0.00   0.00   0.00   0.00
2000  1  1 19   0.00   0.00   0.00   0.00   0.00   0.00   0.00   0.00   0.00   0.00   0.00   0.00   0.00   0.00   0.00   0.00   0.00
2000  1  1 20   0.08   0.08   0.10   0.11   0.12   0.13   0.14   0.15   0.16   0.16   0.17   0.18   0.19   0.20   0.21   0.22   0.15
2000  1  1 21   0.29   0.28   0.27   0.27   0.26   0.24   0.22   0.21   0.20   0.18   0.17   0.16   0.15   0.13   0.11   0.11   0.21
2000  1  1 22   0.49   0.49   0.51   0.52   0.52   0.51   0.50   0.50   0.50   0.49   0.49   0.49   0.50   0.49   0.48   0.49   0.50
2000  1  1 23   0.14   0.17   0.22   0.26   0.31   0.35   0.40   0.44   0.49   0.53   0.58   0.62   0.67   0.71   0.76   0.79   0.46
2000  1  1 24   0.00   0.00   0.00   0.00   0.00   0.00   0.00   0.00   0.00   0.00   0.00   0.00   0.00   0.00   0.00   0.00   0.00
2000  1  2  1   0.00   0.00   0.00   0.00   0.00   0.00   0.00   0.00   0.00   0.00   0.00   0.00   0.00   0.00   0.00   0.00   0.00
```

First header: Title

Second header: YYYY_MM_DD HH followed by the ID of the meteorological sub-unit found in the defined GRID. The last ID ("0") is the average for the entire catchment.

Third header: YYYY_MM_DD HH followed by the relative portion of each meteorological zone.

Precipitation correction and adjustment

After interpolation of the meteorological variables, PREVAH offers a gauge error correction and water balance adjustment for the precipitation data.

Firstly, a gauge error correction may be applied to the interpolated precipitation data. It is calculated for snow and rain separately, using the interpolated wind speed:

$$PR_{korr} = PR_{akt} \cdot \left[1 + 0.07 \cdot \ln\left(v_W + 1\right)\right]$$
$$PS_{korr} = PS_{akt} \cdot \left[1 + 0.20 \cdot \ln\left(v_W + 1\right)\right] \quad (3.5\text{-}1)$$

with

PR_{akt}, PS_{akt}	gauged amount of snow or rain [mm h^{-1}]
PR_{korr}, PS_{korr}	corrected amount of snow or rain [mm h^{-1}]
vW	wind speed [m s^{-1}]

Regional differences in the gauging conditions are considered with the help of wind speed and the distinction of the fluid and solid phase of precipitation. Therefore, further spatial differentiation of the correction is not necessary. Figure 3.5-2 shows the correction factors calculated with Equation 3.5-1 and compares it to the approach of Schulla and Jasper (2000) which is used in WaSiM. While Schulla and Jasper also use wind speed, the approach presented here has the advantage that it does not produce unreasonably high correction factors for high wind speeds.

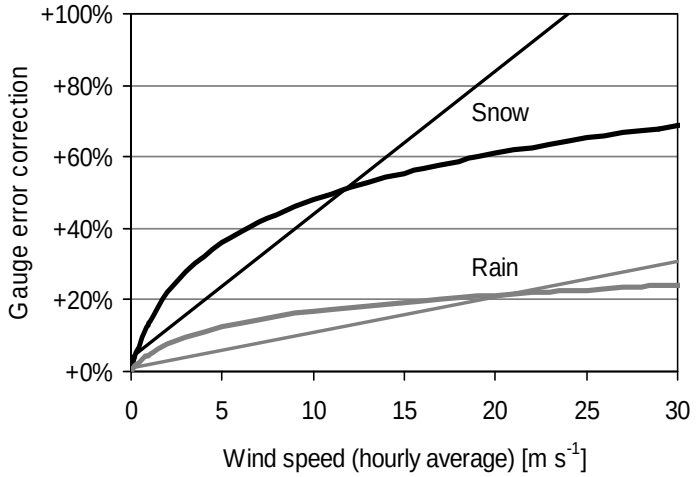

Figure 3.5-2: Wind-dependent gauge error correction for rain and snow as introduced in PREVAH (thick line) compared to correction by Schulla and Jasper (2000) (thin line).

In addition to the gauge error correction, PREVAH also implements a water balance adjustment which can be tuned with the help of two free model parameters (Gurtz et al., 1997a; Pos, 2001):

$$P_{Rain} = P \cdot (1 - p_{Snow}) \cdot (1 + PKOR)$$
$$P_{Snow} = P \cdot p_{Snow} \cdot (1 + SNOKOR) \qquad (3.5\text{-}2)$$

P is the precipitation value obtained from a meteorological tower or provided by the interpolation module of the PREVAH modelling system. P_{Rain} is the adjusted rainfall, P_{Snow} is the adjusted snowfall, p_{Snow} is the snow fraction. *PKOR* and *SNOKOR* are two catchment specific tunable parameters for rainfall and snowfall, respectively. Both parameters have to be determined during the calibration period. This allows for the minimisation of the differences between observed and computed runoff rates and compensates for errors in the measurement, assimilation**,** representativeness and interpolation of precipitation data (Sevruk, 1986). The parameters also indirectly compensate for errors in the estimation of evapotranspiration and snow evaporation. *PKOR* and *SNOKOR* can also be provided as monthly values (Gurtz et al., 2003).

3.5.2 Topography dependent adjustment of radiation and temperature

Calculation of sun co-ordinates, sunset and sunrise, radiation correction

The impacts of topography on radiation and air temperature are considered using the scheme after Oke (1987) (Figure 3.5-3).

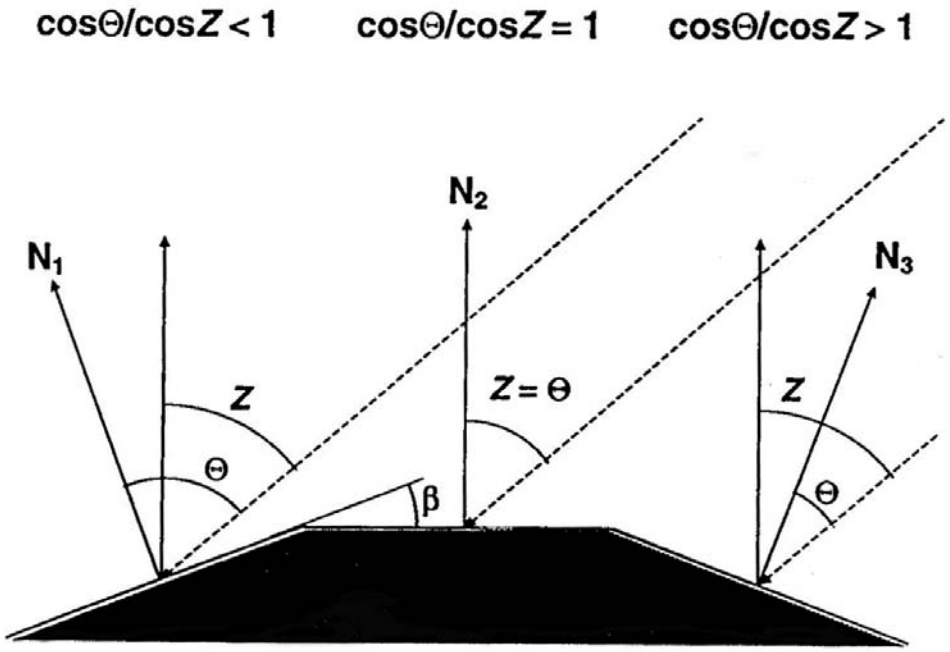

Figure 3.5-3: Schematic representation of topography dependent adjustment of radiation and temperature.

The symbols:

- ϕ geographical latitude (positive north, negative south)
- δ declination of the sun (angle between sun and equatorial plane of the earth)
- Z zenith angle (angle between direction of the sun and local zenith)
- h_s hour angle
- Ω_s azimuth angle (angle between projection of the direction to the sun and north)
- t_J Julian day (1st of January = 1, 31st of December = 365)
- t true local sun time (from average sun time corrected using: Jan: -3.2, Feb: -13.6, Mar: -2.6, Apr: -4.2, May: +2.8, Jun: +2.5, Jul: -3.5, Aug: -6.3, Sep: -0.3, Oct: +10.0, Nov: +16.4, Dec: +11.3 min)
- Θ_s incidence angle between the normal to the local slope and the direction of the sun
- β_t local slope angle
- $\hat{\beta}$ height of the sun above the horizon (as an angle)
- $\hat{\Omega}$ azimuth angle of the local slope (aspect, clockwise from north, i.e. 0 to 359)

The equations for calculating zenith and azimuth angles are given by:

$$\cos Z = \sin\varphi\sin\delta + \cos\varphi\cos\delta\cosh_s = \sin\beta_t \tag{3.5-3}$$

$$\cos\Omega_s = \left(\sin\delta\cos\varphi - \cos\delta\sin\varphi\cosh\right)/\sin Z \tag{3.5-4}$$

$$\delta = -23.4\cdot\cos\left[360\left(t_J + 10\right)/365\right] \tag{3.5-5}$$

$$h_s = 15\left(12 - t\right)\ [°] \tag{3.5-6}$$

with
$$\Omega_s = \arccos\left(\cos\Omega\right) \qquad (t < 12, h_s > 0)$$
$$\Omega_s = 360° - \arccos\left(\cos\Omega\right) \qquad (t > 12, h_s < 0)$$
$$\Omega_s = 180° \qquad (t = 12, h_s = 0)$$

The relations for calculating sunrise and sunset for use within the evaporation routine are given by:

$$\cos h_s = \frac{\sin\phi \sin\delta}{\cos\phi \cos\delta} \rightarrow h_{sr} = \frac{12}{\pi} \cdot \arccos(\cos h_s) = \frac{12}{\pi} \cdot h_s \text{ and } h_{ss} = 24 - h_{sr} \quad (3.5\text{-}7)$$

with h_{ss} time of sunset [h]
h_{sr} time of sunrise [h]

The incoming clear sky direct short-wave radiation I_{max} on a plain perpendicular to the direction of the sun is estimated using an approach for the atmospheric extinction given by Oke (1987):

$$I_{\max} = I_{tof} \cdot \psi_a^{\frac{p/p_0}{\cos Z}} \text{ [W m}^{-2}\text{]} \quad (3.5\text{-}8)$$

with I_{tof} incoming short-wave radiation at the top of atmosphere [W m^{-2}]
(solar constant ≈ 1368 W m^{-2})
p air pressure at the place of interest [hPa]
p_0 air pressure at sea level (≈ 1013 hPa)
ψ_a transmissivity of the atmosphere [-]

A horizontal plane will then have a normal irradiation I_{norm} given by:

$$I_{norm} = I_{\max} \cdot \cos Z \quad (3.5\text{-}9)$$

This type of irradiation estimation is also used in the evaporation module if no sunshine duration data is available.

The angle between the direction to the sun and the normal to a given grid cell (the incidence angle $\hat{\Theta}$) and, hence, the correction factor for the direct irradiation is given by:

$$\cos\hat{\Theta} = \cos\beta_t \cdot \cos Z + \sin\beta_t \cdot \sin Z \cdot \cos(\Omega_s - \hat{\Omega}) \quad (3.5\text{-}10)$$

For a horizontal plane, the correction is then given by:

$$I_{korr} = I_{norm} \cdot \frac{\cos\hat{\Theta}}{\cos Z} \quad (3.5\text{-}11)$$

This correction factor can only be applied with the following restrictions:

- The sun has to be over the horizon
- The elevation angle of the sun should be greater than 12°, since smaller angles result in the optical density of the atmosphere decreasing too quickly (exponent in Equation 3.5-8); if the sun is less than 12° above the horizon, the correction factor is limited to ± 5
- The considered grid cell must not be in the shadow of another cell and $\hat{\Theta} < 90°$ must apply
- The relative sunshine duration has to exceed 0.1, otherwise only diffuse radiation is assumed which will not be corrected

If the model time-step is too large for a reasonable radiation correction (e.g., when using daily time steps), the time step is subdivided into sub-steps. Then, a radiation correction is carried out for each of these sub-steps. The effective correction factor for an entire time interval (time step) is then found as the weighted average of all sub-time-step correction factors. The weights for each sub-step are calculated as the respective normal irradiation divided by the sum of the normal irradiation of all sub-steps within the interval.

$$f_d = \frac{\sum_{i=1}^{n} \frac{\cos\hat{\Theta}_i}{\cos Z_i} I_{norm,i}}{\sum_{i=1}^{n} I_{norm,i}} \tag{3.5-12}$$

with f_d average correction factor for a day [-]
i sub-time-step index 1…n

The correction of the interpolated global radiation itself (as opposed to the calculation of the correction factor) is completed within the evaporation calculation scheme by:

$$RG_{eff} = RG \cdot \left(1 + (1 - cr_0) \cdot SSD \cdot \left[\frac{\cos\hat{\Theta}}{\cos Z} - 1 \right] \right) \tag{3.5-13}$$

with RG_{eff} effective (corrected) global radiation [Wh m^{-2}]
cr_0 empirical factor for consideration of diffuse short-wave radiation (for the Thur-basin around 0.23, see Schulla, 1997)
SSD relative sunshine duration (interpolated, without (!) impacts of topographic shadowing)

Besides the correction of radiation, the azimuth angle Ω_s and the zenith angle Z are used for the analysis of shadowing of cells by other cells.

Modification of temperature

Using the radiation correction term of Equation 3.5-13, it is also possible to modify the air temperature. The parameters needed for this purpose are sunshine duration and an empirical parameter c_t:

$$\begin{aligned}
T_{corr} &= T_{meas} + c_t \cdot SSD \cdot \ln\frac{\cos\hat{\Theta}}{\cos Z} && \text{if} && 0.2 \le \cos\hat{\Theta} \cdot (\cos Z)^{-1} \le 5.0 \\
T_{corr} &= T_{meas} + c_t \cdot SSD \cdot 1.609 && \text{if} && \cos\hat{\Theta} \cdot (\cos Z)^{-1} > 5.0 \\
T_{corr} &= T_{meas} - c_t \cdot SSD \cdot 1.609 && \text{if} && \cos\hat{\Theta} \cdot (\cos Z)^{-1} < 0.2
\end{aligned} \tag{3.5-14}$$

Using sunshine duration accounts for the radiation correction factor being valid for clear sky conditions only. On the other hand, differences between cells with varying aspect will become smaller with higher cloudiness (i.e. shorter sunshine duration). If the sky is fully clouded, no temperature modification is completed. The value of c_t should be calibrated or taken from well-established temperature measurements on plots with varying aspect. Usually, c_t should be less than 5 K.

4. Theoretical basis of PREVAH

4.1 General notes on modelling hydrological processes and systems

A model is a simplified representation of a real system, the corresponding simulation is a, more or less, accurate representation of a number of processes which run in a model. A model can be characterised as follows:

- Representation characteristics: Models as a representation of a natural system can show different grades of adaptation to this system, depending on the stage of system research and the necessity and possibility of a complete representation.
- Shortening and simplification characteristics: Models only include the parts of a natural system which are relevant to the solution of a given problem. Therefore, the model structure is strongly influenced by the goal of the modelling.
- Subject characteristics: The representations of processes are only valid for a defined subject and are limitated to certain operations during a given time period.

To model a river stream system, the following hydrological processes need to be represented with more or less accuracy, depending on the goal of the model:

Atmosphere:

- Correct spatial and temporal estimation of the actual precipitation and other meteorological input variables
- Acquisition of input data necessary to calculate evapotranspiration
- Separation of precipitation into rain and snow
- Correct estimation of snowmelt and icemelt

Land surface: The interception storage, which is provided by the vegetation, needs to be modelled as the first influencing factor. The fraction of precipitation which exceeds this storage reaches the soil surface. Depending on the characteristic catchment area and the moisture-state of the area, this fraction can be assigned to:

- Direct infiltration into the soil
- More or less delayed runoff to the stream network
- Temporary storage on the land surface (swale storage)
- Delayed infiltration into the soil
- Evaporation from the land surface

Ventilated soil zone: The part of the precipitation that infiltrates directly or is delayed to the soil can:

- Flow directly below the soil surface (through the top soil layer) to a river channel (direct or quick interflow)
- Be delayed through the top soil layer to a river channel (delayed interflow)
- Be stored for a shorter or longer time in the ventilated soil zone
- Percolate in the groundwater zone (following gravity)
- Be taken out from the soil through evapotranspiration

Groundwater zone: The water which reaches the groundwater zone can:

- Runoff more or less delayed to the stream network (baseflow)
- Be stored for a longer time in the groundwater zone
- Return to the ventilated soil zone through capillary rise
- Percolate to deep, inactive soil zones
- Be transpired through plants, which feed on groundwater
- Be extracted by humans for various purposes

Stream network: The land surface runoff including glacier runoff, direct or delayed interflow, runoff from groundwater and precipitation that falls directly on the water surface flows through the river bed to the runoff profile of the catchment, whereby the water is temporally stored in the river bed, depending on the river bed characteristics and water level. Through this, the temporal distribution of the runoff as well as the hydrograph is changed.

Additionally, the following can be considered in a model:

- Regulated and non-regulated storage systems
- Dam influences
- Spacious irrigation and drainage
- External in- and outflow to ground and surface water
- Influence of karsts
- Runoff lags due to the utilisation of water

4.2 Interception

4.2.1 Definitions

Interception of precipitation, often called canopy storage in forested environments, plays an important role in calculating water balances (hydrology) and energy budgets (boundary layer climatology). With leaves and woody structures, vegetation modifies the intensity and distribution of precipitation falling through. Interception is technically defined as the plant canopy capturing precipitation and subsequently returning it to the atmosphere through evaporation or sublimation and is the most obvious effect plants have on falling precipitation (Figure 4.2-1). Interception is usually determined by subtracting throughfall from total precipitation input (Gash et al., 1980).

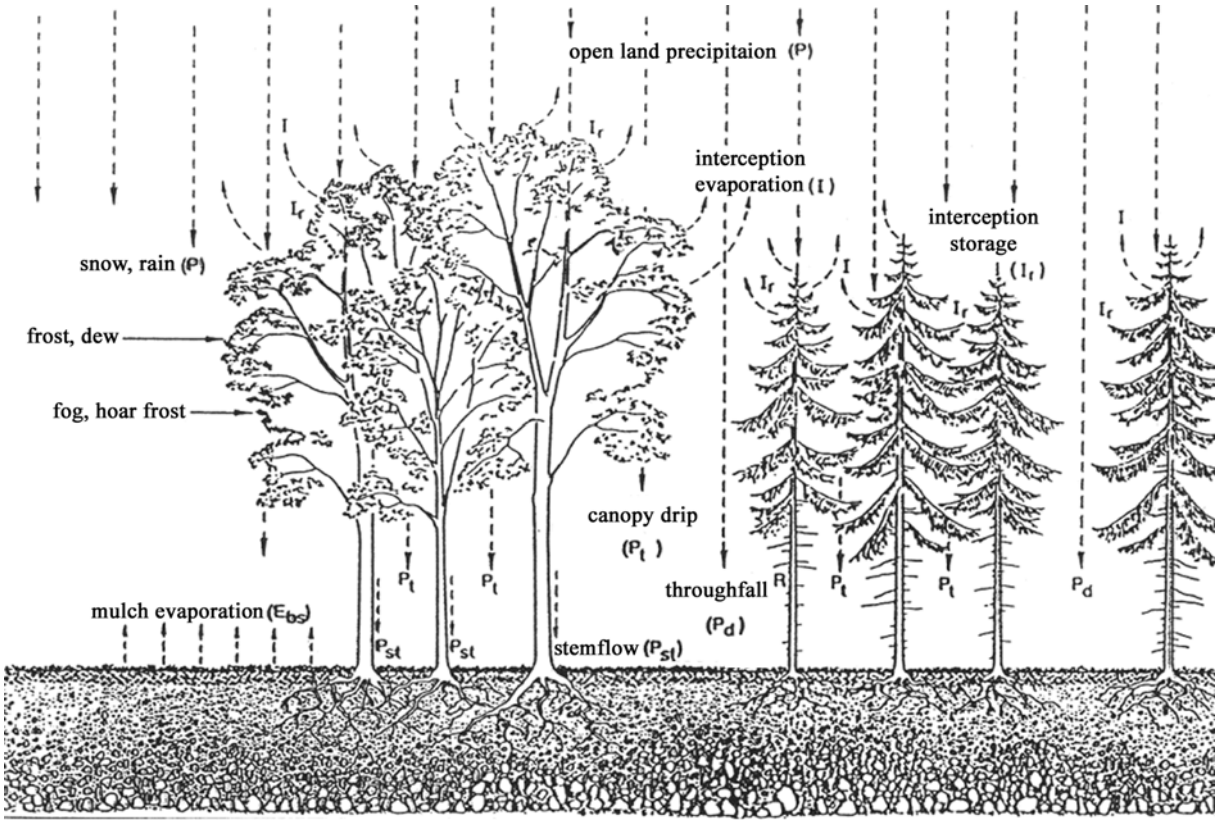

Figure 4.2-1: Schematic of interception for vegetation covered land surface.

The balanced equation from Figure 4.2-1 is

$$P_b = P_d + P_t + P_{St} = P - EI - \Delta SI \text{ [mm]} \quad (4.2\text{-}1)$$

where P_d is the throughfall, P_t the canopy drip, P_{St} the stemflow, P the open land precipitation, EI the interception evaporation and ΔSI the interception storage change. Vegetation can intercept up to 50 % of the rain that falls on its leaves. The leaves of deciduous trees commonly intercept 20 to 30 % of the falling rain. Water dripping off the leaves to the ground surface is technically called leaf or canopy drip.

4.2.2 PREVAH's interception module

The interception model implemented in PREVAH considers variations in interception storage capacity as a function of the vegetation type. Evaporation of intercepted water occurs from vegetated surfaces at the potential rate as long as the reservoir contains sufficient humidity. The surface depression storage capacity of rocky soils and urban areas is also defined for the calculation of direct evaporation.

To conceptualise the process of canopy interception, a simple bucket approach is used. A maximal interception storage capacity SI_{MAX} [mm] is assigned to each class of vegetation and may be set to vary monthly (Gurtz et al., 1997a). The filling of the interception storage SI [mm] is computed as proposed by Menzel (1997) using the actual storage content SI_A:

$$SI(t) = SI_A(t - \Delta t) + (SI_{MAX} - SI_A(t - \Delta t)) \cdot \left(1 - e^{-cPI(t)}\right) \text{ [mm]} \quad (4.2\text{-}2a)$$

$$c = SI_{MAX}^{-1} \text{ [mm}^{-1}\text{]} \quad (4.2\text{-}2b)$$

where t is the computation time, ΔT is the calculation time step and PI is the intensity of precipitation [mm] for the current time step. The consumption or emptying of SI occurs through interception evaporation:

$$SI_E = SI(t) - EI_{\Delta t} \quad (4.2\text{-}3)$$

The interception evaporation *EI* depends on the interception storage filling state *SI*, potential interception evaporation intensity ETP_{SI} and degree of vegetation coverage *VBG*. During the time period ΔT, it is calculated in the following way:

$$EI_{\Delta T} = ETP_{SI} \cdot \Delta T \cdot VBG \quad \text{if } (ETP_{SI} \cdot \Delta T \cdot VBG) \leq SI(t)$$

$$EI_{\Delta T} = SI \quad \text{if } (ETP_{SI} \cdot \Delta T \cdot VBG) > SI(t) \qquad (4.2\text{-}4)$$

$$EI_{\Delta T} = 0 \quad \text{if } SI(t) = 0$$

using: SI_A = interception storage at the beginning of the time interval [mm]
SI_E = interception storage at the end of the time interval [mm]
SI_{max} = interception storage capacity [mm]
PI = precipitation intensity during the time interval [mm h^{-1}]
ΔT = time interval [h]
VBG = vegetation cover grade ($0 \leq VBG \leq 1$)
ETP_{SI} = potential interception evaporation [mm h^{-1}]. It is assumed that ETP_{SI} is equal to the calculated potential evapotranspiration *ETP*.

4.3 Snow and glacier melt

4.3.1 Snow accumulation

The process of snow accumulation and distribution, which involves a variety of meteorological and topographical interactions in a basin during the winter accumulation period, is much more complex than a rain-only situation, since temperature and elevation play a prominent role in determining whether precipitation falls as rain or snow.

In the middle latitudes, precipitation usually falls as a result of the colloidal instability of a mixed water-ice cloud at temperatures below 0 °C. Winter precipitation begins as snow crystals in subfreezing portions of clouds. As the snowflakes fall through the atmosphere, they later melt into raindrops when falling through warmer air at lower elevations. The melting-level air temperature for snowflakes falling through the atmosphere varies from 0 to 4 °C, but it is usually about 1–2 °C. On the Earth's surface, accordingly, snow falls at elevations above the melting level temperature, while rain falls at elevations below the melting level temperature.

For modelling, the separation between snow and rain is realised as follows: the type of precipitation is estimated for each grid cell using the interpolated air temperature in the given time step. If the interpolated air temperature at 2 meters height T_a [°C] is lower than a calibrated threshold temperature T_{GR}, the phase of precipitation is solid. Otherwise, the phase of precipitation is liquid. A transition parameter (T_{TRANS}) defines the air temperature range where the phase of precipitation is considered a mixture of rain and snow. The snow fraction (p_{snow}) is given by (cf. Figure 4.3-1):

$$p_{Snow} = \frac{T_{R/S} + T_{trans} - T}{2 \cdot T_{trans}} \text{ for } (T_{R/S} - T_{trans}) < T < (T_{R/S} + T_{trans}) \qquad (4.3\text{-}1)$$

with p_{snow} fraction of snow to the total precipitation (0..1)
T air temperature [°C]
$T_{R/S}$ temperature at which 50 % of precipitation is falling as snow [°C]
T_{trans} half of the temperature-transition range from snow to rain [°C]

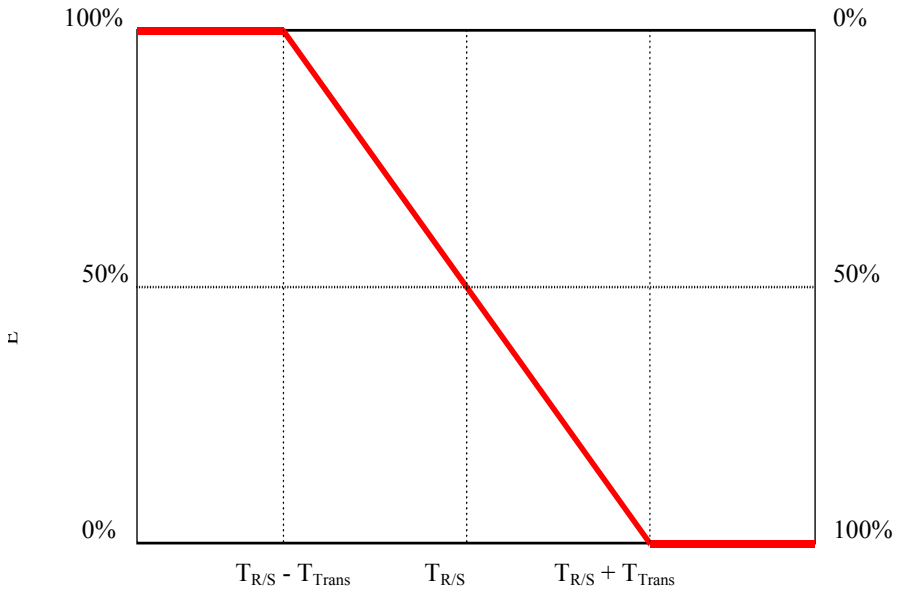

Figure 4.3-1: Separation of precipitation into snow and/or rain depending on temperature.

4.3.2 Snow melt

For the calculation of processes of snow melt, different approaches of different complexity can be used in the PREVAH model.

The Positive Degree-Day Index (PDDI): This classical temperature-index method (Hock, 2003) requires only the availability of interpolated temperature data. If T is below a threshold temperature for snowmelt (T_0), then the melt rate (M) is zero. If T exceeds T_0, then the melt rate is calculated. The temperature dependent melt factor (c_0) can be defined by a sinus shaped function of the threshold values between the annual maximum (set for June 21st) and minimum values (December 21st). In this differentiation, the seasonal variation of the solar radiation is taken into account (Braun, 1985).

$$M = c_0 \cdot (T - T_0) \cdot \frac{\Delta t}{24} \text{ for } T > T_0, \text{ else } M = 0 \qquad (4.3\text{-}2)$$

with M melting rate [mm Δt^{-1}]
c_0 temperature dependent melt factor [mm °C^{-1} d^{-1}]
T air temperature, using modification after Equation (4.3-1) [°C]
T_0 temperature at the beginning of snowmelt [°C]
Δt time step [h]

The temperature-wind-index-approach additionally takes a wind dependent melt factor and the wind speed into account:

$$M = (c_1 + c_2 \cdot u) \cdot (T - T_0) \cdot \frac{\Delta t}{24} \text{ for } T > T_{0,m}, \text{ else } M = 0 \qquad (4.3\text{-}3)$$

with M melt rate [mm DT^{-1}]
c_1 temperature dependent melt factor [mm °C^{-1} d^{-1}]
c_2 wind dependent melt factor [mm (°C m s^{-1} d)$^{-1}$]
u wind speed [m s^{-1}]
T air temperature, using modifications after Equation (4.3-1)
T_0 threshold temperature at the beginning of snow melt [°C]
Δt time step [h]

The Combination approach (COMB): Anderson (1973) extended the PDDI method to introduce a combination of radiation melt for dry periods and advection melt for wet days. Radiation melt occurs when the melt is dominated by radiation energy. This occurs when the precipitation is less than the threshold intensity. In this case, snowmelt is calculated using Equation (4.3-2). Advection melt occurs when rainfall exceeds the threshold intensity. In this case, a simple empirical parameterisation of the energy balance, Equations (4.3-4 and 4.3-5), is applied for the computation of snowmelt (Braun, 1985). The total snowmelt M is the sum of the melt rates given by long wave radiation (M_R), sensible heat flux (M_S), latent heat flux (M_L) and precipitation (M_P). Melt is calculated only at air temperatures above the threshold temperature T_0. For time steps with precipitation ($P \geq 2$ mm d^{-1}), melt is composed of radiation melt, melt from sensible heat, melt from latent heat, and melt from energy import from precipitation:

$$M = (M_R + M_S + M_E + M_P) \cdot \frac{\Delta t}{24} \tag{4.3-4}$$

with M_R radiation melt [mm]
M_S melt by sensible heat [mm]
M_E melt by latent heat [mm]
M_P melt by import of energy by precipitation [mm]
Δt time step [h]

The melt fractions in Equation (4.3-4) are parameterised by:

$$\begin{aligned} M_R &= 1.2 \cdot T \\ M_S &= (c_1 + c_2 \cdot u) \cdot (T - T_0) \\ M_E &= (c_1 + c_2 \cdot u) \cdot (e_s - 6.11)/\gamma \\ M_P &= 0.0125 \cdot P \cdot T \end{aligned} \tag{4.3-5}$$

with T air temperature [°C]
T_0 threshold temperature for melt [°C]
c_1 temperature dependent melt factor [mm (°C d)$^{-1}$]
c_2 wind dependent melt factor [mm (°C m s^{-1} d)$^{-1}$]
u wind speed [m s^{-1}]
γ psychrometric constant [hPa K^{-1}]
e_s saturation vapour pressure at air temperature T [hPa]
(extended approach after Braun, 1985: observed vapour pressure e)
P precipitation [mm]

Storage and refreezing of liquid water in snow cover

The water equivalent of snow cover *SSO* is subdivided into a snow and water fraction. A coefficient *CWL* is used to control the maximum capacity of water storage as a fraction of the total storage (usually around 10 % of the water equivalent). The effective melt is the amount of water exceeding the water holding capacity, where rain and melt are superposed prior to this calculation. The capillary forces of snow cover can hold and store fluid water against gravity. This occurs if rain falls onto snow and infiltrates, or in the case of a positive radiation balance and positive heat flux, which causes melting in the snow cover. The maximal water storage capacity of snow is described by:

$$SLIQ_{\max} = CWL \cdot SSO \tag{4.3-6}$$

using: $SLIQ_{max}$ maximum amount of fluid water which can be held against gravity [mm]
CWL water storage ability [as a decimal, e.g. 0.1]
SSO snow cover [mm water equivalent]

As long as the water storage capacity of snow is not reached, the melting water and rain, respectively, are restrained by the snow cover.

If the storage for the liquid fraction is not emptied at the beginning of a time step, it is required to calculate a refreezing M_{neg} in cases of temperatures below T_0.

$$M_{neg} = c_{rfr} \cdot RMF \cdot (T - T_0) \cdot \frac{\Delta t}{24} \quad (4.3\text{-}7)$$

with M_{neg} „negative melt" (refreezing water) [mm]
c_{rfr} coefficient for refreezing [-]
RMF seasonally dependent radiation melt coefficient [mm (°C d)$^{-1}$]
T air temperature modified by Equation (4.3-1) [°C]
T_0 threshold temperature for the beginning of snow melt [°C]
Δt time step [h]

After calculating the negative melt, the storages of liquid (S_l) and solid (S_s) fractions on the water equivalent are balanced. The refrozen amount of liquid water is added to the solid fraction and subtracted from the liquid fraction (limited by the amount of water in the liquid fraction storage).

There is the possibility to use a simplified energy balance model for snow melt calculation, which was developed by Strasser et al. (2002) and referred to as ESCIMO. The one-layer snow model ESCIMO (Energy-Balance Snow Cover GIS-Integrated Model) was developed for the hydrological simulation of the Weser catchment in Northern Germany (Strasser and Mauser, 2001). It is designed as a physically-based model for the hourly simulation of the energy balance, water equivalent and melt rate of snow cover. The principle and most influential terms of the energy balance are the short and longwave radiation, and sensible and latent heat fluxes. The energy conducted by solid or liquid precipitation and a constant soil heat flux are also taken into account for the energy balance computation, even if their contribution is negligible. The snow albedo is modelled using a function considering the age and surface temperature of the snow pack (Rohrer, 1994a and 1994b). For each time step, the following scheme is adopted (Abbott et al., 1986a and 1986b): calculation of the energy balance; decision whether the precipitation is solid or liquid; estimation of the water mass and energy budget based on the hypothesis of zero snowmelt at the current time step; comparison of the total available energy of the mass sustained as snow to the total available mass at 273.16 K; calculation of the snowmelt produced by the available excess energy; and a subsequent update of the mass and energy budgets. The number of free parameters is limited to the three. These control the simulation of albedo and are the maximal albedo (ALB_{MAX}) and the parameters determining the ageing of the albedo (A_{POS} for positive and A_{NEG} for negative snow temperature). The mathematical representations of the simulated physical processes as used in ESCIMO are described in Strasser et al. (2002).

4.3.3 Glacier melt and runoff

By storing water seasonally during winter and for up to thousands of years, glaciers regulate streamflow by augmenting inputs when precipitation is low, thereby masking the variability of precipitation inputs and prolonging the melt season into summer.

Because it forms from the metamorphosis of snow, the behaviour of glacier ice deviates from other forms of ice. Melt results from influxes of solar radiation, sensible heat of air and rain, latent heat of condensation (dew and frost) and heat conducted from supraglacial debris (enhanced melt up to a threshold depth of debris; thick deposits insulate the ice).

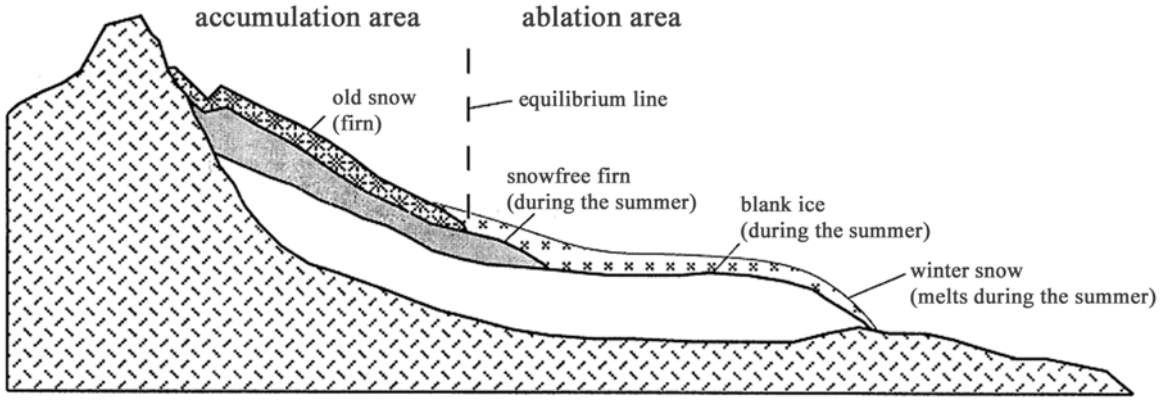

Figure 4.3-2: Longitudinal section of a glacier.

Melt of firn and ice

There are two methods for calculating glacier melt: a classical temperature index method and an extended temperature index method after Hock (1998) which includes information on the global radiation during each time step on each grid cell to modify the melt. The melt after the classical temperature index approach is calculated by:

$$M = \begin{cases} \frac{1}{n} DDF_{snow/firn/ice} \cdot (T - T_0) : & T > T_0 \\ 0 \qquad\qquad\qquad\quad : & T \le T_0 \end{cases} \tag{4.3-8}$$

with
- M melt [mm DT^{-1}]
- n number of time steps per day [d^{-1}]
- DDF 3 degree-day-factors for snow, firn and ice, respectively [mm °C^{-1} d^{-1}]
- T air temperature in a standard elevation of 2 m above land surface [°C]
- T_0 threshold temperature for melt

The melt is calculated for snow, firn and ice separately using specific parameters. If a glacier cell is covered with snow, the melt calculation is completed using the parameters DDF_{snow} and no firn or ice melt is calculated. If the cell is not covered by snow, then the melt calculation is completed using the parameters according to the cell code: DDF_{ice} for ice cells (code 1) or DDF_{firn} for firn cells (code 2). Typically, the relationship $DDF_{ice} > DDF_{firn} > DDF_{snow}$ holds. All three parameters are constant in space and time for the entire model run. The parameter values are ranging from 2 to 10 mm °C^{-1} day^{-1}.

Using the extended melt approach from Hock (1998), the melt of snow, firn, and ice is calculated by:

$$M = \begin{cases} \left(\frac{1}{n} MF + \alpha_{snow/firn/ice} \cdot I_0\right) \cdot (T - T_0) & : \quad T > T_0 \\ 0 & : \quad T \le T_0 \end{cases} \tag{4.3-9}$$

with
- M melt [mm DT^{-1}]
- n number of time steps per day [d^{-1}]
- MF melt factor with identical values for snow, firn and ice (around 2 mm °C^{-1} d^{-1})
- α empirical coefficients for snow and firn (identical, approx. 0.002) and for ice (around 0.001) [mm Wh^{-1} m^2 °C^{-1} day^{-1}]
- I_0 potential direct incoming short-wave radiation (visible incoming sun radiation) for each HRU (depends on aspect and slope angle, time and season, but not on cloudiness) [Wh m^{-2}]
- T air temperature in a standard elevation of 2 m above ground surface [°C]
- T_0 threshold temperature for melt

The correction of the melt factor is completed using the relationship between the observed global radiation at a meteorological station and the theoretical potential global radiation at the same location. This relationship represents the effects of cloudiness multiplied by the potential radiation I_0 on the actual cell. The latter meas-

ure represents the local real global radiation. Since the model uses global radiation interpolated from non-shaded stations, and since it already performs a radiation correction considering local topography, the term $I_0\ G_S\ I_S^{-1}$ is replaced internally by the interpolated global radiation. The actual correction is performed in the evaporation module. However, for using this melt model approach, it is necessary to enable the radiation correction and to use Penman-Monteith, Turc/Ivanov or Wendling evaporation for corrected radiation. Further, it is recommended not to use net radiation instead of global radiation. If no radiation correction is performed, no variations in the melt pattern will be recognisable since only the interpolated radiation is used for scaling the melt. The model stops its execution if no radiation is found during the initialisation.

The parameters α_{ice}, α_{firn}, and α_{snow} are becoming smaller in this order and range between 10^{-4} and $5 \cdot 10^{-3}$ mm Wh^{-1} m^2 $°C^{-1}$ d^{-1}. The radiation is given in [Wh m^2], scaling the small α-values to the order of reasonable degree day factors. Since the product of α and interpolated global radiation is added to the melt factor *MF*, the latter is smaller than the degree day factors in a classical temperature index approach. MF has a value of around 2 mm $°C^{-1}$ d^{-1}.

If a glaciated HRU is coded as ice, but is covered with snow, the current melting is calculated using the parameters for snow. Only in cases of snow free ice area is the melt calculated using the ice parameters.

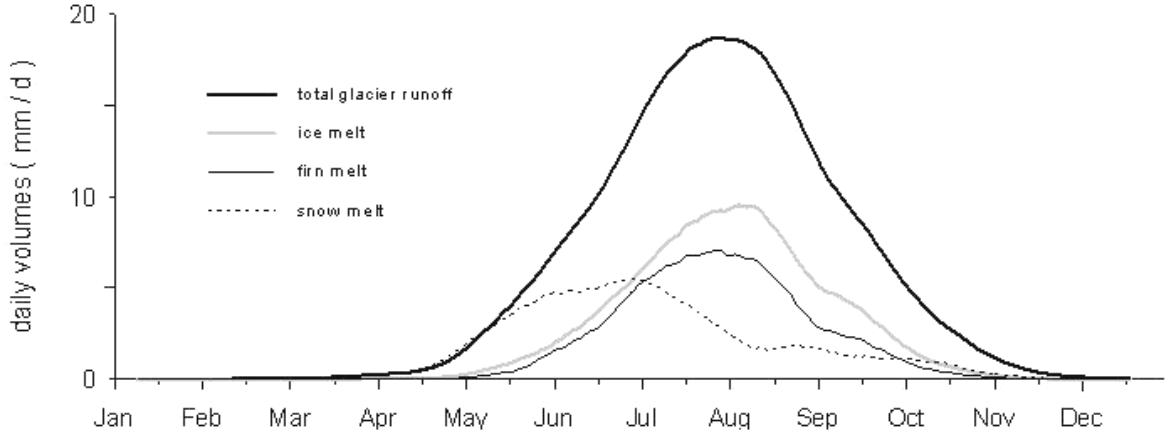

Figure 4.3-3: 21 day moving average of melt components from 1981 to 2000 in the Rhone catchment.

Routing of the different melt components through the glacier

For glaciated sub-basins, there are three melt components calculated following Equations (4.3-8) and (4.3-9), respectively. These components are then delayed and routed to the sub-basin outlet using a set of parallel single linear reservoirs in combination with a translation movement using individual storage and translation times:

- Ice (ablation zone): very short storage and translation times (in the model, k_{ice} of 1 to 10 hours), output is added to the fast runoff component Q0
- Snow on ice (ablation zone): longer storage time (k_{snow} of 10 to 100 h), translation time of about 2 h, output is added to the delayed runoff component Q1
- Firn and snow on firn (accumulation zone): long storage and translation times, (k_{firn} of around 100 to 1000 h) melt water is added to baseflow storage input (i.e. SLZ)

Rainfall falling on the three glacier sections described is treated as melt water and directly enters the respective storages.

For model calibration, it is important to initialise the three parallel reservoirs with matching initial values. If the calibration begins when the total glacier is frozen, e.g. in January, then only the firn reservoir must be initialised with a small initial outflow, the other two reservoirs may be initialised with zero.

The total runoff from the glacier sub-basins is handled in the discharge routing module as the runoff of any other sub-basin.

4.4 Water in the soil-plant-atmosphere system

4.4.1 Characterisation of soil water

The mass and energy exchange between soil, vegetation and atmosphere significantly determines the charge and consumption of the water storage of an area. A positive *DS* (reserve) develops if *P > (ET + R)*, a negative *DS* (consumption) when *P < (ET + R)*. This exchange occurs mainly in the vertical direction, as most of the precipitation is returned to the atmosphere through evapotranspiration, whereby the soil-moisture-zone is the dominant turnover space. This is also shown with the help of the soil column in Figure 4.4-1 where the components and sub-processes of the water cycle in the land phase can be observed. As this is only a section of a catchment area, input and output to the subsystem have to be considered additionally to achieve a closed water balance. Only for the case of negligible horizontal flows, can the water balance be calculated alone from the vertical flows.

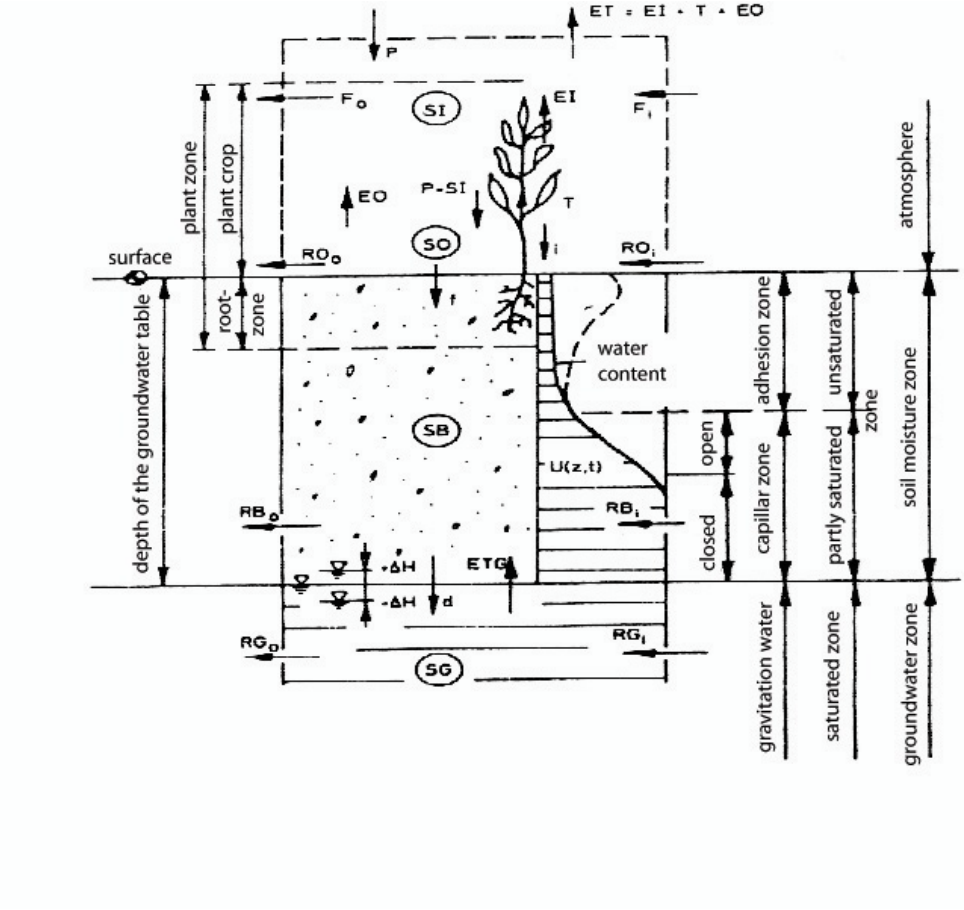

Figure 4.4-1: Schematic representation of the soil-plant-atmosphere system.

The soil-water-budget is determined through three processes: (1) infiltration of water through the surface with the generation of soil moisture, (2) unsaturated water flow through the ventilated soil zone and (3) groundwater flow through saturated granular soil or bedrock. The soil pores in the ventilated and moistened zone may also contain air beneath water. At the groundwater surface, atmospheric pressure is registered, beneath the groundwater layer, pressure rises linearly. Above the groundwater surface, capillary forces may saturate a porous medium to a certain extent. Higher in the soil column, the soil is only temporally saturated after the infiltration of precipitation.

As the hollow space between the soil grains can take up liquid and/or gaseous matter, the soil can store or pass on water. The rate of the storage and conductance ability depends on the volume and size distribution of the hollow spaces, and is thus determined from the grain size and their distribution.

The pore volume (porosity) is defined as:

$$n = \frac{holow\ space\ volume}{total\ volume} \tag{4.4-1}$$

n can be found in the range of 0.25 to 0.75, depending on the soil texture.

The water or moisture content of a soil is defined as**:**

$$\Theta = \frac{water\ volume}{total\ volume} \tag{4.4-2}$$

From the degree of saturation $s = \Theta / n$, we can draw conclusions on the temporal development of the water content.

The field capacity and wither point are characteristic values of the water fixation. The field capacity *FC* represents the amount of water a soil can hold against gravity without influence of the evapotranspiration. It is determined after a longer precipitation period, after the gravity water has largely petered out.

If the water content falls under a certain value, most plants wither irreversibly. This is called the permanent wilting point *WP*.

The absorption and capillary water in the range between *FC* and *WP* can be used from the plants. Therefore the plant usable or plant available field capacity is defined:

$$AFC = FC - WP. \tag{4.4-3}$$

Table 4.4-1: Classification of the plant available field capacity AFC.

AFC-steps	storage capacity [mm]	volume %
very good	> 100	24
good	60 – 100	16
moderate	45 – 60	11
low	30 – 45	8
very low	15 – 30	4.5
extremely low	< 15	1.5
rocky, urban area	0	0

It depends on the vegetation which part of the precipitation reaches the soil surface and which part is held back by interception. Vegetation and soil characteristics are influenced by the infiltration of precipitated water to the soil.

Table 4.4-2: Recommendation for the soil-model-parameters in dependency of the soil type (after Haberlandt, 1989): Porosity n, *field capacity* FC, *wilting point* WP.

soil type		n Vol-.%	FC Vol-.%	WP Vol-.%
sand	S	28 – 35	8 – 15	1 – 7
sand, clayey	Sl	30 – 40	10 – 16	2 – 5
clayey sand	lS	32 – 42	13 – 24	5 – 8
sandy clay	sL	33 – 45	22 – 30	8 – 13
clayey silt	lU	43 – 45	28 – 35	8 – 14
clay	L	35 – 50	20 – 35	12 – 19
silty clay	UL	43 – 46	32 – 43	14 – 20
silt	U	40 – 52	28 – 35	18 – 22
sandy potters's clay	sT	42 – 55	32 – 40	16 – 24
silty potter's clay	uT	49 – 60	37 – 46	18 – 24
potter's clay	T	50 – 65	40 – 55	25 – 35

The plant available soil moisture storage is depleted by evapotranspiration. It is assumed that the maximal content of the soil moisture storage corresponds to the maximum plant available soil moisture SFC_{MAX} [mm]. Such a water content is available for transpiration. The parameterisation of SFC_{MAX} requires the availability to estimate the specific plant AFC [Vol%] and the knowledge of the soil depth T_B [m]. SFC_{MAX} is then parameterised for each vegetated hydrological response unit according to the following equation:

$$SFC_{MAX} = AFC \cdot T_B \cdot 10.0 \tag{4.4-4}$$

Additionally, it is assumed that the soil water is only available up to a depth close to the rooting depth T_{WU} [m]. The rooting depth varies seasonally and according to the land use. To account for capillary rise, an additional depth of 15 cm is included in the parameterisation of the effective soil depth, which is relevant for the parameterisation of the effective SFC_{EFF}:

$$SFC_{\mathrm{EFF}} = AFC \cdot (T_{WU} + 0.15) \cdot 10.0 \tag{4.4-5}$$

It may happen that soils are less deep than the roots. In this case, the available field capacity is limited by $SNFC_{MAX.}$ The actual maximal plant available soil moisture storage $SNFC$ is therefore defined as:

$$SFC = MIN\left[SNFC_{EFF}, SNFC_{MAX}\right] \tag{4.4-6}$$

where $SNFC_{EFF}$ is the effective plant available soil moisture storage.

SFC is parameterised separately for non vegetated surfaces. If no vegetation is present, then soils can be depleted by direct soil evaporation up to a depth of 25 cm:

$$SFC = AFC \cdot 0.25 \cdot 10.0 \tag{4.4-7}$$

Urban areas are an exception to this rule, where values of SFC ranging between 4 and 5 mm are assumed.

4.4.2 Potential evapotranspiration

Plants need water to build up substance and as a dissolver-, transport-, welling- and cooling-resource. Through transpiration, the water vapour transfer to the atmosphere, a steady transport of plant available water from the roots to the leaves is assured. The leaves are specially adapted to the regulation of the gas exchange. The transpiration suction of the leaves is the pushing force of the water transport through the plants. It depends on the suction power gradient between the soil and atmosphere. Therefore, the evapotranspiration is an important factor for the water and energy balance of a land surface.

Definitions

Evapotranspiration is defined as the sum of all processes by which water in the liquid or solid phase at or near the earth's land surface becomes atmospheric water vapour. Evapotranspiration is a combined process of both evaporation from soil and plant surfaces as well as transpiration through plant canopies. Evapotranspiration is responsible for the occurrence of more than 50% of the energy flux from a land surface to the atmosphere, which shows the importance of this variable.

Evaporation occurs from uncovered surfaces (soil-, snow- or ice-evaporation), the precipitation which is restrained in the plant canopy (intercepted evaporation) and from free water surfaces (water evaporation). Evaporation can be defined as the process by which liquid water is converted into a gaseous state. Evaporation may only occur when water is available. It is also required that the humidity of the atmosphere is below the humidity of the evaporating surface (at 100% relative humidity, there is no evaporation). The evaporation process requires large amounts of energy. For example, the evaporation of one gram of water at a temperature of 0° C requires 600 calories of heat energy.

Transpiration is the physiological regulated loss of water vapour to the atmosphere through the stomata of plants and can be regarded as evaporation from the plant's vascular system. The water is absorbed by the roots, rises by capillary action to stomatal cavities in the leaves where it finally evaporates and is diffused through stomata (Greek "stomatos": mouth). Under dry, windy and/or hot and sunny conditions, transpiration may exceed the rate at which water can be supplied from the soil. By closing the stomates, plants prevent water loss, but also restrict access to atmospheric CO_2 for photosynthesis.

The standard rates are defined in the following ways:

– *Potential evaporation* in [mm] is defined as the amount of water which evaporates from an idealised, extensive free water surface under given atmospheric circumstances.

– A reference value for the *potential plant evapotranspiration* in [mm] is defined as the evapotranspiration that occurs from an idealised grassy surface with a vegetation height of 12 cm, an albedo of 0.23 and a surface resistance of 69 s m^{-1}. The latter is a measure for the ability of the atmosphere to remove water from the plant surface through processes of evaporation and transpiration, assuming unlimited water supply and no advection (wind).

The evapotranspiration joins the environmental compartments of air, water, soil and vegetation in multiple ways (cf. Figure 4.4-2)

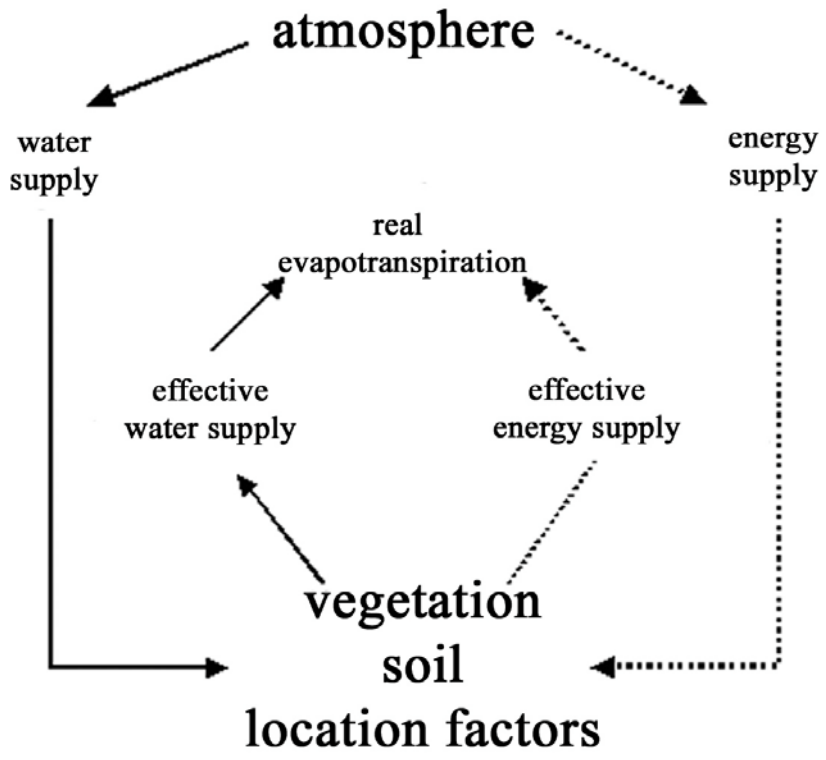

Figure 4.4-2: The evapotranspiration in the complex system atmosphere-plant-soil.

Potential evapotranspiration after Penman (1948) and Penman-Monteith (1975, 1981)

The most widely adopted scheme for the estimation of evapotranspiration in distributed hydrological models relies on the Penman (1948) and Penman-Monteith equation (Monteith, 1975; Menzel, 1997; DVWK, 1996; Gurtz et al., 1997a; Schulla and Jasper, 2000).

The Penman (1948) equation is referred to as

$$ETP = \frac{UFK}{\rho_w L} \quad \frac{\Delta \cdot R_N + \gamma +_a}{\Delta + \gamma} \tag{4.4-8}$$

using

$$E_a = 0.263 \left(0.5 + 0.537\ u\right)\left(e_s\text{-}e\right) \,{}^{L}\!/_{86400} \tag{4.4-9}$$

and the Penman-Monteith (1975, 1981) equation is as follows:

$$ETP = \frac{UFK}{\rho_w L} \quad \frac{\Delta \cdot \left(R_N\text{-}G\right) + \dfrac{\rho\ c_p\ \left(e_s\text{-}e\right)}{r_a}}{\Delta + \gamma\ \left(1 + {}^{r_s}\!/_{r_a}\right)} \tag{4.4-10}$$

where
- ETP potential evapotranspiration [mm d^{-1}]
- E_a aerodynamic term [W m^{-2}], ventilation
- ρ density of dry air [kg m^{-3}]
- ρ_w density of water ≅ 1000 [kg m^{-3}]
- γ psychrometric constant [hPa K^{-1}]
- c_p specific heat of dry air at constant pressure [J kg^{-1} K^{-1}]
- e actual water vapour pressure [hPa]
- e_s saturated vapour pressure at actual temperature [hPa]
- Δ first derivative of the saturated vapour pressure curve (around temperature T) [hPa K^{-1}]
- R_N net radiation [W m^{-2}]

G	ground heat flux [W m^{-2}]
L	latent evaporation heat[J kg^{-1} K^{-1}]
r_a	aerodynamic diffusion resistance [s m^{-1}]
r_s	stomata diffusion resistance, surface resistance [s m^{-1}]
u	wind speed 2 m above ground [m s^{-1}]
UFK	86'400'000 (conversion from m s^{-1} to mm d^{-1})

The latent evaporation heat is a temperature dependent term

$$L = 2501 - 2.37\ T \text{ [kJ kg}^{-1}\text{] using } T = \text{air temperature [°C]} \tag{4.4-11}$$

The saturated vapour pressure e_s can be calculated with the Magnus-equation

$$e_s = 6.11\ \exp\left(\frac{17.3\ T}{237.3 + T}\right) \text{[hPa]} \tag{4.4-12}$$

The actual water vapour pressure e is calculated from the relative humidity U with

$$e = U \cdot e_s \text{ [hPa]} \tag{4.4-13}$$

Δ is the first derivative of the saturated vapour pressure curve around air temperature T (Magnus-equation).

$$s = \frac{\partial e_s}{\partial T} = \frac{4098\ e_s}{(237.3 + T)^2} \text{ [hPa K}^{-1}\text{]} \tag{4.4-14}$$

The term γ is called psychrometric constant and is a function of the air pressure and air temperature.

$$\gamma = \frac{p\ \cdot\ c_p}{m \cdot L} = 0.016286\ \frac{p}{L} \text{[hPa K}^{-1}\text{]} \tag{4.4-15}$$

c_p = specific heat of dry air at constant pressure = 1000 [J kg^{-1} K^{-1}]

m = ratio of the molar masses water vapour to dry air = 0.622 [-]

The air pressure p can be expressed with the barometric height equation.

$$p = 1013\ e^{-\frac{H}{7991+29.33T}} \text{ [hPa] using H = height above sea level [m]} \tag{4.4-16}$$

The air density is estimated as a function of temperature:

$$\rho = 0.349\ \frac{\mathrm{p}}{275\ +\ \mathrm{T}} \text{ [km m}^{-3}\text{]} \tag{4.4-17}$$

The ground heat flux G can be expressed as a fraction of the net radiation (R_N):

$$G = C_R \cdot Rn \text{ [W m}^{-2}\text{]} \tag{4.4-18}$$

C_R = ground factor ≈ 0.3 for urban areas, rocky areas and water
≈ 0.2 for grassy surfaces
≈ (0.3 - 0.03 LAI) for vegetation covered surfaces

LAI = leaf area index

The net radiation is derived from the balanced short-wave (Rsw) and long-wave (Rlw) radiation:

$$Rn = Rsw + Rlw \text{ [W m}^{-2}\text{]} \tag{4.4-19}$$

The balanced short-wave radiation is determined in the following way:

$$Rsw = RG\ (1 - \alpha\ ) \text{ [W m}^{-2}\text{]} \tag{4.4-20}$$

with α = albedo [-] and RG = global radiation [W m^{-2}]

To determine the balanced long-wave radiation, SSD which is the ratio of the measured sunshine duration n to the maximum possible sunshine duration N is needed:

$$SSD = \frac{\text{sunshine duration}}{\text{max. possible sunshine duration}} = \frac{n}{N} \text{ [h h}^{-1}\text{]} \quad (4.4\text{-}21)$$

Following this, f is derived as a factor which considers the reverberation from clouds:

$$f = f(SSD) = (c_0 + (1 - c_0) \cdot SSD) \text{ using } c_0 = 0.23 \text{ for the Thur River catchment} \quad (4.4\text{-}22)$$

and ε is the net emission of the considered surface:

$$\varepsilon = (a_e + b_e \sqrt{e}) \ , \ a_e = 0.48 \ , \ b_e = -0.065 \quad (4.4\text{-}23)$$

Giving the balanced long-wave radiation:

$$Rlw = -f(SSD)\ \varepsilon D (275 + T)^4 \text{ [W m}^{-2}\text{]} \quad (4.4\text{-}24)$$

where σ is the Stefan-Boltzmann constant ($5.68 \cdot 10^{-8}$ W m^{-2} K^{-4}).

The aerodynamic diffusion resistance r_a is:

$$r_a = \frac{4.72 \cdot \left(\ln \frac{z}{z_0} \right)^2}{1 + 0.54u} \text{ [s m}^{-1}\text{]} \quad (4.4\text{-}25)$$

using z height above ground where the wind speed is measured [m]
z_0 aerodynamic roughness-length as a parameter of every form of land use ($z_o \approx 0.125 \cdot (h - d)$ [m])
u wind speed 2 m above ground [m s^{-1}]
h height of vegetation [m]
d height displacement = 0.6 h

The surface resistance r_s is calculated for the daytime as:

$$\frac{1}{r_{sT}} = \frac{(1 - A)}{r_{sc}} + \frac{A}{r_{ss}} \quad (4.4\text{-}26)$$

using r_{sT} minimal surface resistance in daytime [s m^{-1}]
r_{sc} minimal surface resistance of the plants with full water supply and dense cover [s m^{-1}]
r_{ss} surface resistance for uncovered ground ($\approx$ 150 s m^{-1}) [s m^{-1}]
1-A factor to characterise the evaporating vegetation cover
$A = f^{LAI}$ using $f \approx 0.7$

At night, the following equation applies:

$$\frac{1}{r_{sN}} = \frac{LAI}{2500} + \frac{A}{r_{ss}} \quad (4.4\text{-}27)$$

using r_{sN} minimal surface resistance at night [s m^{-1}]

The terms z_0 and LAI (additionally, the degree of vegetation cover and radix depth to calculate the utilisation of the soil moisture) show a vegetation specific annual fluctuation.

The averaged surface resistance r_s throughout a day:

$$\frac{1}{r_s} = \frac{T_L}{24 r_{sT}} + \left(1 - \frac{T_L}{24}\right) \frac{1}{r_{sN}} \quad (4.4\text{-}28)$$

using T_L day length [h]

Potential evapotranspiration after Wendling (1975):

The estimation of potential evapotranspiration (ETP) after Wendling (1975) (see also DVWK, 1996) is applicable only when using a time step of one day or longer. The potential evapotranspiration is then given by:

$$ETP = (RG(1.1 - \alpha) + 93 \cdot f_k) \frac{T + 22}{150(T + 123)} \text{ [mm d}^{-1}\text{]} \quad (4.4\text{-}29)$$

using RG global radiation in [J cm^{-2} d^{-1}], transformed from [W m^{-2}] using the multiplier 8.64
α albedo (0 to 1) [-]
f_k empirical correction value which takes into account the parameters that cannot becollected using the radiation and temperature (coastal 0.6, lowland 1, assessed empirical value for northern Switzerland, compared to Penman-Monteith evapotranspiration: 0.5) [-]
T daily mean value of air temperature [°C]

Potential evapotranspiration after Hamon (1961) (from Federer and Lash, 1983)

$$ETP = 0.1651 \cdot f_i \cdot h_d / 12 \cdot \frac{216.7 \cdot e_s}{T + 273.3} \text{ [mm d}^{-1}\text{]} \quad (4.4\text{-}30)$$

using f_i empirical factor, varies monthly (Table 4.4-2)
h_d day length [h]
e saturated vapour pressure at temperature T [hPa]
T air temperature [°C]

Table 4.4-2: Monthly correction factor f_i for Hamon-evapotranspiration (valid for northern Switzerland).

Month	Jan.	Feb.	Mar.	Apr.	May	Jun.	Jul.	Aug.	Sep.	Oct.	Nov.	Dec.
f_i	0.5	0.6	0.8	1.1	1.2	1.3	1.2	1.1	1.0	0.9	0.7	0.5

Potential evapotranspiration after Turc/Ivanov:

The Turc (1961) scheme (DVWK, 1996) is applied in France and in arid/semi-arid regions when air temperature exceeds 5 °C. For temperatures below 5°C, the scheme after Ivanov (see DVWK, 1996) is used. Both schemes are applicable only using a time step of one day or more.

Turc scheme, for T ≥ 5°C

$$ETP = 0.0031 (RG + 209.4) \frac{T}{T + 15} ETPF_{mon} \text{ [mm d}^{-1}\text{]} \quad (4.4\text{-}30)$$

Ivanov scheme, for T < 5°C

$$ETP = f_k \cdot 0.00006 (T + 25)^2 (100 - RH) \text{ [mm d}^{-1}\text{]} \quad (4.4\text{-}31)$$

using RG global radiation in [J cm^{-2} d^{-1},], calculated from [W m^{-2}] using the multiplier 8.64
$ETPF_{mon}$ empirical factor varies monthly (see Table 4.4-3)
f_k empirical correction value, cf. Wendling (1975)
T daily mean value of air temperature [°C]
RH relative humidity [%]

Table 4.4-3: Empirical coefficient $ETPF_{mon}$ for ETP_{TURC} (valid for central Europe).

Month	Jan.	Feb.	Mar.	Apr.	May	Jun.	Jul.	Aug.	Sep.	Oct.	Nov.	Dec.
$ETPF_{mon}$	0.7	0.85	0.95	1.05	1.25	1.15	1.05	0.95	0.9	0.8	0.75	0.7

In the PREVAH model, the potential evapotranspiration is calculated as daily averaged values in mm d^{-1}. In case of using a computation time step of 1 hour, the daily values are distributed to the hours of the day between the time of sunrise and sunset. The disaggregation of daily evapotranspiration to the different day hours is carried out depending on the cloudiness for cloudy sky (relative sunshine duration smaller than 0.7) and for clear sky using the distribution functions from the following schematic (Figure 4.4-3).

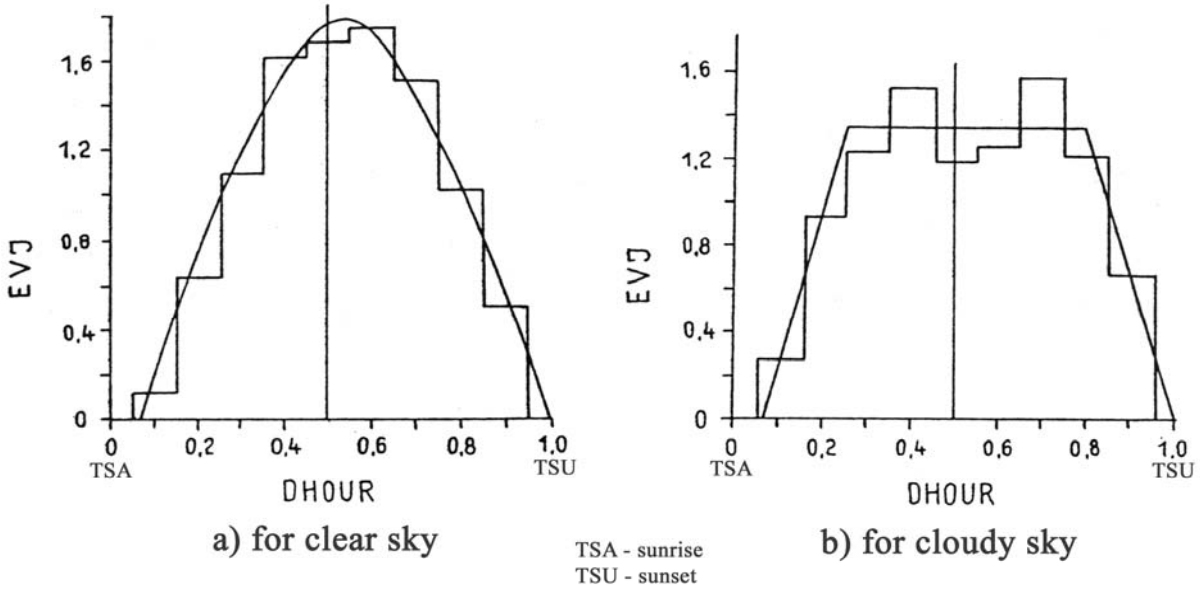

Figure 4.4-3: Mean distribution function of the evapotranspiration during a day.

In the appendix, the equations optionally used in PREVAH to calculate the short and long wave radiation are supplied.

4.4.3 Real evapotranspiration

The real evapotranspiration *ETR* from the soil surface and soil itself is controlled by different factors (Figure 4.4-4): meteorological conditions and the resulting energy supply; water supply at the surface and in the ventilated soil zone; height of the groundwater table; and further location-specific factors (morphology, geology, soil type, cropping, vegetation type and succession).

The direct evaporation from a land surface or the soil is an unproductive process. With sufficient moisture, it is only determined by meteorological conditions. Transpiration through the stomata is a plant physiological process. It is the base of nutrient supply and biomass production, and is therefore called productive evaporation. Plants have the possibility to reduce the transpiration in case of water shortages by closing their stomata. Water for transpiration is supplied through a network of roots of varying length, whose size and position changes with the growth of the plant and moisture supply. For this reason, the distance of the water transport between the soil and roots is significantly shorter in comparison to the evaporation. Further, the available soil space for water supply becomes larger. Beside the transpiration demand, it is the water transport ability which regulates the transpiration rate. Again, the water transport ability depends on the development stage of a plant. Therefore, the transpiration process is a very important part of the highly non linear soil-plant-atmosphere system.

For uncovered soil, only evaporation occurs. For covered soil, the fraction of transpiration rises with increasing vegetation density. Lastly, for a closed vegetation cover, the fraction of evaporation is extremely small.

The modelling of the evapotranspiration always needs to be regarded in close relation to the modelling of soil moisture. It strongly depends on the spatial and temporal process scales considered and the temporal and spatial differentiation of the model input data available.

In practice, the *ETR* is generally calculated on the basis of *ETP* and then adjusted to actual moisture, soil and vegetation conditions at the location of focus.

During dry periods, evapotranspiration is reduced constantly. This is tantamount to an increase in the suction power and, therefore, the binding intensity of the soil water and soil resistance. Real evapotranspiration may drop substantially under the potential evapotranspiration. This process can be described with the extraction- or reduction-function r(Θ):

$$ETR = r\,(\Theta) \cdot ETP \tag{4.4-32}$$

As the function $r(\Theta)$ theoretically can not be differentiated, the chosen function type differs from model to model. To simplify the complicated functions, a stepwise linear characteristic is commonly used.

For covered soil, *rb* applies:

$$\begin{aligned} rb(\Theta) &= 1 && \text{for} \quad \Theta_0 \le \Theta \le \Theta_S \\ rb(\Theta) &= (\Theta - \Theta_{WP})/(\Theta_0 - \Theta_{WP}) && \text{for} \quad \Theta_{WP} \le \Theta < \Theta_0 \\ rb(\Theta) &= 0 && \text{for} \quad \Theta < \Theta_{WP} \\ \Theta_0 &= cu \cdot \Theta_{FC} && cu = 0.4 \text{ to } 0.8 \text{ (parameter)} \end{aligned} \tag{4.4-33}$$

Uncovered soil is characterised by *ru*:

$$\begin{aligned} ru(\Theta) &= 1 && \text{for} \quad \Theta_{FC} \le \Theta \le \Theta_S \\ ru(\Theta) &= (\Theta - \Theta_{WP})/(\Theta_{FC} - \Theta_{WP}) && \text{for } \Theta_{WP} \le \Theta < \Theta_{FC} \\ ru(\Theta) &= 0 && \text{for} \quad \Theta < \Theta_{WP} \end{aligned} \tag{4.4-34}$$

Θ is the volumetric soil moisture content, Θ_S, Θ_{FC}, Θ_{WP} are the values of Θ at saturation, field capacity and wilting point, respectively.

If the fraction of the plant-covered soil is defined with the vegetation-covering-grade *VBG* ($0 \le VBG \le 1$), *ETR*(*b*+*u*) of partly covered soil can be estimated as:

$$ETR(b+u) = ETP\,[(rb(\Theta) \cdot VBG) + (ru(\Theta) \cdot (1 - VBG))] \tag{4.4-35}$$

If potential evapotranspiration is calculated with the Penman-Monteith equation, *ETR* can be estimated either directly over the moisture dependent reduction function or the resistance analogy method, where the stomatal resistance is adjusted depending on the particular soil moisture (for $\Theta \le \Theta_0$).

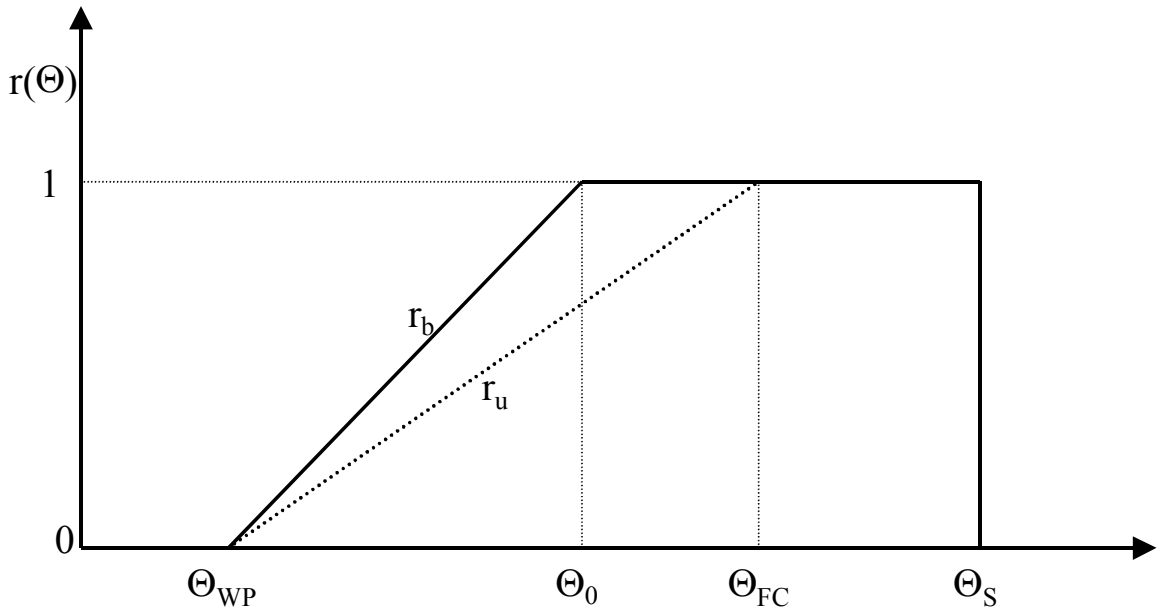

Figure 4.4-4: Schematic for the estimation of real evapotranspiration depending on soil moisture Θ.

4.5 Runoff generation, runoff components and runoff concentration

4.5.1 Generation of soil moisture, land surface runoff, interflow and percolation

The runoff (R or Q) is defined as the water volume per time unit ([m^3 s^{-1}] or [l s^{-1}]) that leaves a catchment through a surface runoff profile (e.g. river profile) and possibly also through subsurface ways. This water originates from the catchment area which, in turn, is limited by the watersheds. Surface and subsurface catchment areas are distinguished. The surface catchment area is defined by natural watersheds like mountain ridges, its area corresponds to the horizontal projection of the area which is enclosed by the watersheds. The subsurface catchment area is affected by the geological conditions. The characteristics of the geological layers, and geological faults, cleavages or vugs, may influence water flow such that inflows or outflows are virtually impossible to determine.

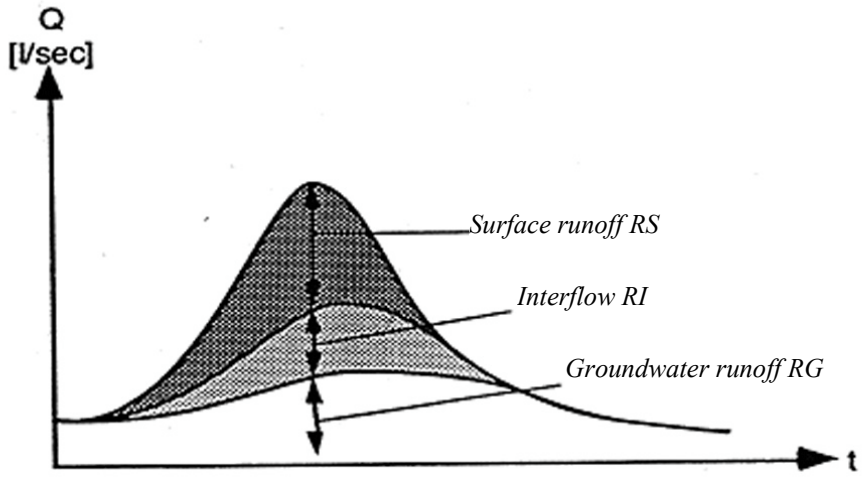

Figure 4.5-1: Composition of a runoff hydrograph from the surface runoff RS, the interflow RI and the groundwater runoff (baseflow) RG.

The runoff hydrograph consists of different runoff components generated in different parts of the catchment at the land surface, in the unsaturated soil zone and in the saturated groundwater zone using different runoff generation sub-models. The flowing of the generated runoff to the outlet profile of the catchment at the land surface, through the soil and in the river network occurs with different velocities and is described by runoff concentration sub-models. The runoff generation and concentration modules can be coupled similarly as in the PREVAH model.

Equations of the runoff-generation module used in PREVAH

Here, we present the equations for the water flows within the runoff generation module of PREVAH (see Chapter 2). The water flows are computed for each HRU at each time step *dt* [h] as represented schematically in Figure 2-2. Table 4.5-1 summarises the variables and parameters of the soil and runoff generation modules.

Table 4.5-1: Main variables and parameters of the soil and runoff-generation modules.

Name	Unit	Definition
State Variables		
SNFC	[mm]	Maximum plant available soil moisture storage
SSM	[mm]	Plant available soil moisture storage
DSUZ	[mm h^{-1}]	Inflow into the runoff generation module
SUZ	[mm]	Upper storage reservoir
PERC	[mm h^{-1}]	Deep percolation rate
RS	[mm h^{-1}]	Surface runoff
RI	[mm h^{-1}]	Interflow
SG1	[mm]	Fast response groundwater reservoir
SG2	[mm]	1st order slow response groundwater reservoir
SG3	[mm]	2nd order slow response groundwater reservoir
GR1	[mm h^{-1}]	Recharge of SG1
GR2	[mm h^{-1}]	Recharge of SG2
GR3	[mm h^{-1}]	Recharge of SG3
RG1	[mm h^{-1}]	Fast response groundwater runoff component
RG2	[mm h^{-1}]	Delayed groundwater runoff component
R_{TOT}	[mm h^{-1}]	Total runoff
Tuneable parameters		
BETA	[-]	Soil moisture recharge parameter
SGR	[mm]	Threshold content of SUZ for generation of surface runoff
$SG1_{MAX}$	[mm]	Maximum content of the fast response groundwater reservoir SG1
K0	[h]	Storage time for surface runoff
K1	[h]	Storage time for interflow
K2	[h]	Storage time for quick response baseflow
K3	[h]	Storage time for delayed baseflow
$PERC_{MAX}$	[mm dt^{-1}]	Maximal deep percolation rate

The inflow *DSUZ* into the storages of the runoff generation module is relative to *SFC*:

$$DSUZ(t) = P_b(t) \cdot \left(\frac{SSM(t-1)}{SNFC} \right)^{BETA} \quad (4.5\text{-}1)$$

BETA is a dimensionless non-linearity parameter that controls the redistribution of the available water amount for runoff generation P_b [mm h^{-1}] between the plant available soil moisture storage reservoir (*SSM*) and upper storage reservoir SUZ.

The *SUZ* reservoir temporarily stores water amounts that can either drain by gravitation in the groundwater storages *SLZ*, or generate surface runoff and interflow. *SUZ* contains the water available for land surface runoff generation and the fraction of the soil moisture content which exceeds the field capacity and contributes to runoff generation (Figure 4.5-2) and percolation. The soil moisture recharge (*SMR*) is the difference between P_b and *DSUZ*. *SMR* increases with increasing *BETA* (Uhlenbrook, 1999).

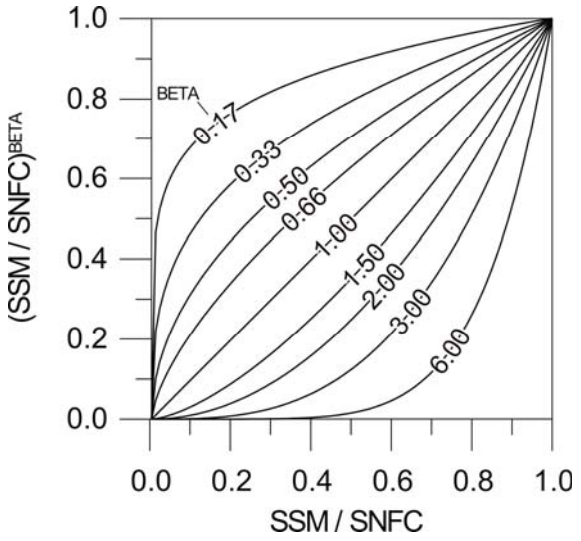

Figure 4.5-2: Relation of storage inflow (abscissa) to storage outflow (ordinate) depending on the parameter BETA.

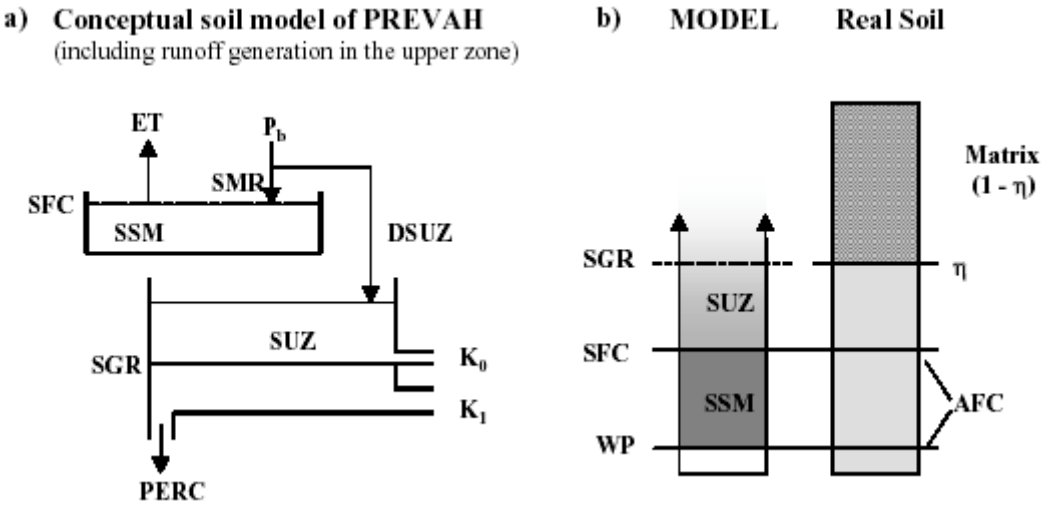

Figure 4.5-3: Conceptualisation of the soil model in PREVAH (left) and schematic conceptualisation of the real soil and its parameterisation in the hydrological model (right).

As a first step, the storage reservoir *SUZ* is incremented by *DSUZ*:

$$SUZ_1(t) = SUZ(t-1) + DSUZ(t) \cdot dt \qquad (4.5\text{-}2)$$

SUZ is emptied by deep percolation *PERC* into the reservoirs of the saturated zone *SG1, SG2, SG3*, by surface runoff *RS* and interflow *RI*:

$$SUZ_2(t) = SUZ_1(t) - PERC(t) \cdot dt \tag{4.5-3}$$

$$\text{with } PERC(t) = MIN\left[\left(SUZ_1(t) \cdot dt^{-1}\right), PERC_{MAX}\right] \tag{4.5-4}$$

The percolation rate *PERC* is a tuneable parameter. *PERC* (Eq. 4.5-4) is limited by the content of *SUZ* obtained from Equation 4.5-2. The generation of surface runoff *RS* (Eq. 4.5-5) and interflow *RI* (Eq. 4.5-5) depends on the content of the linear reservoir *SUZ*, as obtained from Equation 4.5-2:

$$\begin{aligned} RS(t) &= \left(SUZ_2(t) - SGR\right) \cdot \left(1 - e^{-dt/K0}\right) \cdot dt^{-1} \quad if \quad SUZ_2(t) > SGR \\ RS(t) &= 0 \quad if \quad SUZ_2(t) \le SGR \\ RI(t) &= SUZ_2(t) \cdot \left(1 - e^{-dt/K1}\right) \cdot dt^{-1} \quad if \quad SUZ_2(t) > 0 \\ RI(t) &= 0 \quad if \quad SUZ_2(t) = 0 \end{aligned} \tag{4.5-5}$$

where *SGR* is a model parameter defining a threshold content of *SUZ* [mm] that must be exceeded to allow for surface runoff generation. The two storage times *K0* and *K1* [h] are tuned through model calibration and adopted as catchment specific parameters to govern the generation of surface runoff and interflow, respectively.

The content of *SUZ* at the end of the time-step is:

$$SUZ(t) = SUZ_2(t) - \left(RI(t) + RS(t)\right) \cdot dt \tag{4.5-6}$$

4.5.2 Groundwater storage and generation of baseflow

The principle of parallel connection of single linear storages is used in PREVAH to compute the base runoff. It is implemented in the sub-model SLOWCOMP from Schwarze et al. (1999). The groundwater storage is divided into a quick-leaking storage *SG1* and a slow-leaking storage *SG2*. The capacity of *SG1* for the fast groundwater components is limited through a given maximal storage charge $SG1_{MAX}$. Further, the free storage volume of *SG1* can only be filled as fast as it would leak when fully charged; the corresponding storage time is *CGH*. Subsequently, *SG2* only receives the fraction of percolation which is not absorbed by *SG1*.

Additionally, a smaller, even slower leaking storage *SG3* is usually added to *SG2* in parallel. The mean storage time *K3* is assigned as $9 \cdot K2$, the input consumes $^1/_9$ of the input to *SG2*. The total content of the groundwater storages (also called *SLZ*, for "storage lower zone") is the sum of the three partial storages *SG1*, *SG2* and *SG3*. Total base runoff is combined from the outflow of the three partial storages.

The storage times for *SG1* (*CGH*) and SG2 (*K2*) are parameters which need to be estimated empirically for the particular catchment. This may be achieved through an analysis of the runoff hydrographs (Schwarze et al. 1999). *K3* (for SG3) is derived from *K2*, and therefore does not need to be estimated.

The recharge rates *GR1*, *GR2* and *GR3* of the groundwater storage reservoirs *SG1, SG2* and *SG3* are determined as a function of the deep percolation rate *PERC*. The computation of the water flows within the groundwater storages and the corresponding runoff components follows the method developed in the sub-model SLOWCOMP by Schwarze et al. (1999):

$$\begin{aligned} if \quad SG1(t) \ge SG1_{MAX} \quad & GR1(t) = 0 \\ & GR2(t) = PERC(t) \cdot 8/9 \\ & GR3(t) = PERC(t) \cdot 1/9 \end{aligned} \tag{4.5-7}$$

$$\begin{aligned} if \quad SG1(t) < SG1_{MAX} \quad & GR1 = MIN\left(PERC(t), GR1_{MAX}(t)\right) \\ & GR2 = \left(PERC(t) - GR1\right) \cdot 8/9 \\ & GR3(t) = \left(PERC(t) - GR1\right) \cdot 1/9 \end{aligned} \tag{4.5-8}$$

$$\text{with } GR1_{MAX}(t) = \left[\frac{\left(SG1_{MAX} - SG1(t)\right)}{K2_H} \right] \tag{4.5-9}$$

where $SG1_{MAX}$ is a threshold factor which restricts the content of the quick response groundwater reservoir *SG1*. $SG1_{MAX}$ is not exceeded during the time step *dt*.

Equations 4.5-10 to 4.5-12 describe the computation of the change in storage for the three groundwater reservoirs during *dt*.

$$SG1(t) = SG1(t-1) \cdot e^{-dt/K2} + \left[\left(1 - e^{-dt/k2}\right) \cdot GR1(t) \cdot K2\right] \tag{4.5-10}$$

$$SG2(t) = SG2(t-1) \cdot e^{-dt/K3} + \left[\left(1 - e^{-dt/k3}\right) \cdot GR2(t) \cdot K3\right] \tag{4.5-11}$$

$$SG3(t) = SG3(t-1) \cdot e^{-dt/K4} + \left[\left(1 - e^{-dt/k4}\right) \cdot GR3(t) \cdot K4\right] \tag{4.5-12}$$

The generation of the groundwater runoff components is governed by the tuneable storage times *K2* and *K3*:

$$RG1(t) = \frac{SG1(t)}{K2} \tag{4.5-13}$$

$$RG2(t) = \frac{SG2(t)}{K3} + \frac{SG3(t)}{K4} \tag{4.5-14}$$

$$\text{with } K4 = K3 \cdot 1/9 \tag{4.5-15}$$

K2 and *K3* are the storage times [h] governing the generation of a quick response (*RG1*) and delayed (*RG2*) groundwater runoff, respectively. The additional reservoir *SG3* also generates a delayed groundwater component (*RG3*), whose storage time *K4* is parameterised as a function of *K3* (Equation 4.5-15). The storage times of the groundwater runoff components can be either tuned through model calibration or determined by an analysis of the hydrograph's recession curve (Schwarze et al., 1999).

The total runoff generation R_{TOT} in time step *dt* is determined by adding all components generated in the upper storage reservoir and groundwater reservoirs:

$$R_{TOT}(t) = RS(t) + RI(t) + RG1(t) + RG2(t) \tag{4.5-16}$$

R_{TOT} is assumed to be instantaneously routed to the catchment outlet.

4.5.3 Runoff concentration

Runoff routing and estimation of the total runoff

When elaborating a model concept, simulation of storage and translation processes in the catchment area and stream system is approached with simple mathematical models. The model parameters are estimated such that the processes in the natural system are approximated as accurately as possible. A commonly used concept to represent storage effects is the so-called single linear storage (SLS; Figure 4.5-4) which can be combined with a translation element.

$$S = k \cdot q \quad \text{or} \quad q = (1/k) \cdot S \tag{4.5-17}$$

using:

S = storage
q = outflow
k = storage constant as the residence time
p = inflow

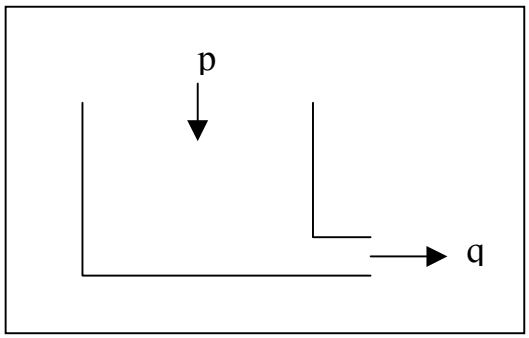

If the storage change as shown in Equation 4.5-18

$$p - q = dS / dt \tag{4.5-18}$$

is inserted in Equation 4.5-17, the differential equation for the SLS is achieved:

$$p = q + k \cdot (dq / dt) \qquad (4.5\text{-}19)$$

The corresponding solution is:

$$q(t) = q(t_0) \cdot \exp(-(t-t_0) / k)) + p(\tau) \cdot (1 / k) \cdot \exp(-(t-t_0) / k) \cdot \mathrm{d}(\tau) \qquad (4.5\text{-}20)$$

using: $q(t_0)$ = storage outflow at time t_0
$q(t)$ = storage outflow at time t

The first term takes into account the idle process during periods without inflow (p=0), whereas the second term describes the outflow $q(t)$ which results from the system input p and corresponds to the convolution integral

$$q(t) = p(\tau) \cdot h(t - \tau)\, \mathrm{d}(\tau).$$

From this, we get the pulse response from the SLS:

$$h(t) = (1 / k) \cdot \exp(-t / k) \qquad (4.5\text{-}21)$$

This means that the storage experiencing a pulsed input will drain according to an e-function.

Assuming a rectangular input pulse with $0 \leq t \leq \Delta t$ results in a rising outflow hydrograph:

$$q(t) = p(t) \cdot (1 - \exp(-t / k)) \qquad (4.5\text{-}22)$$

The recession of the hydrograph is calculated using the idle term for $t > \Delta t$ and $q_{\Delta t}$ as outflow at the end of the rectangular pulse:

$$q(t) = q_{\Delta t} \cdot \exp(-(t - \Delta t) / k) \qquad (4.5\text{-}23)$$

The parameter k (storage constant of the *SLS*) corresponds to the residence time of the water in the *SLS*. If the *SLS* is applied to calculate the runoff concentration of effective precipitation to direct runoff in a flood event, k may be estimated as half of the time between the end of the precipitation and the end of the flood event (concentration time T_C).

Linear translation element (LTE)

The single linear storage does not take into account translation processes in the considered hydrological system. The outflow always begins at the same time as the initiating inflow, which is unlikely to happen in reality. Therefore, a completion with the linear translation element is required. It forwards every input without any modification. The inflow $p(t)$ to a translation element, which is passed through with a translation time T, is used to calculate the outflow:

$$q(t)=p(t-T) \qquad (4.5\text{-}24)$$

Regarding the runoff concentration of a catchment or the characteristics of river runoff, both storage and translation processes are involved. In general, these processes are simulated more accurately with a combined model (storage and translation). The system parameter T for a pure translation system is interpreted from the time displacement of specific points on the in- and outflow hydrographs.

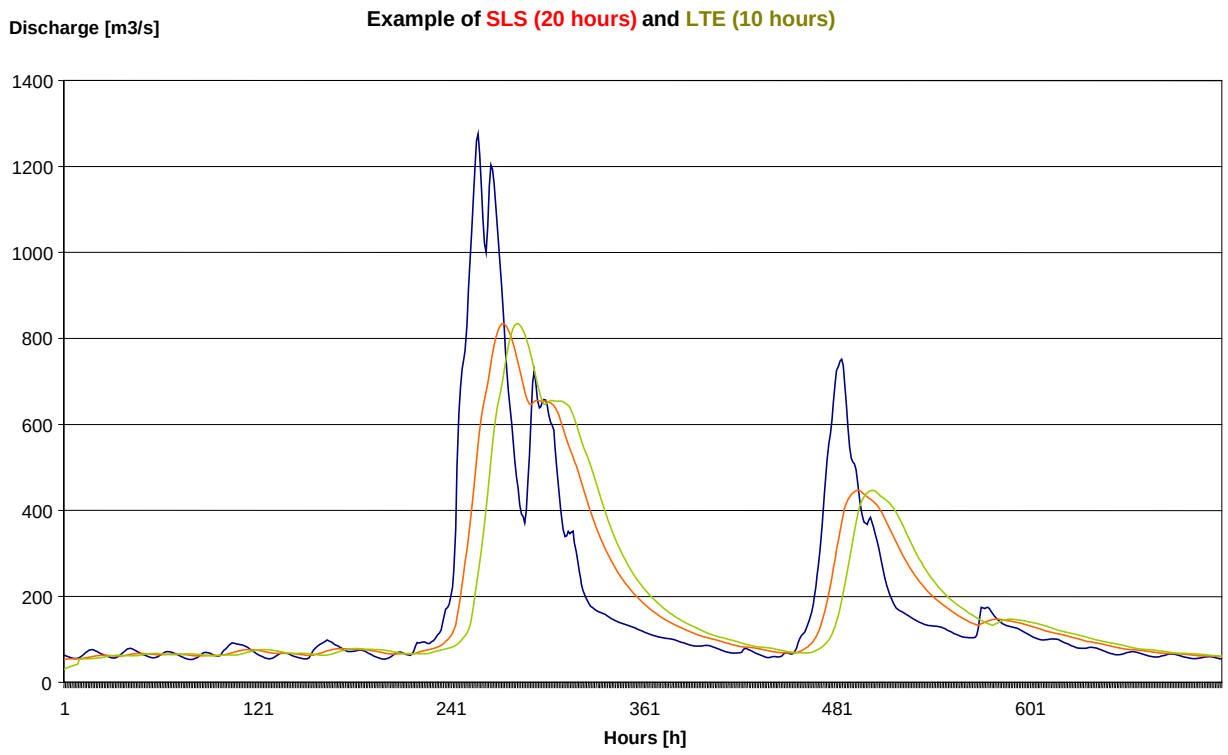

Figure 4.5-4: Example of a single linear storage (SLS) and a Linear translation element (LTE).

SLS and *LTE* may be also adopted in order to approximate the retention of lakes (Figure 4.5-5).

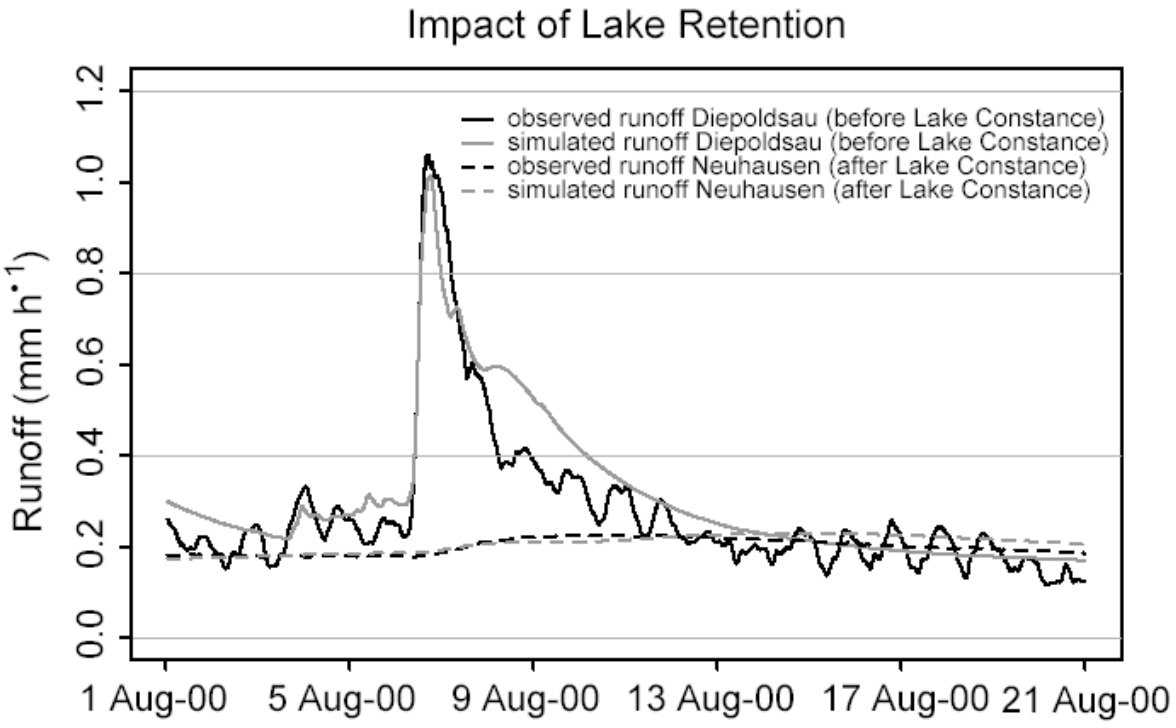

Figure 4.5-5: Impact of Lake Constance retention on the August 2000 flood-peak, illustrated by the simulated and observed discharges at the gauges Diepoldsau and Neuhausen (Verbunt et al., 2006).

Flood routing in the river bed system

Regarding the wave flow phases, we have to answer the question of how the different flood waves from the catchment areas are combined the moment they reach the main river (forecast of flood water). The development of these waves in an open stream system is, in general, in an unsteady state, a flow process which is changing gradually. This process can be described on the basis of the "Saint-Venent-Equation" which is composed of the dynamic base equation and continuity equation. As there is no known analytic solution for this equation, different simplified approaches were developed, e.g. the diffusion-wave-model and kinematic-wave-model.

As an alternative to these hydraulic models, which require a demanding calculating capacity to obtain a numerical solution, hydrologists developed simpler mathematical terms. These models, which show a robust behaviour, are called hydrological or conceptual models. They are based on the following equation, which is valid for an extended river section:

$$Q_z - Q_a = \frac{dS}{dt} \tag{4.5-25}$$

using: S storage capacity of the river section
Q_z inflow to river section
Q_a outflow from river section

The dynamic equation is substituted through a more or less empirical dependency between S and Q_z and/or Q_a. One of these model concepts is the Muskingum-Model after McCarthy (1938)

$$S = K\left[g \cdot Q_z + (1-g) \cdot Q_a\right] \tag{4.5-26}$$

using an accumulation constant K an a dimensionless weighting factor g with values from 0 to 1

Another flood routing model concept is the Kalinin-Miljukov-Model, (Kalinin and Miljukov, 1957) consisting of a cascade of n linear storages using

$$S = K \cdot Q_{a,} \tag{4.5-27}$$

In PREVAH, this term is integrated for the calculation of flood routing in the river bed by the Storage-Translation-Model, consisting of a SLS coupled with a pure translation element.

5. Assimilation and use of hydrological data

5.1 Model requirements

The most important hydrological data are time series of observed discharges at river gauges. These data are required in order to calibrate the model and estimate model efficiency. The format is identical to the format for meteorological station data, except the second row which does not contain the altitude but the catchment area of a gauging station. This is important if the discharges (in [m^3 s^{-1}]) are converted into specific discharges (in [mm Δt^{-1}]), as latter is the unit required by the model.

5.2 Computation of model efficiency

To calibrate and validate a model, the calculated (y_i) and observed (x_i) values are compared assess the simulation and modelling quality, respectively. Beside the visual control of the graphical diagram, quality and error criteria should be used to obtain a more objective rating of the differences between the simulated and observed values. For the use of mathematical parameter optimisation, such objective quality criteria are essential since the parameter optimisation tries to maximise and minimise the particular quality criteria, respectively. The choice of a quality criteria and the corresponding timeframe needs to be completed carefully and in a sophisticated way, depending on the conceptual formulation.

The runoff is the most commonly used term to compare processes in hydrological modelling. However, there can also be other terms used such as evapotranspiration, soil moisture or fill level of storage to obtain a quality assessment of a simulation. It has to be considered that the quality of a simulation depends on the regarded temporal resolution.

The objective statistical coefficients that were used to evaluate the simulated variables *S* with respect to the observed variables *O* are:

Empirical coefficient of correlation R_{os}:

This quality criterion is used in analogy to the correlation coefficient of the linear regression. As the required linearity is mostly not fulfilled, and the simulated runoff is not a random variable, the term "correlation coefficient" should be substituted with "sum of the deviation products" or at least used with apostrophes. It has to be recognised that the range of the variant calculation only varies between -1 and +1 and, therefore, changes in the simulation are more difficult to discover than with other quality criteria. We have the possibility to compare different catchment areas.

$$R_{os} = \frac{\sum_{i=1}^{N} \left(S_i - \overline{S}\right)\left(O_i - \overline{O}\right)}{\sqrt{\sum_{i=1}^{N} \left(S_i - \overline{S}\right)^2 \sum_{i=1}^{N} \left(O_i - \overline{O}\right)^2}} \tag{5.2-1}$$

with $\overline{O}$ and $\overline{S}$ the mean of the observations O_i and simulated S_i values, respectively and N the number of observations. R_{os} tends to unity the more the simulated values have similar dynamics with respect to the observations.

Root mean square error RMSE:

$$RMSE = \sqrt{\frac{\sum_{i=1}^{N} \left(S_i - O_i\right)^2}{N}} \tag{5.2-2}$$

RMSE allows for the quantification of the magnitude of the deviation of the simulated from the observed values.

Mean absolute deviation MAD:

$$MAD = \frac{\sum_{i=1}^{N} |S_i - O_i|}{N} \tag{5.2-3}$$

MAD must be minimised in the calibration phase to obtain a better quantitative agreement for the simulated variable with respect to the observation.

Efficiency score E_2 (Legates and McCabe, 1999; Nash and Sutcliffe, 1970):

$$E_2 = 1 - \frac{\sum_{i=1}^{n} | O_i - S_i |^2}{\sum_{i=1}^{n} \left| O_i - \left[\frac{1}{n} \sum_{i=1}^{n} O_i \right] \right|^2} \tag{5.2-4}$$

E_2 quantifies the relative improvement of the model compared to the mean of the observations. An efficiency below zero indicates that average daily measured stream flow would have been as good a predictor as the modelled stream flow. A perfect model prediction has a score equal to one. Any positive value corresponds to an improvement. E_2 tends towards unity when S_i tends towards O_i. Further, the logarithmic formulation of E_2 (Schulla, 1997; Hock, 1999) is considered:

$$E_2^{\log} = 1 - \frac{\sum_{i=1}^{n} | \ln(O_i) - \ln(S_i) |^2}{\sum_{i=1}^{n} \left| \ln(O_i) - \left[\frac{1}{n} \sum_{i=1}^{n} \ln(O_i) \right] \right|^2} \tag{5.2-5}$$

The logarithmic efficiency score E_2^{log} gives valuable indications on the model performance in the case of discharge simulations during low-flow periods in winter (Gurtz et al., 2001). The range of both E_2 and E_2^{log} is [-∞,1]. The logarithmic form should possibly be used in addition to the linear variant.

5.3 Computation of flood statistics

Three peak-specific efficiency scores are computed by the PREVAH sub-module FLOODSTAT. They follow the recommendations of Lamb (1999) and allow in-depth analysis of the peak simulation ability of the PREVAH model parameter set in use (see Viviroli, 2007 for details). The efficiency scores are defined as follows:

Sum of time- and size-weighted peak errors (Lamb, 1999)

$$P - QT = \sum_{i=1}^{m} \sqrt{\left[(P_i - p_i) / p^* \right]^2 + \left[(T_i - t_i) / t^* \right]^2} \tag{5.3-1}$$

with $P_i = i^{th}$ observed peak, $p_i = i^{th}$ simulated peak, p^* = difference between largest and smallest observed peak, T_i = time of i^{th} observed peak, t_i = time of i^{th} simulated peak, t^* = time steps between occurrence of first and last observed peak and m = number of extracted peaks in the peak flow record (usually three times the number of years considered, see FLOODSTAT OPTIONS in the WINPREVAH documentation for details). A *P-QT* score of 0 means complete correspondence of observed and simulated peaks; with rising score the deviations in timing and size of the peaks increase. *P-QT* is a relative score with no upper limit, and since the score is scaled relative to p^* and t^*, its meaning is specific and can not be compared between different peak flow records.

Sum of absolute errors SAE *in peak flow record (Lamb, 1999)*

$$P - SAE = \sum_{i=1}^{m} |P_i - p_i| \tag{5.3-2}$$

Sum of weighted absolute errors WAE *in entire runoff record*

$$WAE = \sum_{t=1}^{n} Q_t{}^{a} \left| Q_t - q_t \right| \tag{5.3-3}$$

with Q_t = observed runoff, q_t = simulated runoff, a = exponent (1.5 is recommended) and n = total number of runoff records.

Additionally, three further statistical scores are computed:

NSE: Efficiency score following Nash and Sutcliffe (1970) (see Section 5.2)

SPM_R: Spearman rank-correlation coefficient (see e.g. Bahrenberg et al., 1990) between observed and simulated peaks in the peak flow record.

$$SPM\_R = 1 - \frac{\sum_{i=1}^{m} \left| R_i - r_i \right|}{m(m^2 - 1)} \tag{5.3-4}$$

With R_i = rank of i^{th} observed peak, p_i = rank of i^{th} simulated peak and m = number of extracted peaks. It is assumed that there are no peaks of exactly identical magnitude. This coefficient may be used to assess the ability of the current parameter set to reproduce the magnitude order of flood peaks.

SPM_P: Significance level of *SPM_R*. Example: In a two-sided test with an α error limit of 5%, a value below 0.975 means that there is no significant correlation between observed and simulated peaks. Note that normal distribution is assumed which applies only to record sets of 30 or more samples.

Please note that it is difficult to obtain high standard efficiencies and peak record efficiencies with the same set of PREVAH parameters. Depending on the accuracy desired by the user and the application goal, it may be necessary to use different parameter sets for the ideal representation of normal and extreme flow periods, respectively. However, a parameter set for simulating peak flows should achieve at least acceptable standard efficiencies (performance over the whole simulation period focusing on non-extreme runoff), since simulation results are more trustworthy when PREVAH is able to capture basic hydrological characteristics of the catchment in consideration (Viviroli, 2007).

6. Model calibration

6.1 Introduction

As a standard procedure for model calibration and validation, the available data sets for hydrological simulations in a catchment are divided into two non-overlapping periods. If the global time series is longer than five years, at least three years are used as the calibration period. The first year of the simulation period should be used as an initialisation period and then excluded from the evaluation. This decision is based on the uncertainty of the values for the snow water equivalent and different water storages at initialisation. This restriction is less important in regions where snow accumulation plays a marginal role in the runoff generation process.

The remaining period is used for verification of the model quality without further adjustments of the tuneable parameters. The analysis of the hydrological behaviour of the catchment generally includes the entire available time series. The quality of the model simulation can be assessed by using different observed variables. The comparison of different outputs of a model run with selected observed variables allows a multiple-response verification of the model's capabilities. Hydrometeorological observations available for model evaluation include:

- Discharge observations
- Soil moisture time series
- Observed fluctuations of the groundwater level
- Lysimeter data (evapotranspiration, percolation, storage changes)
- Records of snow height and snow water equivalent
- Snow patterns derived by satellite observations
- Latent heat flux values observed by eddy correlation and computed using the Bowen ratio method

6.2 Trial and error calibration

If calibration of PREVAH is completed manually, the output is compared with observed values and evaluated by means of objective statistical criteria. A graphical comparison between observation and simulation is made in the calibration phase for a subjective assessment of the simulation quality. This allows an expertise-based assessment of the model's free parameters. As a further index of the model quality, the quantitative difference between computed and measured data is taken into account and analysed (e.g. between computed and observed average yearly discharge). The most sensitive catchment specific tuneable parameters to be calibrated are:

- Adjustment factors for precipitation (snow and rain)
- Parameters of the snowmelt module
- Parameters of the glacial melt module
- Non-linearity exponent controlling the soil moisture recharge
- Threshold storage parameter for the generation of surface runoff
- Maximal storage available for fast baseflow (Schwarze et al., 1999)
- Storage times which govern the process of runoff generation (surface runoff, interflow, delayed and fast baseflow)
- Percolation rate

6.3 Automatic calibration

6.3.1 Procedure and set-up

To perform the automatic model calibration, observed runoff data for the catchment in the defined simulation period are required. The general idea behind an automatic calibration is to allow the calibration module to find the best settings for the selected tuneable parameters with help of a set of model runs which are evaluated by means of different objective functions. These functions are computed on the basis of the determined efficiency and volume error of the model simulations with PREVAH. The model parameters are calibrated pair-wise (two parameters at a time). The following procedure is applied for the automatic calibration of PREVAH:

– A set of so-called parameter pairs is defined. Maximum and minimum limits are set for each parameter. Thus, a parameter space is defined (see also the documentation of the tool VIEWOPTIM).

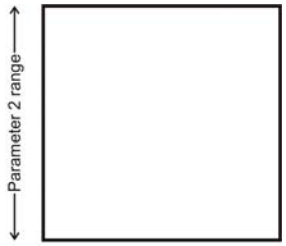

– The parameter space is subdivided into 9 sections, each of them covering $^1/_9$ of the area of the parameter space.

– The parameter combinations found at the 4 main intersections of the parameter space are used for running PREVAH.

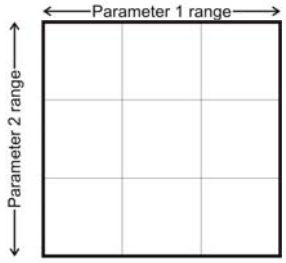

– The objective scores are computed as defined in the next section, so that the calibration module can decide which of these 4 runs (and corresponding parameter configurations) was the most accurate.

– The parameter space is then reduced (white area), a new parameter space is centred on the best parameter configuration of the previous iteration. $^5/_9$ of the original parameter space area is discarded (grey area).

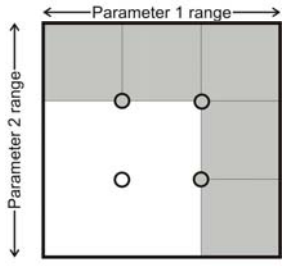

– The new parameter-space is then is subdivided anew into 9 sections, and the procedure described above is repeated. This is continued until a pre-defined number of iterations is reached or until the improvement in model efficiency as compared to the last iteration remains under a defined threshold.

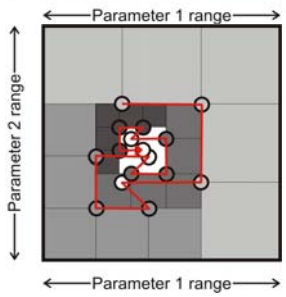

Table 6.3-1: Default parameter-pairs for automatic calibration of PREVAH for Swiss glaciated catchments. These default settings assume that the recommended snowmelt module "4. EMA with varying melt factor" is used.

PAIR	Parameter 1	Parameter 2
1	Rain correction [%]	Snow correction [%]
2	Threshold Temperature Rain-snow [°C]	Transition Temperature Rain-snow [°C]
3	Maximal degree day factor [mm d^{-1} K^{-1}]	Minimal degree day factor [mm d^{-1} K^{-1}]
4	Threshold Temperature Rain-snow [°C]	Threshold Temperature snowmelt [°C]
5	Exponent for soil moisture recharge [-]	Percolation [mm h^{-1}]
6	Refreezing factor [mm d^{-1} K^{-1}]	Rad. melt factor snow [mm h^{-1} K^{-1} W^{-1} m^2]
7	Threshold storage for surface runoff [mm]	Storage time for surface runoff [h]
8	Storage time for interflow [h]	Percolation [mm h^{-1}]
9	Storage time for fast baseflow [h]	Maximum storage for fast baseflow [mm]
10	Storage time for delayed baseflow [h]	Percolation [mm h^{-1}]
11	Temperature melt factor for ice [mm d^{-1} K^{-1}]	Rad. melt factor ice [mm h^{-1} K^{-1} W^{-1} m^2]

Table 6.3-2: Recommended parameter-pairs for automatic calibration of PREVAH for large catchments with no glaciers and daily meteorological input. These default settings require that the snowmelt module "0. Positive degree day index (PDDI)" (see Section 4.5.1) is used.

PAIR	Parameter 1	Parameter 2
1	Rain correction [%]	Snow correction [%]
2	Threshold Temperature Rain-snow [°C]	Transition Temperature Rain-snow [°C]
3	Maximal degree day factor [mm d^{-1} K^{-1}]	Minimal degree day factor [mm d^{-1} K^{-1}]
4	Refreezing factor [mm d^{-1} K^{-1}]	Threshold Temperature snowmelt [°C]
5	Exponent for soil moisture recharge [-]	Percolation [mm h^{-1}]
6	Threshold storage for surface runoff [mm]	Storage time for surface runoff [h]
7	Storage time for interflow [h]	Percolation [mm h^{-1}]
8	Storage time for fast baseflow [h]	Maximum storage for fast baseflow [mm]
9	Storage time for delayed baseflow [h]	Percolation [mm h^{-1}]

The number of iterations can be defined by the user although 4 to 8 iterations for each parameter pair are recommended. If the calibration module does not register an improvement from the previous iteration step, further iterations are skipped and the calibration continues with the subsequent parameter pair. The set-up of the automatic calibration is controlled by WINPREVAH (see Part III of the PREVAH documentation).

6.3.2 The 3×3 objective scores

Three scores are computed to assign a total score to each model run and determine the best model run during automatic model calibration. Each score is computed on the basis of three objective functions which in turn can be weighted separately. Thus, a specific score and objective function can have larger or smaller influence on the total score.

Linear Score (ALIN)

The linear score analyses the quality of the model run with respect to the linear efficiency score E_2^{lin} (Nash and Sutcliffe, 1970; Legates and McCabe, 1999). Three weighted objective functions are defined to assess ALIN:

– The linear efficiency score during the calibration period.
The range of this score is between -∞ and 1. The goal of the calibration should be to maximise this score. To scale this score to a range between 0 and 1, a simple fuzzy function is introduced:

$$ALIN_{PERIOD} = \begin{cases} 0 & if \quad E_2^{lin} < E_{2\_MIN}^{lin} \\ \dfrac{\left(E_2^{lin} - E_{2\_MIN}^{lin}\right)}{\left(E_{2\_MAX}^{lin} - E_{2\_MIN}^{lin}\right)} & if \quad E_{2\_MIN}^{lin} \le E_2^{lin} \le E_{2\_MAX}^{lin} \\ 1 & if \quad E_2^{lin} > E_{2\_MAX}^{lin} \end{cases} \tag{6.3-1}$$

The fuzzy function is governed by two parameters: the user-definable maximum and minimum values for E_2^{lin}. As a result, the score of a simulation with respect to the linear efficiency score during the entire calibration period is established ($ALIN_{PERIOD}$).

– The year-to-year standard deviation (STDEV) of the linear efficiency score during the calibration years. The range of this score is between 0 and ∞. This score should allow that all the years in the calibration period have a similar linear efficiency score. The goal of the calibration should be to maximise this score (and thus minimise year-to-year standard deviation). To scale this score to a range between 0 and 1, a simple fuzzy function is introduced:

$$ALIN_{YY} = \begin{cases} 1 & if \quad \mathrm{STDEV_{YY}}\left(\mathrm{E}_2^{lin}\right) < \mathrm{STDEV_{YY\_MIN}} \\ \left(1 - \dfrac{\left(\mathrm{STDEV_{YY}}\left(\mathrm{E}_2^{lin}\right) - \mathrm{STDEV_{YY\_MIN}}\right)}{\left(\mathrm{STDEV_{YY\_MAX}} - \mathrm{STDEV_{YY\_MIN}}\right)}\right) & if \quad \mathrm{STDEV_{YY\_MIN}} \le \mathrm{STDEV_{YY}}\left(\mathrm{E}_2^{lin}\right) \le \mathrm{STDEV_{YY\_MAX}} \\ 0 & if \quad \mathrm{STDEV_{YY}}\left(\mathrm{E}_2^{lin}\right) > \mathrm{STDEV_{YY\_MAX}} \end{cases} \tag{6.3-2}$$

The fuzzy function is governed by two parameters: the maximum and minimum standard deviation of E_2^{lin} from year to year (STDEV_{YY}). These two parameters have to be defined by the user to establish the score of a simulation with respect to the variability of linear efficiency score during the different years of the calibration period ($ALIN_{YY}$).

– The month-to-month standard deviation of the linear efficiency score during the calibration years. The range of this score is between 0 and ∞. This score should allow that, during the calibration period, all the months have a similar linear efficiency score. The goal of the calibration should be to maximise this score (and thus minimise month-to-month standard deviation). To scale this score to a range between 0 and 1, a simple fuzzy function is introduced:

$$ALIN_{MM} = \begin{cases} 1 & if \quad \mathrm{STDEV_{MM}}\left(\mathrm{E}_2^{lin}\right) < \mathrm{STDEV_{MM\_MIN}} \\ \left(1 - \dfrac{\left(\mathrm{STDEV_{MM}}\left(\mathrm{E}_2^{lin}\right) - \mathrm{STDEV_{MM\_MIN}}\right)}{\left(\mathrm{STDEV_{MM\_MAX}} - \mathrm{STDEV_{MM\_MIN}}\right)}\right) & if \quad \mathrm{STDEV_{MM\_MIN}} \le \mathrm{STDEV_{MM}}\left(\mathrm{E}_2^{lin}\right) \le \mathrm{STDEV_{MM\_MAX}} \\ 0 & if \quad \mathrm{STDEV_{MM}}\left(\mathrm{E}_2^{lin}\right) > \mathrm{STDEV_{MM\_MAX}} \end{cases} \tag{6.3-3}$$

The fuzzy function is governed by two parameters: the maximum and minimum standard deviation of E_2^{lin} from month to month (STDEV_{MM}). These two parameters have to be defined by the user to establish the score of a simulation with respect to the variability of linear efficiency score during the different months in the calibration period ($ALIN_{MM}$).

ALIN is then computed as follows:

$$ALIN = ALIN_{PERIOD} \cdot \frac{w_1^{lin}}{\left(w_1^{lin} + w_2^{lin} + w_3^{lin}\right)} + ALIN_{YY} \cdot \frac{w_2^{lin}}{\left(w_1^{lin} + w_2^{lin} + w_3^{lin}\right)} + ALIN_{MM} \cdot \frac{w_3^{lin}}{\left(w_1^{lin} + w_2^{lin} + w_3^{lin}\right)} \tag{6.3-4}$$

with w_1^{lin}, w_2^{lin}, w_3^{lin} as the weight of the three fuzzy scores obtained through application of the previously defined fuzzy functions. All parameters and weights of the fuzzy function have to be assigned at the beginning of the simulation.

Logarithmic Score (ALOG)

The logarithmic score analyses the quality of the model run with respect to the logarithmic efficiency score E_2^{log}. Three weighted objective functions are defined to assess ALOG:

– The logarithmic efficiency score during the calibration period.
The range of this score is between -∞ and 1. The goal of the calibration should be to maximise this score. To scale this score to a range between 0 and 1, a simple fuzzy function is introduced:

$$ALOG_{PERIOD} = \begin{cases} 0 & if \quad E_2^{\log} < E_{2\_MIN}^{\log} \\ \dfrac{\left(E_2^{\log} - E_{2\_MIN}^{\log}\right)}{\left(E_{2\_MAX}^{\log} - E_{2\_MIN}^{\log}\right)} & if \quad E_{2\_MIN}^{\log} \le E_2^{\log} \le E_{2\_MAX}^{\log} \\ 1 & if \quad E_2^{\log} > E_{2\_MAX}^{\log} \end{cases} \tag{6.3-5}$$

The fuzzy function is governed by two parameters: the maximum and minimum E_2^{log}. These two parameters have to be defined to establish the score of a simulation with respect to the logarithmic efficiency score during the calibration period ($ALOG_{PERIOD}$).

– The year-to-year standard deviation of the logarithmic efficiency score during the calibration years. The range of this score is between 0 and ∞. This score should allow that all the years in the calibration period have a similar logarithmic efficiency score. The goal of the calibration should be to maximise this score (and thus minimise year-to-year standard deviation). To scale this score to a range between 0 and 1, a simple fuzzy function is introduced:

$$ALOG_{YY} = \begin{cases} 1 & if \quad \mathrm{STDEV_{YY}}\left(\mathrm{E_2^{log}}\right) < \mathrm{STDEV_{YY\_MIN}} \\ \left(1 - \frac{\left(\mathrm{STDEV_{YY}}\left(\mathrm{E_2^{log}}\right) - \mathrm{STDEV_{YY\_MIN}}\right)}{\left(\mathrm{STDEV_{YY\_MAX}} - \mathrm{STDEV_{YY\_MIN}}\right)}\right) & if \quad \mathrm{STDEV_{YY\_MIN}} \le \mathrm{STDEV_{YY}}\left(\mathrm{E_2^{log}}\right) \le \mathrm{STDEV_{YY\_MAX}} \\ 0 & if \quad \mathrm{STDEV_{YY}}\left(\mathrm{E_2^{log}}\right) > \mathrm{STDEV_{YY\_MAX}} \end{cases} \tag{6.3-6}$$

The fuzzy function is governed by two parameters: the maximum and minimum standard deviation of E_2^{log} from year to year ($STDEV_{YY}$). These two parameters have to be defined by the user to establish the score of a simulation with respect to the variability of logarithmic efficiency score during the different years of the calibration period ($ALOG_{YY}$).

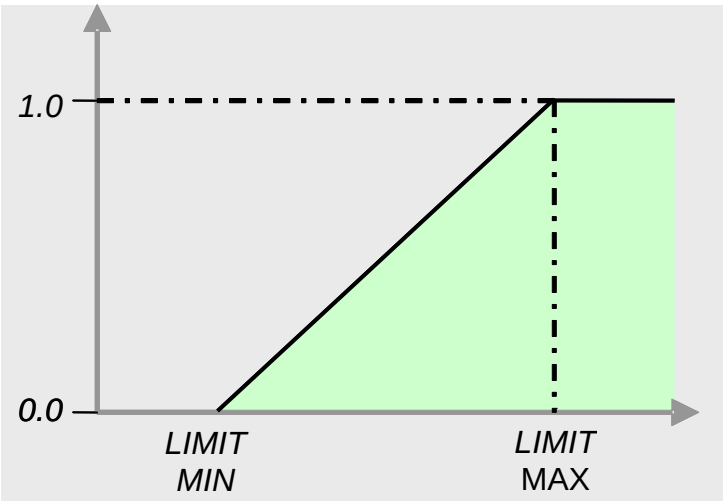

Figure 6.3-1: Minimum and maximum limits of the fuzzy functions needed to scale the objective functions to a range between 0 and 1.

– The month-to-month standard deviation of the logarithmic efficiency score during the calibration years. The range of this score is between 0 and ∞. This score should allow that, during the calibration period, all the months have a similar logarithmic efficiency score. The goal of the calibration should be to maximise this score (and thus minimise month-to-month standard deviation) To reduce this score to a range between 0 and 1, a simple fuzzy function is introduced:

$$ALOG_{MM} = \begin{cases} 1 & if \quad \mathrm{STDEV_{MM}}\left(\mathrm{E_2^{log}}\right) < \mathrm{STDEV_{MM\_MIN}} \\ \left(1 - \frac{\left(\mathrm{STDEV_{MM}}\left(\mathrm{E_2^{log}}\right) - \mathrm{STDEV_{MM\_MIN}}\right)}{\left(\mathrm{STDEV_{MM\_MAX}} - \mathrm{STDEV_{MM\_MIN}}\right)}\right) & if \quad \mathrm{STDEV_{MM\_MIN}} \le \mathrm{STDEV_{MM}}\left(\mathrm{E_2^{log}}\right) \le \mathrm{STDEV_{MM\_MAX}} \\ 0 & if \quad \mathrm{STDEV_{MM}}\left(\mathrm{E_2^{log}}\right) > \mathrm{STDEV_{MM\_MAX}} \end{cases} \tag{6.3-7}$$

The fuzzy function is governed by two parameters: the maximum and minimum standard deviation of E_2^{log} from month to month ($STDEV_{MM}$). These two parameters have to be defined by the user to establish the score of a simulation with respect to the variability of logarithmic efficiency score during the different months in the calibration period ($ALOG_{MM}$).

ALOG is then computed as follows:

$$ALOG = ALOG_{PERIOD} \cdot \frac{w_1^{\log}}{\left(w_1^{\log} + w_2^{\log} + w_3^{\log}\right)} + ALOG_{YY} \cdot \frac{w_2^{\log}}{\left(w_1^{\log} + w_2^{\log} + w_3^{\log}\right)} + ALOG_{MM} \cdot \frac{w_3^{\log}}{\left(w_1^{\log} + w_2^{\log} + w_3^{\log}\right)} \tag{6.3-8}$$

with w_1^{log}, w_2^{log}, w_3^{log} as the weight of the three fuzzy scores obtained through application of the previously defined fuzzy functions. All the parameters and weights of the fuzzy function have to be assigned at the beginning of the simulation.

Volumetric Score (AVOL)

The Volumetric score analyses the quality of the model run with respect to the volumetric deviation in percent (DV) between observed and simulated runoff. DV is defined as follows:

$$DV = \left| \sum_{i=1}^{n} \frac{S_i}{O_i} - 1 \right| \tag{6.3-9}$$

S_i is the simulated runoff at the time step i, O_i is the observed runoff at time step i. n is the number of time steps. Three weighted objective functions are defined for AVOL:

– The volumetric score during the calibration period.
The range of this score is between 0 and ∞. The goal of the calibration should be to minimise this score. To scale this score to a range between 0 and 1, a simple fuzzy function is introduced:

$$AVOL_{PERIOD} = \begin{cases} 1 & if \quad DV < DV_{MIN} \\ \left(1 - \frac{(DV - DV_{MIN})}{(DV_{MAX} - DV_{MIN})}\right) & if \quad DV_{MIN} \le DV \le DV_{MAX} \\ 0 & if \quad DV > DV_{MAX} \end{cases} \tag{6.3-10}$$

The fuzzy function is governed by two parameters: the maximum and minimum *DV*. These two parameters have to be defined by the user to establish the score of a simulation with respect to the volumetric score during the full calibration period ($AVOL_{PERIOD}$).

– The year-to-year standard deviation of the volumetric score during the calibration years.
The range of this score is between 0 and ∞. This score should allow that all the years in the calibration period have a similar volumetric score. The goal of the calibration should be to maximise this score (and thus minimise year-to-year standard deviation) To scale this score to a range between 0 and 1, a simple fuzzy function is introduced:

$$AVOL_{YY} = \begin{cases} 1 & if \quad STDEV_{YY}(DV) < STDEV_{YY\_MIN} \\ \left(1 - \frac{(STDEV_{YY}(DV) - STDEV_{YY\_MIN})}{(STDEV_{YY\_MAX} - STDEV_{YY\_MIN})}\right) & if \quad STDEV_{YY\_MIN} \le STDEV_{YY}(DV) \le STDEV_{YY\_MAX} \\ 0 & if \quad STDEV_{YY}(DV) > STDEV_{YY\_MAX} \end{cases} \tag{6.3-11}$$

The fuzzy function is governed by two parameters: the maximum and minimum standard deviation of *DV* from year to year ($STDEV_{YY}$). These two parameters have to be defined by the user to establish the score of a simulation with respect to the variability of volumetric score during the different years of the calibration period ($AVOL_{YY}$).

– The month-to-month standard deviation of the volumetric score during the calibration years.
The range of this score is between 0 and ∞. This score should allow that, during the calibration period, all the months have a similar volumetric score. The goal of the calibration should be to maximise this score (and thus minimise month-to-month standard deviation). To scale this score to a range between 0 and 1, a simple fuzzy function is introduced:

$$AVOL_{MM} = \begin{cases} 1 & if \quad STDEV_{MM}(DV) < STDEV_{MM\_MIN} \\ \left(1 - \frac{(STDEV_{MM}(DV) - STDEV_{MM\_MIN})}{(STDEV_{MM\_MAX} - STDEV_{MM\_MIN})}\right) & if \quad STDEV_{MM\_MIN} \le STDEV_{MM}(DV) \le STDEV_{MM\_MAX} \\ 0 & if \quad STDEV_{MM}(DV) > STDEV_{MM\_MAX} \end{cases} \tag{6.3-12}$$

The fuzzy function is governed by two parameters: the maximum and minimum standard deviation of *DV* from month to month ($STDEV_{MM}$). These two parameters have to be defined by the user to establish the score of a simulation with respect to the variability of volumetric score during the different months in the calibration period ($AVOL_{MM}$).

AVOL is then computed as follows:

$$AVOL = AVOL_{PERIOD} \cdot \frac{w_1^{vol}}{\left(w_1^{vol} + w_2^{vol} + w_3^{vol}\right)} + AVOL_{YY} \cdot \frac{w_2^{vol}}{\left(w_1^{vol} + w_2^{vol} + w_3^{vol}\right)} + AVOL_{MM} \cdot \frac{w_3^{vol}}{\left(w_1^{vol} + w_2^{vol} + w_3^{vol}\right)} \tag{6.3-13}$$

with w_1^{vol}, w_2^{vol}, w_3^{vol} as the weight of the three fuzzy scores obtained through application of the previously defined fuzzy functions. All the parameters and weights of the fuzzy function have to be assigned at the beginning of the simulation.

Table 6.3-3: Recommended settings for the nine objective functions used for the calibration of PREVAH.

#	Description	SCORE	WEIGHT	$LIMIT_{MIN}$	$LIMIT_{MAX}$	Function
1	Linear efficiency – full period	$ALIN_{PERIOD}$	6	0.25	0.95	E_2^{lin}
2	Linear efficiency – year-by-year	$ALIN_{YY}$	4	0.1	0.01	$STDEV(E_2^{lin})$
3	Linear efficiency – month-by-month	$ALIN_{MM}$	2	0.5	0.02	$STDEV(E_2^{lin})$
4	Logarithmic efficiency – full period	$ALOG_{PERIOD}$	3	0.25	0.95	E_2^{log}
5	Logarithmic efficiency – year-by-year	$ALOG_{YY}$	2	0.1	0.01	$STDEV(E_2^{log})$
6	Logarithmic efficiency – month-by-month	$ALOG_{MM}$	1	0.5	0.02	$STDEV(E_2^{log})$
7	Volume error – full period	$AVOL_{PERIOD}$	10	0.1	0.01	DV
8	Volume error – year-by-year	$AVOL_{YY}$	4	0.15	0.02	STDEV(DV)
9	Volume error – month-by-month	$AVOL_{MM}$	3	0.10	0.02	STDEV(DV)

The column SCORE in Table 6.3-3 defines the different functions (see Equations 6.3-1 to 6.3-16).

Table 6.3-3 indicates the recommended (and default) weights of each function for building the corresponding summary score and overall score, as well as the "worst case" (minimum) and "best case" (maximum) limits.

6.3.3 Overall score (ATOT)

The overall score is a weighted function of the three scores ALIN, ALOG and a VOL (cf. Figure 6.3-2):

$$ATOT = ALIN^{w^{lin}/w^{tot}} \cdot ALOG^{w^{\log}/w^{tot}} \cdot AVOL^{w^{vol}/w^{tot}} \quad (6.3\text{-}14)$$

with $w^{lin} = w_1^{lin} + w_2^{lin} + w_3^{lin}$; $w^{\log} = w_1^{\log} + w_2^{\log} + w_3^{\log}$; $w^{vol} = w_1^{vol} + w_2^{vol} + w_3^{vol}$ (6.3-15)

and $w^{tot} = w^{lin} + w^{\log} + w^{vol}$ (6.3-16)

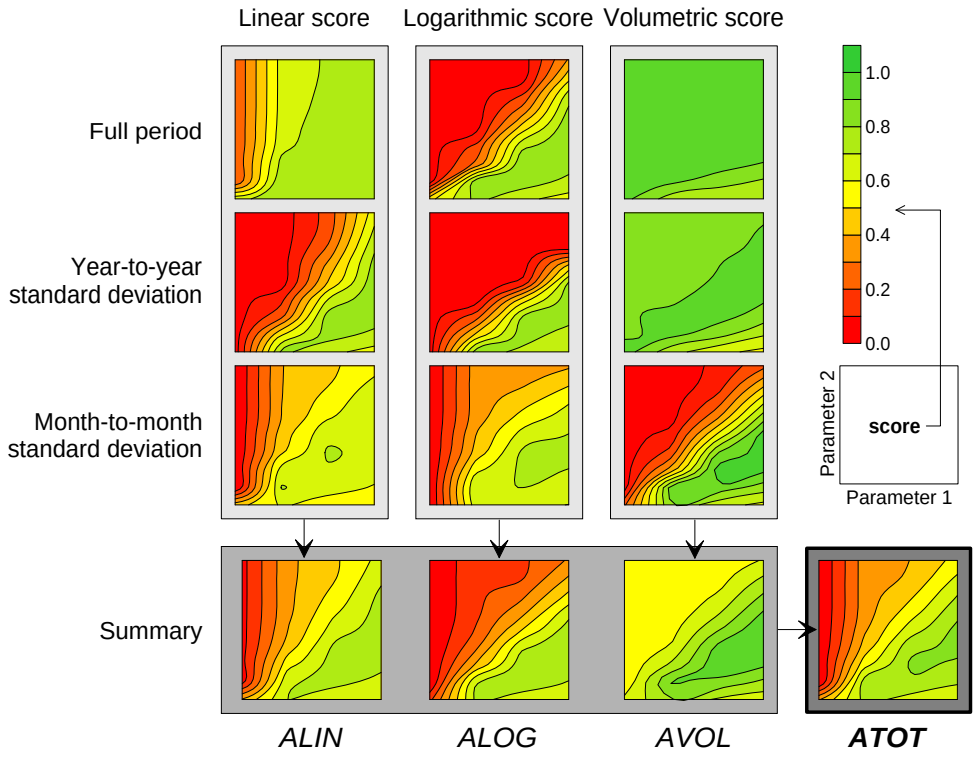

Figure 6.3-2: Composition of overall score from partial scores (Viviroli, 2007).

Figure 6.3-3 shows the course of these overall scores during a calibration process. PREVAH maintains a log of the corresponding values which is written to a file (see Part III, Chapter I: VIEWOPTIM).

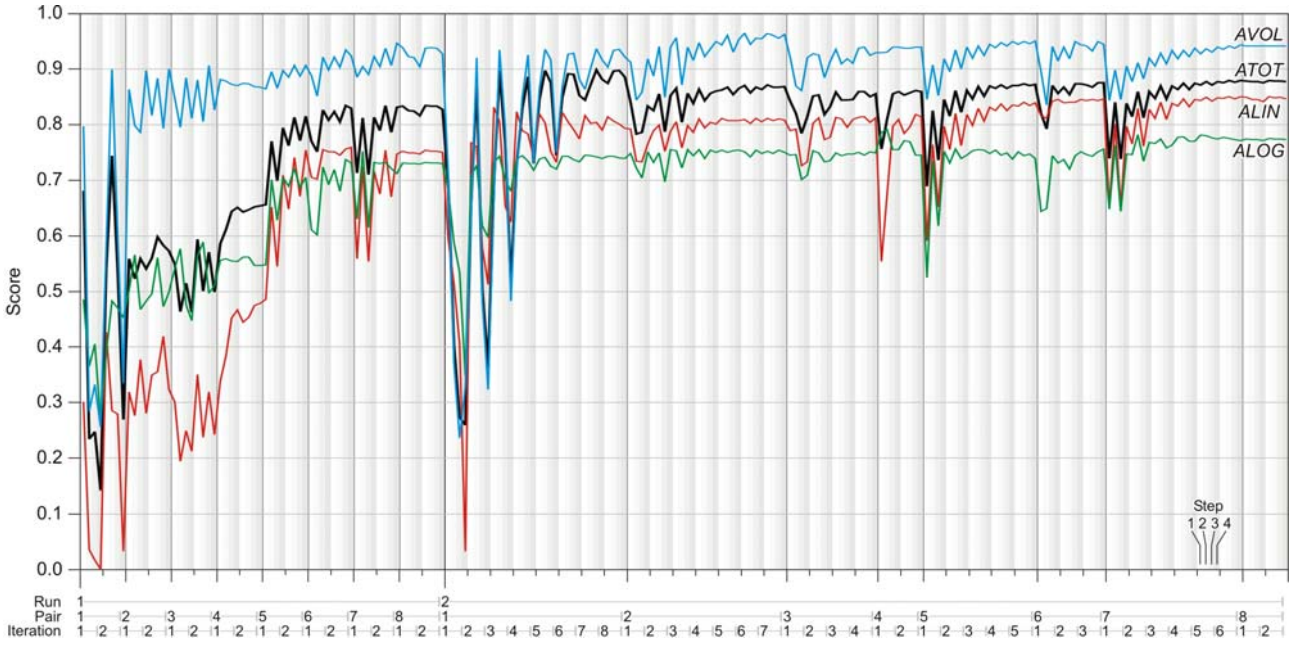

Figure 6.3-3: Full visualisation of the log file (.log) of the calibration module of WINPREVAH. ALIN is the linear score, ALOG the logarithmic score, AVOL the volumetric score and ATOT the total score (Viviroli, 2007).*

Acknowledgements

PREVAH was originally developed by Joachim Gurtz at the ETH Zürich and has received major input from Karsten Jasper, Simon Jaun, Jörg Schulla, Jan Schwanbeck, Mark Verbunt, Daniel Viviroli and Massimiliano Zappa. Furthermore, the following persons are acknowledged for their contributions to the development and testing of PREVAH:

Phillippe Achleitner
Carolin Antoni
Alexandre Badoux
Andri Baltensweiler
Claudine Berthod
Miriam Bohrer
Thomas Bosshard
Massimo Corti
Gion Decurtins
Philipp Flach
Daniel Gasser
Regine Hock
Raphael Hubacher
Susanne Huber
Lisette Klok
Gernot Koboltschnig
Herbert Lang
Patrick Lazzarotto
Lucas Menzel
Jürg Merz
Heidi Mittelbach
Annina Morger
Madlaina Perl
Femke Pos
Kees Roelofsma
Stefan Schmidle
Christoph Sonderegger
Stefan Vogt
Christoph Walther
Bernhard Wehren
Rolf Weingartner
Thomas Wöhling

The Federal Office for the Environment (FOEN) and Federal Office of Meteorology and Climatology (MeteoSwiss) are acknowledged for the invaluable gauge data they have provided over the years. Major research projects were hosted by the Institute for Atmospheric and Climate Science, ETH Zürich (IACETH), Institute of Geography, University of Berne (GIUB) and Swiss Federal Institute for Forest, Snow and Landscape Research in Birmensdorf (WSL). The Federal Office for the Environment (FOEN) and the Swiss Agency for Development and Cooperation (SDC) have provided additional funding.

Thanks also to Sabina Steiner who has helped editing this publication and to Stefan Zach (Part I) and Raelene Sheppard (Parts II and III) for their proof-reading.

References

Cited literature

Abbott, M. B., Bathurst, J. C., Cunge, J. A., O'Connell, P. E., Rasmussen, J. (1986a): An introduction to the European Hydrological System – Système Hydrologique Européen, "SHE", 1: History and philosophy of a physically-based, distributed modelling system. *Journal of Hydrology*, **87**, 45–59.

Abbott, M. B., Bathurst, J. C., Cunge, J. A., O'Connell, P. E., Rasmussen, J. (1986b): An introduction to the European Hydrological System – Système Hydrologique Européen, "SHE", 2: Structure of a physically-based, distributed modelling system. *Journal of Hydrology*, **87**, 61–77.

Anderson, E. A. (1973): *National Weather Service River Forecast System – Snow Accumulation and Ablation Model.* NOAA Technical Memo. Silver Spring: U.S. Department of Commerce, NWS.

Angström, A. (1918): *A study of the radiation of the atmosphere.* Smithsonian Institution Miscellaneous Collections, **65**, 159–161.

Bahrenberg G., Giese E., Nipper J. (1990): *Statistische Methoden in der Geographie. Band 1: Univariate und bivariate Statistik.* Stuttgart (D): Teubner.

Becker, A., Braun, P. (1999): Disaggregation, aggregation and spatial scaling in hydrological modelling. *Journal of Hydrology*, **217**, 239–252.

Becker, A., Nemec, J. (1987): Macroscale hydrologic models in support to climate research. In: Solomon, S. I., Beran, M., Hoog, W., eds. *The Influence of Climate Change and Climatic Variability on the Hydrologic Regime and Water Resources*. IAHS Publication, **168**. Wallingford (UK): IAHS, p. 431–445.

Bergström, S. (1976): *Development and Application of a Conceptual Runoff Model for Scandinavian Catchments.* Bulletin Series A, **52**, University of Lund (SWE).

Bergström, S. (1992): *The HBV Model – its Structure and Applications.* SMHI Reports Hydrology, **4**. Norrköping (SWE): SMHI.

Beven, K. J. (2000): *Rainfall-runoff Modelling: The Primer.* Chichester (UK): John Wiley & Sons.

Beven, K. J., Kirkby M. J. (1979): A physically based, variable contributing area model of basin hydrology. *Hydrological Sciences Bulletin*, **24**, 43–70.

BfR (1980): *Bodeneignungskarte der Schweiz. Grundlagen für die Raumplanung.* Bern: Bundesamt für Raumplanung.

Binley, A., Beven, K. J. (1993): *Three Dimensional Modelling of Hillslope Hydrology*. Advances in hydrological processes. Chichester (UK): John Wiley & Sons.

Blöschl, G., Sivapalan, M. (1995): Scale issues in hydrological modelling – a Review. *Hydrological Processes*, **9**, 251–290.

Braun, L. (1985): *Simulation of snowmelt-runoff in lowland and lower alpine regions of Switzerland.* Zürcher Geographische Schriften, **21**, ETH Zürich.

Burrough, P., McDonnell, R. A. (2000): *Principles of Geographical Information Systems.* New York: Oxford University Press.

Crawford, N. H., Linsley, R. S. (1966): *Digital simulation in hydrology: The Stanford Watershed Model IV.* Technical Report, **39**: Department of Civil Engineering, Stanford University, Paolo Alto, California.

Deutsch, C. V., Journel, A. G. (1997): *GSLIB: Geostatistical Software Library and User's Guide.* New York: Oxford University Press.

DVWK (1996): *Ermittlung der Verdunstung von Land- und Wasserflächen.* DVWK-Merkblätter zur Wasserwirtschaft, **238**. Bonn (D): Wirtschafts- und Verlagsgesellschaft Gas und Wasser.

Dyck, S., Peschke, G. (1995): *Grundlagen der Hydrologie*, Berlin (D): Verlag für Bauwesen.

Engel, B. A. (1996): Methodologies for development of hydrological response units based on terrain, land cover and soils data. In: *GIS and environmental modelling*. Fort Collins, CO, US: GIS World Books, p. 123–128.

FAO-UNESCO (1988): *Soil Map Of World*, Revised Legend. World Soil Resources Reports, **60**. Rome (IT): FAO.

Federer, C. A., Lash, D. (1983): *BROOK – a hydrologic simulation model for eastern forests.* Water Resources Research Center, University of New Hampshire.

Fekete, B. M., Vörösmarty, C. J., Lammers R. B. (2001): Scaling gridded river networks for macroscale hydrology: Development, analysis, and control of error. *Water Resources Research*, **37**, 1955–1967.

Flügel, W. A. (1995): Delineating hydrological response units by geographical inforamtion system analyses for regional hydrological modelling using PRMS/MMS in the drainage basin of the river Bröl, Germany. *Hydrological Processes*, **9**, 423–436.

Flügel, W. A. (1997): Combining GIS with regional hydrological modelling using hydrologic response units (HRUs): An application from Germany. *Mathematics and Computers in Simulation*, **43**, 297–304.

Freeze, R. A., Harlan, R. L.(1969): Blueprint for a physically-based digitally simulated hydrologic response model. *Journal of Hydrology*, **9**, 237–258.

Garen, D., Marks, D. (2001): Spatial fields of meteorological input data including forest canopy corrections for an energy budget snow simulation model. In: Dolman, A. J., Hall, A. J., Kavvas, M. L., Oki, T., Pomeroy, J. W., eds. *Soil-Vegetation-Atmosphere Transfer Schemes and Large Scale Hydrological Models*. IAHS Publication, **270**. Wallingford (UK): IAHS, p. 349–353.

Gash, J. H. C., Wright, I. R., Lloyd, C. R. (1980): Comparative estimates of interception loss from three coniferous forests in Great Britain. *Journal of Hydrology*, **48**, 89–105.

Gurtz, J., Baltensweiler, A., Lang, H., Menzel, L., Schulla, J. (1997a): *Auswirkungen von klimatischen Variationen von Wasserhaushalt und Abfluss im Flussgebiet des Rheins.* Schlussbericht NFP 31:"Klimaänderungen und Naturkatastrophen". Zürich: vdf Hochschulverlag.

Gurtz, J., Schulla, J., Lang, H. (1997b): Methodische Aspekte der Modellierung von Wasserhaushalt und Abfluss in Gebirgsgebieten. In: *Symposium zur Modellierung in der Hydrologie*, TU Dresden (D), p. 166–178.

Gurtz, J., Baltensweiler, A., Lang, H. (1999): Spatially distributed hydrotope-based modelling of evapotranspiration and runoff in mountainous basins. *Hydrological Processes*, **13**, 2751–2768.

Gurtz, J., Zappa, M., Jasper, K., Verbunt, M., Badoux, A., Vitvar, T., Lang, H. (2001): *Modelling of runoff and its components and model validation in Swiss Pre-Alpine and Alpine catchments.* Freiburger Schriften zur Hydrologie, **13**. Institute of Hydrology, University of Freiburg i.Br. (D), p. 206–220.

Gurtz, J., Zappa, M., Jasper, K., Lang, H., Verbunt, M., Badoux, A., Vitvar, T. (2003): A Comparative Study in Modelling Runoff and its Components in Two Mountainous Catchments. *Hydrological Processes*, **17**, 297–311.

Haberlandt, E. (1989): Zur Bestimmung von Parametern für hydrologische Modelle. Diplomarbeit. Dresden: TU Dresden, Bereich für Hydrologie und Meteorologie.

Haddeland, I., Matheussen, B. V., Lettenmaier, D. P. (2002): Influence of spatial resolution in a macroscale hydrologic model. *Water Resources Research*, **38**, 1124.

Hock, R. (1998): *Modelling of Glacier Melt and Discharge*. Diss ETH, **12430**, Department of Geography, ETH Zürich.

Hock, R. (1999): Distributed temperature-index ice- and snowmelt model including potential direct solar radiation. *Journal of Glaciology*, **45**, 101–111.

Hock, R. (2003): Evaluation and recent developments in temperature index melt modelling in mountain regions. *Journal of Hydrology*, **282**, 104–115.

Horton, R. E. (1933): The role of infiltration in the hydrologic cycle. *Transactions of the American Geophysical Union*, **14**, 446–460.

Isaaks, E. H., Srivastava, R. M. (1989): *An Introduction to Applied Geostatistics.* New York: Oxford University Press.

Jensen, H. (1986): *Kurzfristige Abflussvorhersagen für den Rhein bei Rheinfelden. Teil 1 und Teil 2*. Berichte und Skripte, **25** and **26**, Geographisches Institut der ETH Zürich.

Kalinin, G. P., Miljukov, P. I. (1957): On the computation of unsteady flow in open channels. *Meteorologiya i Gidrologiya*, **10**, 10–18 (in Russian).

Kasten F., Czeplak, G. (1980): Solar and terrestrial radiation dependent on the amount and type of cloud. *Solar Energy*, **24**, 177–189.

Kirkby, M. (1988): Hillslope runoff processes and models. *Journal of Hydrology*, **100**, 315–339.

Klemes, V. (1990): The Modelling of Mountain Hydrology: the Ultimate Challenge. In: Molnar, L., ed. *Hydrology of Mountainous Areas*, IAHS Publication, **190**. Wallingford (UK): IAHS, p. 29–43.

Klok, E. J., Jasper, K., Roelofsma, K. P., Badoux, A., Gurtz, J. (2001): Distributed hydrological modelling of a glaciated Alpine river basin. *Hydrological Sciences Journal*, **46**, 553–570.

Kouwen, N., Soulis, E. D., Pietroniro, A., Donald, J. Harrington, R. A. (1993): Grouped Response Units for distributed hydrologic modelling. *Journal of Water Resources Planning and Management – ASCE*, **119**, 289–305.

Lamb, R. (1999): Calibration of a conceptual rainfall-runoff model for flood frequency estimation by continuous simulation. *Water Resources Research*, **35**, 3103–3114.

Legates, D. R., McCabe, G. J. (1999): Evaluating the use of "Goodness-of-Fit" measures in hydrologic and hydroclimatic model validation. *Water Resources Research*, **35**, 233–241.

McCarthy, G. T. (1938): *The Unit Hydrograph and Flood Routing*. Presented at Conference of the North Atlantic Division, US Army Corps of Engineers, 24 June 1938.

Menzel, L. (1997): *Modellierung der Evapotranspiration im System Boden-Pflanze-Atmosphäre.* Zürcher Geographische Schriften, **67**, ETH Zürich.

Monteith, J. L. (1965): Evaporation and environment. *Symposium of the Society of Experimental Biologists*, **19**, 205–234.

Monteith, J. L. (1975): *Vegetation and the atmosphere, vol. 1: Principles.* London (UK): Academic Press.

Monteith, J. L. (1981): Evaporation and surface temperature. *Quarterly Journal of the Royal Meteorological Society*, **107**, 1–27.

Moore, I. D., Turner, A. K., Wilson, J. P., Jenson, S. K., Band, E. B. (1993): GIS and Land-Surface-Subsurface Process Modelling. In: *Environmental Modelling with GIS*. New York (US): Oxford University Press, p. 196–230.

Nash J. E., Sutcliffe J. V. (1970): River flow forecasting through conceptual models: Part I – a discussion of principles. *Journal of Hydrology*, **10**, 282–290.

Nemec, J. (1993): *Comparison and selection of existing hydrological models for the simulation of the dynamic water balance processes in basins of different sizes and on different scales.* CHR/KHR-Report, **II-7**. Lelystad (NL): International Commission for the Hydrology of the Rhine basin.

Oke, T. R. (1987): *Boundary Layer Climates,* 2nd edition. London (UK) and New York (US): Routledge.

Penman, H. L. (1948): Natural evaporation from open water, bare soil and grass. *Proceedings of the Royal Meteorological Society, London*, A, **193**, 120–145.

Penman, H. L. (1956): Estimating evaporation. *Transactions of the American Geophysical Union,* **37**, 43–46.

Pos F. (2001): *Spatially distributed modelling of snow accumulation and melt in pre-alpine and alpine catchments*. Diplomarbeit ETH Zürich. Zürich.

Refsgaard, J. C. (1997): Parameterisation, calibration, validation of distributed hydrological models. *Journal of Hydrology*, **198**, 69–97.

Rohrer, M. B., Braun, L. N., Lang, H. (1994a): Long term records of snow cover water equivalent in the Swiss Alps: 1. Analysis. *Nordic Hydrology*, **25**, 53–64.

Rohrer, M. B., Braun, L. N., Lang, H. (1994b): Long-term records of snow cover water equivalent in the Swiss Alps. 2. Simulation. *Nordic Hydrology*, **25**, 65–78.

Ross, B. B., Contractor, D. N., Shanholtz, V. O. (1979): A finite element model of overland and channel flow for assessing the hydrologic impact of land-use change. *Journal of Hydrology*, **41**, 1–30.

Ross, C. N. (1921): The calculation of flood discharge by the use of time contour plan isochrones. *Transactions of the Institute of Engineers (Australia)*, **2**, 85–92.

Schulla, J. (1997): *Hydrologische Modellierung von Flussgebieten zur Abschätzung der Folgen von Klimaänderungen.* Zürcher Geographische Schriften, **69**, ETH Zürich.

Schulla, J., Jasper, K. (2000): *Model Description WaSiM-ETH*. Zürich: Institute for Atmospheric and Climate Science.

Schwarze, R., Droege, W., Opherden, K. (1999): Regional analysis and modelling of groundwater runoff components from catchments in hard rock areas. In: Diekkrüger, B., Kirkby, M. J., Schröder, U., eds. *Regionalisation in Hydrology*. IAHS Publication, **254**. Wallingford (UK): IAHS, p. 221–232.

Sevruk, B., ed. (1986): *Correction of Precipitation Measurements. ETH/IASH/WMO Workshop on the Correction of Precipitation Measurements*. Zürcher Geographische Schriften, **23**, ETH Zürich.

Sherman, L. K. (1932): Streamflow from rainfall by unit-hydrograph method. *Engineering news Record.*, **108**, 501–505.

Singh, V. P. (1995): *Computer models of Watershed Hydrology*. Highlands Ranch, CO (US): Water Resources Publications.

Singh, V. P. (1997): Effect of spatial and temporal variability in rainfall and watershed characteristics on stream flow hydrograph. *Hydrological Processes*, **11**, 1649–1669.

Sonderegger, C. (2004): *Rainfall-Runoff Modelling of a Sub-Catchment of the Yangtze River in China.* Diploma Thesis, ETH and University of Zürich.

Strahler, A. N. (1952): Hypsometric (area-altitude) analysis of erosional topography. *Bulletin of the Geological Society of America*, **63**, 1117–1142.

Strasser, U., Mauser, W. (2001): Modelling the spatial and temporal variations of the water balance for the Weser catchment 1965–1994. *Journal of Hydrology*, **254**, 199–214.

Strasser, U., Etchevers, P., Lejeune, Y. (2002): Intercomparision of two snow models with different complexity using data from an alpine site. *Nordic Hydrology*, **33**, 15–26.

Susong, D., Marks, D., Garen, D. (1999): Methods for developing time-series climate surfaces to drive topographically distributed energy- and water-balance models. *Hydrological Processes*, **13**, 2003–2021.

Tarboton, D. G., Bras, R. L., Rodríguez-Iturbe, I. (1993): On the extraction of channel networks from digital elevation data. In: Beven, K. J., Moore, I. D., eds. *Terrain Analysis and Distributed Modelling in Hydrology*. Chichester (UK): Wiley, p. 85–104.

Uhlenbrook, S. (1999): *Untersuchung und Modellierung der Abflußbildung in einem mesoskaligen Einzugsgebiet.* Freiburger Schriften zur Hydrologie, **10**, Freiburg i. Br. (D).

Uhlenbrook, S., Leibundgut, Ch. (2002): Process-oriented catchment modelling and multiple-response validation. *Hydrological Processes*, **16**, 423–440.

Verbunt, M., Gurtz, J., Jasper, K., Lang, H., Warmerdam, P., Zappa, M. (2003): The hydrological role of snow and glaciers in alpine river basins and their distributed modelling. *Journal of Hydrology*, **282**, 36–55.

Verbunt, M., Zappa, M., Gurtz, J., Kaufmann, P. (2006): Verification of a coupled hydrometeorological modelling approach for alpine tributaries in the Rhine basin. *Journal of Hydrology* **324**, 224–238.

Viviroli, D. (2007): *Ein prozessorientiertes Modellsystem zur Abschätzung seltener Hochwasserabflüsse für unbeobachtete Einzugsgebiete der Schweiz.* Geographica Bernensia, **G77**. Berne: Institute of Geography, University of Berne.

Wendling, U. (1975): Zur Messung und Schätzung der potentiellen Verdunstung. *Zeitschrift für Meteorologie*, **25**, 103–111.

Zappa, M. (1999): *Untersuchungen zur Aufbereitung unterschiedlicher Rauminformationen für die flächendifferezierte Einzugsgebietsmodellierung.* Diploma thesis, ETH Zürich.

Zappa, M. (2002): *Multiple-Response Verification of a Distributed Hydrological Model at Different Spatial Scales.* Diss ETH, **14895**, ETH Zürich.

Zappa, M., Gurtz, J. (2002): The Experience of Using a Response Units Based Model for Distributed Hydrological Simulations at Different Scales. In: *Water Resources and Environment Research,* Proceedings of ICWRER 2002, 22–25 July 2002 Dresden (D), **28**, I, 96–100.

Zappa, M., Gurtz, J. (2003): Plot-scale simulation of soil moisture and evapotranspiration during the 1999 MAP-Riviera campaign. *Hydrology and Earth System Sciences*, **7**, 903–919.

Zappa, M., Kan, C. (2007): Extreme heat and runoff extremes in the Swiss Alps. *Natural Hazards and Earth System Sciences*, **7**, 375–389.

Zappa, M., Pos, F., Strasser, U., Gurtz, J. (2003): Seasonal water balance of an alpine catchment as evaluated by different methods for spatially distributed snow melt modelling. *Nordic Hydrology*, **34**, 179–202.

Further reading

Badoux, A. (1999): *Untersuchung zur flächendifferenzierten Modellierung von Abfluss und Schmelze in teilvergletscherten Einzugsgebieten*. Diploma thesis, ETH Zürich.

Bartlet, P., Lehning, M. (2002): A physical SNOWPACK model for the Swiss avalanche warning. Part I: numerical model. *Cold Regions Science and Technology*, **35**, 123–145.

Beven, K. J., Wood, E. F., Sivapalan, M. (1988): On hydrological heterogeneity – catchment morphology and catchment response. *Journal of Hydrology*, **100**, 353–375.

BfS (1995): *Die Bodennutzung der Schweiz. Arealstatistik 1979/85*. Bern: Bundesamt für Statistik.

Blöschl, G. (1996): *Scale and Scaling in Hydrology*. Wiener Mitteilungen Wasser - Abwasser - Gewässer, **132**, TU Wien, Institut für Hydraulik, Gewässerkunde und Wasserwirtschaft.

Bohrer, M. (1998): *Räumlich differenzierte Erfassung der Einzugsgebietskennwerte und Modellierung des Wasserhaushalts im Rietholzbachgebiet unter Nutzung eines GIS*. Diploma thesis, ETH Zürich and University of Zürich.

Braun, L., Brun, E., Durand, Y., Martin, E. (1994): Simulation of discharge using different methods of meteorological data distribution, basin discretisation and snow modelling. *Nordic Hydrology*, **25**, 129–144.

Breinlinger, R., Gamma, P., Weingartner, R. (1992): *Characteristics of small basins*. Hydrological Atlas of Switzerland, Plate **1.2**. Berne: Swiss National Hydrological and Geological Survey.

Brutsaert, W. (1975): On a derivable formula for long-wave radiation from clear skies. *Water Resources Research*, **11**(5), 742–744.

Brutsaert, W. (1982): *Evaporation into the atmosphere*. Dordrecht (NL): Kluwer Academic Publishers.

Bründl, M., Etter, H. J., Steiniger, M., Klinger, C., Rhyner, J., Ammann, W. J. (2004): IFKIS – a basis for managing avalanche risk in settlements and on roads in Switzerland. *Natural Hazards and Earth System Sciences*, **4**, 257–262.

Collins, E. H. (1934): *Relationship of degree-days above freezing to runoff.* Transactions of the American Geophysical Union, Reports and Papers, Hydrology, 624–629.

Essery, R., Martin, E., Douville, H., Fernandez, A., Brun, E. (1999): A comparison of four snow models using observations from an alpine site. *Climate Dynamics*, **15**, 583–593.

Famiglietti, J. S., Wood, E. F. (1995): Effects of spatial variability and scale on areally averaged evapotranspiration. *Water Resources Research*, **31**, 699–712.

Ferguson, R. I. (1999): Snowmelt Runoff Models. Progress *In Physical Geography*, **23**, 205–227.

Grayson, R., Blöschl, G., eds. (2001): *Spatial patterns in catchment hydrology: observations and modelling.* Cambridge (UK): Cambridge University Press.

Green, W. H., Ampt, G. A. (1911): Studies on Soil Physics: I. The flow of air and water through soils. *Journal of Agricultural Sciences,* **4**, 1–24.

Gurtz, J., Baltensweiler, A., Lang, H. (1999): Spatially distributed hydrotope-based modelling of evapotranspiration and runoff in mountainous basins. *Hydrological Processes*, **13**, 2751–2768.

Gurtz, J., Huber, S., Lang, H., Baltensweiler, A. (1997): *Spatial distributed modelling of the evapotranspiration and the water balance in an alpine basin.* XXII General Assembly of European Geophysical Society, Symposium BAHC 03 "Mountain Eco-Hydrology", Vienna, March 1997.

Gurtz, J., Peschke, G., Mendel, O. (1990): *Hydrologic processes in small experimental areas influenced by vegetation cover. In: Hydrological research basins and the environment.* International Conference in 1990, Proceedings and Information, **44**, Wageningen (NL), p. 61–69.

Gurtz, J., Verbunt, M., Jasper, K., Lang, H., Zappa, M. (2002): *Spatial and temporal variations of hydrological processes in mountainous regions and their modelling.* In: Water Resources and Environment Research. ICWRER 2002, 22–25 July 2002 Dresden (D). Proceedings, **28**, I, 47–51.

Gurtz, J., Verbunt, M., Zappa, M., Moesch, M., Moser U. (2003b): Long-term hydrometeorological measurements and model based analyses in the hydrological research catchment Rietholzbach. *Journal of Hydrology and Hydromechanics*, **51**, 162–174.

Gurtz, J., Zappa, M., Verbunt, M., K. Jasper (2003c): Advanced applications of distributed hydrological models in mountainous catchments. In: de Jong, C., Collins, D., Ranzi, R., eds. *Climate and Hydrology in Mountain Areas.* Chichester: Wiley.

Hamon W. R. (1961): Estimating potential evapotranspiration. *Journal of the Hydraulics Division, Proceedings of the American Society of Civil Engineers*, **87**, 107–120.

Jasper, K. (2001): *Hydrological modelling of alpine river catchments using output variables from atmospheric models.* Diss ETH, **14385**, Department of Geography, ETH Zürich.

Jasper, K., Gurtz, J., Lang, H. (2002): Advanced flood forecasting in Alpine watersheds by coupling meteorological observations and forecasts with a distributed hydrological model. *Journal of Hydrology*, **267**, 40–52.

Kenward, T., Lettenmaier, D. P., Wood, E. F., Fielding, E. (2000): Effects of digital elevation model accuracy on hydrologic predictions. *Remote Sensing of Environment*, **74**, 432–444.

Kirnbauer, R., Blöschl, G., Gutknecht, D. (1994): Entering the era of distributed snow models. *Nordic Hydrology*, **25**, 1–24.

Klemes, V. (1983): Conceptualisation and scale in hydrology. *Journal of Hydrology*, **65**, 1–23.

Koboltschnig, G. (2007): Mehrfachvalidierung hydrologischer Eis- und Schneeschmelzmodelle in hochalpinen, vergletscherten Einzugsgebieten. Ph.D. Thesis, University of Natural Resources and Applied Life Sciences, Vienna.

Koboltschnig, G., Holzmann, H., Schoener, W., Zappa, M. (2007): Contribution of glacier melt to stream runoff: if the climatically extreme summer of 2003 had happened in 1979. *Annals of Glaciology*, **46**, 46A196.

Konzelmann, T., Calanca, P., Müller, G., Menzel L., Lang, H. (1997): Energy balance and evapotranspiration in a high mountain area during summer. *Journal of Applied Meteorology*, **36**, 966–973.

Kuo, W. L., Steenhuis, T. S., Mcculloch, C. E., Mohler, C. L., Weinstein, D. A., Degloria, S. D., Swaney, D. P. (1999): Effect of grid size on runoff and soil moisture for a variable-source-area hydrology model. *Water Resources Research*, **35**, 3419–3428.

Lang, H. (1981): Is Evaporation an Important Component in High Alpine Hydrology? *Nordic Hydrology*, **12**, 217–224.

Lang, H. (1986): Forecasting meltwater runoff from snow-covered areas and from glacier basins. In: Kraijenhoff, D. A., Moll, J. R., eds. *River Flow Modelling and Forecasting*, D. Reidel publishing company, p. 99–127.

Lang, H., Braun, L. (1990): On the information content of air temperature in the context of snow melt estimation. In: Molnar, L., ed. *Hydrology of Mountanious Areas*. IAHS publication, **190**. Wallingford (UK): IAHS, p. 347–354.

Leibundgut, Ch., Uhlenbrook, S., McDonnell, J., eds. (2001): *Runoff generation and implications for river basin modelling.* Proceedings from the International Workshop, 9–13 October 2000. Freiburger Schriften zur Hydrologie, **13**, Institute of Hydrology, University of Freiburg i.Br. (D).

Maisch, M., Wipf, A., Denneler, B., Battaglia, J., Benz, C. (1999): *Die Gletscher der Schweizer Alpen. Gletscherhochstand 1850, aktuelle Vergletscherung, Gletscherschwund-Szenarien.* Projektschlussbericht im Rahmen des Nationalen Forschungsprogrammes "Klimaänderungen und Naturkatastrophen", NFP-31. Zürich: vdf Hochschulverlag.

Martinec, J., Rango, A. (1986): Parameter values for snowmelt runoff modelling. *Journal of Hydrology*, **84**, 197–219.

Menzel, L. (1996): Modelling Canopy Resistances and Transpiration of Grassland. *Physics and Chemistry of the Earth*, **21**, 123–129.

Muster, H. (1994): Ermittlung von Gebietsniederschlägen. In: *Niederschlag-Abfluss-Modelle für kleine Einzugsgebiete und ihre Anwendung*, 18. Fortbildungslehrgang Hydrologie des DVWK, 19.–23. September 1994, Karlsruhe (D).

Ohmura, A. (2001): Physical Basis for the Temperature-Based Melt-Index Method. *Journal of Applied Meteorology*, **40**, 753–761.

Oltchev, A., Cermak, J., Gurtz, J., Tishenko, A., Kiely, G., Nadezhdina, N., Zappa, M., Lebedeva, N., Vitvar, T., Albertson, J. D., Tatarinov, F., Tishenko, D., Nadezhdin, V., Kozlov, B., Ibrom, A., Vygodskaya, N., Gravenhorst, G. (2002): The response of the water fluxes of the boreal forest region at the Volga's source area to climatic and land-use changes. *Physics and Chemistry of the Earth*, **27**, 675–690.

Peschke, G.(1987): Soil Moisture and Runoff Components from a Physically Founded Approach. *Acta hydrophysica*, **31**, 191–205.

Pfaundler, M., Zappa, M. (2006): Die mittleren Abflüsse über die ganze Schweiz – Ein optimierter Datensatz im 500×500 m^2 Raster. *Wasser, Energie, Luft*, **98**(4), 291–298.

Ranzi, R., Zappa, M., Bacchi, B. (2007): Hydrological aspects of the Mesoscale Alpine Programme: findings from field experiments and simulations. *Quarterly Journal of the Royal Meteorological Society*, **133**, 867–880.

Rotach, M. W., Calanca, P., Graziani, G., Gurtz, J., Steyn, D. G., Vogt, R., Andretta, M., Christen, A., Cieslik, S., Connolly, R., De Wekker, S. F. J., Galmarini, S., Kadygrov, E. N., Kadygrov, V., Miller, E., Neininger, B., Rucker, M., Van Gorsel, E., Weber, H., Weiss, A., Zappa, M. (2004): Turbulence structure and exchange processes in an Alpine Valley – The Riviera project. *Bulletin of the American Meteorological Society*, **85**, 1367–1385.

Seibert, J., McDonnell, J. J. (2002): On the dialog between experimentalist and modeler in catchment hydrology: Use of soft data for multi-criteria model calibration. *Water Resources Research*, **38**, 1241–1254.

Singh, V. P., Woolhiser, D. A. (2002): Mathematical modelling of watershed hydrology. *Journal of Hydrologic Engineering*, **7**, 270–292.

Slater, A. G., Schlosser, C. A., Desborough, C. E., Pitman, A. J., Henderson-Sellers, A., Robock, A., Vinnikov, K. Y., Mitchell, K., the PILPS 2(d) Contributors (2001): The representation of snow in land-surface schemes; results from PILPS 2(d). *Journal of Hydrometeorology*, **2**, 7–25.

Turc L. (1961): Evaluation des besoins en eau d'irrigation, évapotranspiration potentielle, formulation simplifié et mise à jour. *Annales Agronomiques,* **12**, 13–49.

Vàzquez, R. F., Feyen, L., Feyen, J., Refsgaard, J. C. (2002): Effect of grid size on effective parameters and model performance of the MIKE-SHE code. *Hydrological Processes*, **16**, 355–372.

Verbunt, M. (2005): *From Small-scale Modelling of Alpine Catchments Towards Probabilistic Flood Forecasting in the Rhine Basin.* Ph.D. Thesis, **16115**, Institute for Atmospheric and Climate Science, ETH Zürich.

Verbunt, M., Zappa, M., Gurtz, J., Kaufmann, P. (2006): Verification of a coupled modelling approach for different catchments in upper Rhine basin. *Journal of Hydrology*, **324**(1–4), 224–238.

WMO (1983): *Guide to meteorological instruments and observing practices.* Fifth edition. WMO publication, **8**. Geneva: World Meteorological Organisation.

WMO (1986): *Intercomparison of models for snowmelt runoff.* Operational Hydrology Report, **23**. Geneva: World Meteorological Organisation.

Wendling U. (1975): Zur Messung und Schätzung der potentiellen Verdunstung. *Zeitschrift für Meteorologie*, **25**, 103–111.

Wöhling, T., Lennartz, F., Zappa, M. (2006): Technical note: Updating procedure for flood forecasting with conceptual HBV-type models. *Hydrology and Earth System Sciences*, **10**, 783–788.

Wolock, D. M., Price, C. V. (1994): Effects of digital elevation model map scale and data resolution on a topography based watershed model. *Water Resources Research*, **30**, 3041–3052.

Wood, E. F. (1997): Effects of Soil Moisture Aggregation on Surface Evaporative Fluxes. *Journal of Hydrology*, **190**, 397–412.

Wood, A. W., Lettenmaier, D. P., Palmer, R. N. (1997): Assessing climate change implications for water resource planning. *Climatic Change*, **37**, 203–228.

Wood, E. F., Sivapalan, M., Beven, K. J., Band, L. (1988): Effects of spatial variability and scale with implications to hydrologic modelling. *Journal of Hydrology*, **102**, 29–47.

WSL [Forschungsanstalt für Wald, Schnee und Landschaft] (1988): *Schweizerisches Landesforstinventar. Ergebnisse der Erstaufnahme 1982–86.* Berichte der WSL, **305**. Birmensdorf: WSL.

Zappa, M., Kan, C. (2007): Extreme heat and runoff extremes in the Swiss Alps. *Natural Hazards and Earth System Sciences*, **7**, 375–389.

Zhang, W., Montgomery, D. R. (1994): Digital elevation model grid size, landscape representation, and hydrologic simulations. *Water Resources Research*, **30**, 1019–1028.

Zappa, M., Badoux, A., Gurtz, J. (2000): The application of a complex distributed hydrological model in an highly glaciated alpine river catchment. In: Horvatic, J., ed. *Proceedings of the 33rd Conference of International Association for Danube Research*. Limnological Reports, **33**, 23–28.

Zappa, M., Matzinger, N., Gurtz, J. (2001): Hydrological and Meteorological Measurements at Claro (CH) – Lago Maggiore Target Area in the MAP-SOP 1999 RIVIERA Experiment – Including First Evaluation. In: Bacchi, B., Ranzi, R., eds. *Hydrological aspects in the Mesoscale Alpine Programme-SOP experiment*. Technical Report, **10**, Deptartment of Civil Engineering, University of Brescia (IT).

Appendix

Radiation equations used in PREVAH

Short wave radiation *Rsw*

Default using observed and spatially interpolated global radiation (RG):

$$Rsw = (1 - \alpha) \cdot RG$$

where α is the albedo

Penman (1948):

$$Rsw = (1 - \alpha) \cdot G_0 \cdot (0.18 + 0.55 \cdot n/N)$$

where G_0 is the potential incoming clear sky direct radiation [W m^{-2}] and n/N is the relative sunshine duration

Penman (1956):

$$Rsw = (1 - \alpha) \cdot G_0 \cdot (0.20 + 0.48 \cdot n/N)$$

Golchert (1981):

$$Rsw = (1 - \alpha) \cdot G_0 \cdot (A_G + B_G \cdot n/N)$$

where A_G and B_G are dimensionless monthly varying constants after Golchert (1981)

Kasten und Czeplak (1980):

$$G_T = G_0 (1 - 0.7CN^3)$$

$$Rsw = (1 - \alpha) \cdot G_T \cdot (1 - 0.55 \cdot CN - 0.25 \cdot CN^4)$$

where G_T is the global radiation with cloud coverage [W m^{-2}] and CN is the cloud coverage ($^1/_8$ to $^8/_8$)

Morecs (1981):

$$\eta = 1$$

$$Rsw = (1 - \alpha) G_0 (\eta (A_M + B_M n / N) + C_M (1 - \eta))$$

where A_M, B_M and C_M are dimenstionless constants after Morecs (1981); while B_M is monthly varying, A_M and C_M are constant over the year

Schulla (1997):

$$Rsw = (1 - \alpha) G_0 (0.23 + 1.77 n / N) - 2.28 (n / N)^2 + 1.28 (n / N)^2$$

Long wave radiation *Rlw*

Penman (1948):

$$Rlw = -\sigma T_K^4 (0.56 - 0.09\sqrt{0.75e}) \cdot (0.1 + 0.9n/N)$$

where σ is the Stefan-Bolzmann constant and T_K is the air temperature in Kelvin

Penman (1956):

$$Rlw = -\sigma T_K^4 (0.47 - 0.0077\sqrt{0.75e}) (0.2 + 0.8n / N)$$

Angstroem (1918):

$$L_{DN0} = \sigma T_K^4 \left(0.79 - 0.174 * 10^{-0.055*0.75e}\right)$$

where L_{DN0} is the reflectance of the atmosphere

Feussner(s.a.):

$$L_{DN0} = \sigma T_K^4 \left(1 - 10^{-0.424*(0.75e_L)^{0.2}}\right)$$

Kasten and Czeplak (1980):

$$L_{DN0} = \sigma T_K^6 A_{CZ} E_{PS0} - B_{CZ}$$

where A_{CZ} [-], B_{CZ} [W m^{-2}] and E_{PS0} [K^{-2}] are constants after Kasten and Czeplak (1980)

with sunshine duration:

$$Rlw = A_T \left(L_{DN0} - \sigma T_K^4\right)\left(0.2 + 0.8n / N\right)$$

where A_T is the reflectance coefficient of the surface for longwave radiation

with cloud amount:

$$Rlw = A_T \left(L_{DN0}\left(1 + 0.27CN^2\right) - \sigma T_K^4\right)$$

Brutsaert (1975):

$$Rlw = A_T \sigma T_K^4 \left(1.28\left(e / T_K\right)^{1/7} - 1\right)\left(0.2 + 0.8n / N\right)$$

Schulla (1997):

$$Rlw = \sigma T_K^4 \left(0.52 - 0.065\sqrt{e}\right)\left(0.23 + 0.77n / N\right)$$

Institute for Atmospheric and Climate Science
IAC*ETH*

ISBN 978-3-905835-01-0